

Doped Layered Phosphate Catalysts for the Activation of Glycerol

By Douglas J Parker BSc(Hons) AMRSC

A thesis submitted in partial fulfilment for the requirements for the degree of
Master of Science (by Research) at the University of Central Lancashire

April 2014

Declaration

Concurrent registration for two or more academic awards

I declare that while registered as a candidate for the research degree, I have not been a registered candidate or enrolled student for another award of the University or other academic or professional institution

Material submitted for another award

I declare that no material contained in the thesis has been used in any other submission for an academic award and is solely my own work

Collaboration

Where a candidate's research programme is part of a collaborative project, the thesis must indicate in addition clearly the candidate's individual contribution and the extent of the collaboration. Please state below:

Signature of Candidate *Douglas J Parker*

Type of Award **MSc (by research)**

School **School of Forensic and Investigative Science**

Abstract

Glycerol is a plentiful chemical side-product from many industrial processes including the production of biofuels, simple fermentations and reactions used to synthesise alkenes such as propene. The rising cost of safely disposing of chemical waste is forcing companies to find new and innovative ways of either reusing waste products or ways to minimise the amount of waste produced. Waste glycerol can be converted into more highly desirable compounds such as glycerol carbonate. However, the most common method of converting glycerol to glycerol carbonate is to react it with phosgene which is highly toxic. Glycerol carbonate is a highly sought after compound because of the magnitude of its uses from polymers and cleaning solvents to cosmetics and curing agents.

Recent research has started to focus on finding new green methods for synthesising glycerol carbonate, by way of catalysis. Previous work in this area was carried out by Aresta *et al.* in which γ -zirconium phosphate was used to catalyse the reaction between glycerol and urea to form glycerol carbonate. It is thought that the reaction proceeds via a two-step reaction. Firstly the glycerol and urea react forming glycerol carbamate, this intermediate then cyclicises around to form the carbonate. The advantage in using urea for this reaction as opposed to carbon dioxide is that ammonia gas is evolved during the reaction, allowing for a potentially greener method to synthesise another valuable industrial chemical. The work presented here is the synthesis of a library of novel metal-substituted layered phosphate catalysts and the assessment of their potential as catalysts, in the synthesis of glycerol carbonate via the glycerolysis of urea.

Acknowledgements

Firstly I would like to thank my supervisors Professor Gary Bond and Dr. Jennifer Readman, who have provided me with lots of support and encouragement over the past year and have always found the time to help me. Also a special thank you to Jen for keeping my spirits high by providing ample quantities of very delicious cake!

I would also like to acknowledge the help and support of Dr Richard McCabe whose helpful advice and vast knowledge of all things relating to chemistry has proved to be most insightful and invaluable to me in completing my thesis. Also I like to thank all the technical staff in the school, especially a big thank you to Jim, Tamar and Pat for keeping everything running smoothly in the analytical suite and to Dr Runjie Mao for helping me with the micrometrics equipment. Also I would like to say a big thank you to Sal who never failed to dig out obscure bits of equipment and chemicals whenever I asked.

I would like to thank both the School of Forensic and Investigative Sciences and the School of Pharmacy and Biomedical Sciences for allowing me to use their facilities and equipment.

And finally I would like to thank all my friends at UCLan for making my time here most enjoyable and my family for being a constant source of support.

List of Abbreviations

AlPO	Aluminium Phosphate
α -ZrP	Alpha Zirconium Phosphate
γ -ZrP	Gamma Zirconium Phosphate
GTBE	Glycerol <i>tert</i> -butyl ether
NMR	Nuclear Magnetic Resonance
FoM	Figure of Merit
XRD	Powder X-Ray Diffraction
XRF	X-Ray Fluorescence
MQMAS	Multiple Quantum Magic Angle Spinning
SEM	Scanning Electron Microscopy
EDX	Energy Dispersive X-ray spectroscopy
TGA	Thermogravimetric Analysis
BET	Brunauer, Emmett and Teller
DRIFTS	Diffuse Reflectance Infrared Fourier Transform Spectroscopy

Contents

List of Figures	VII
-----------------------	-----

List of Tables.....	X
---------------------	---

Chapter 1: Introduction

1.1: Glycerol, waste product or valuable raw material?	1
1.2: Existing and new methods of glycerol carbonate synthesis	6
1.3: Aluminium phosphates and derivatives.....	9
1.4: Zirconium phosphates and derivatives	14
1.5: Aims of Research.....	17

Chapter 2: The synthesis and characterisation of doped metal phosphates

2.1: Introduction	18
2.2: Synthesis of catalysts	18
2.3: Materials	19
2.4: Methods of characterisation and analysis	21
2.5: Characterisation of Aluminium Phosphate series catalysts.....	24
2.5.1: Infrared Spectroscopy	24
2.5.2: X-Ray Diffraction and X-Ray Fluorescence analysis	30
2.5.3: Solid-state NMR	33
2.5.4: Surface properties and decomposition analysis	37
2.6: Characterisation of α -zirconium phosphate catalyst.....	43
2.6.1: Infrared Spectroscopy	43
2.6.2: X-Ray Diffraction and X-Ray Fluorescence analysis	44
2.6.3: Solid-state NMR	45
2.6.4: Surface properties and decomposition analysis	45
2.7: Summary	48

Contents

Chapter 3: Catalytic testing and results

3.1: Introduction	49
3.2: Method development and reaction set-up.....	50
3.3: Results	52
3.3.1: Ammonia capture results.....	52
3.3.2: Glycerol carbonate yields.....	53
3.4: Summary	55

Chapter 4: Conclusions and future work

4.1: Conclusions	56
4.2: Future work.....	61
4.3: Summary	64

Appendices.....	65
Appendix 5.1: Ammonia capture data	66
Appendix 5.2: XRF spectra	70
Appendix 5.3: ²⁷ Al NMR spectra.....	73
Appendix 5.4: 1D-MQMAS NMR spectra	76
Appendix 5.5: Annotated catalytic reaction NMRs.....	79
Appendix 5.6: Refined lattice parameters	100
References.....	106

List of Figures

Figure 1.1: Derivatives of glycerol, chemical pathway [3]	2
Figure 1.2: Fine chemical derivatives of glycerol	3
Figure 1.3: The direct carboxylation of glycerol via $n\text{-Bu}_2\text{Sn}(\text{OMe})_2$ catalysis	6
Figure 1.4: Crystal structure of berlinite [21].....	9
Figure 1.5: Crystal structure of α -zirconium phosphate [36].....	14
Figure 1.6: The glycerolysis of urea via catalytic reaction	17
Figure 2.1: IR spectrum of DJP011 (Ti doped).....	25
Figure 2.2: IR spectrum of DJP015	26
Figure 2.3: IR Spectrum of DJP017 (Zn doped)	27
Figure 2.4: IR Spectrum of DJP018 (Ga doped).....	28
Figure 2.5: IR spectrum of DJP019 (Co doped)	29
Figure 2.6: XRD patterns for aluminium phosphate series catalysts	32
Figure 2.7: ^{31}P NMR spectrum of DJP011 (Ti doped)	34
Figure 2.8: ^{31}P NMR spectrum of DJP015.....	34
Figure 2.9: ^{31}P NMR spectrum of DJP017 (Zn doped)	35
Figure 2.10: ^{31}P NMR spectrum of DJP018 (Ga doped).....	35
Figure 2.11: ^{31}P NMR spectrum of DJP019 (Co doped).....	36
Figure 2.12: Scanning electron micrographs of DJP015(a) and DJP017(b)	38
Figure 2.13: TGA curve of DJP011 (Ti doped).....	40
Figure 2.14: TGA curve of DJP015	40
Figure 2.15: TGA curve of DJP017 (Zn doped)	41
Figure 2.16: TGA curve of DJP018 (Ga doped)	41
Figure 2.17: TGA curve of DJP019 (Co doped)	42
Figure 2.18: IR spectrum of DJP016	43
Figure 2.19: ^{31}P NMR spectrum of α -ZrP catalyst	45
Figure 2.20: Scanning electron micrograph of DJP016	46
Figure 2.21: TGA curve of DJP016.....	47
Figure 3.1: Correlation between glycerol carbonate and ammonia evolved	51
Figure 3.2: Graph showing the cumulative ammonia captured per reaction.....	52
Figure 4.1: ^{13}C NMR of catalytic reaction showing no ethylenediamine peak.....	57
Figure 4.2: Proposed structure of undoped AlPO with template. Adapted from [59]	58
Figure 5.1: XRF spectrum for DJP011	70
Figure 5.2: XRF spectrum for DJP015.....	70

List of Figures

Figure 5.3: XRF spectrum for DJP016	71
Figure 5.4: XRF spectrum for DJP017	71
Figure 5.5 XRF spectrum for DJP018	72
Figure 5.6 XRF spectrum for DJP019	72
Figure 5.7: ²⁷ Al NMR spectrum of DJP011.....	73
Figure 5.8: ²⁷ Al NMR spectrum of DJP015.....	73
Figure 5.9: ²⁷ Al NMR spectrum of DJP017.....	74
Figure 5.10: ²⁷ Al NMR spectrum of DJP018	74
Figure 5.11: ²⁷ Al NMR spectrum of DJP019	75
Figure 5.12: 1D-MQMAS spectrum of DJP011	76
Figure 5.13: 1D-MQMAS spectrum of DJP015	76
Figure 5.14: 1D-MQMAS spectrum of DJP017	77
Figure 5.15: 1D-MQMAS spectrum of DJP018	77
Figure 5.16: 1D-MQMAS spectrum of DJP019	78
Figure 5.17: Annotated ¹³ C NMR for DJP000 (reaction 1).....	79
Figure 5.18: Annotated ¹³ C NMR for DJP000 (reaction 2).....	80
Figure 5.19: Annotated ¹³ C NMR for DJP000 (reaction 3).....	81
Figure 5.20: Annotated ¹³ C NMR for DJP011 (reaction 1).....	82
Figure 5.21: Annotated ¹³ C NMR for DJP011 (reaction 2).....	83
Figure 5.22: Annotated ¹³ C NMR for DJP011 (reaction 3).....	84
Figure 5.23: Annotated ¹³ C NMR for DJP015 (reaction 1).....	85
Figure 5.24: Annotated ¹³ C NMR for DJP015 (reaction 2).....	86
Figure 5.25: Annotated ¹³ C NMR for DJP015 (reaction 3).....	87
Figure 5.26: Annotated ¹³ C NMR for DJP016 (reaction 1).....	88
Figure 5.27: Annotated ¹³ C NMR for DJP016 (reaction 2).....	89
Figure 5.28: Annotated ¹³ C NMR for DJP016 (reaction 3).....	90
Figure 5.29: Annotated ¹³ C NMR for DJP017 (reaction 1).....	91
Figure 5.30: Annotated ¹³ C NMR for DJP017 (reaction 2).....	92
Figure 5.31: Annotated ¹³ C NMR for DJP017 (reaction 3).....	93
Figure 5.32: Annotated ¹³ C NMR for DJP018 (reaction 1).....	94
Figure 5.33: Annotated ¹³ C NMR for DJP018 (reaction 2).....	95
Figure 5.34: Annotated ¹³ C NMR for DJP018 (reaction 3).....	96
Figure 5.35: Annotated ¹³ C NMR for DJP019 (reaction 1).....	97

List of Figures

Figure 5.36: Annotated ^{13}C NMR for DJP019 (reaction 2).....	98
Figure 5.37: Annotated ^{13}C spectrum for DJP019 (reaction 3)	99

List of Tables

Table 1.1: Glycerol market breakdown [3]	1
Table 2.1: Summary of starting materials and reaction conditions	20
Table 2.2: IR data for DJP011	25
Table 2.3: IR data for DJP015	26
Table 2.4: IR data for DJP017	27
Table 2.5: IR data for DJP018	28
Table 2.6: IR data for DJP019	29
Table 2.7: XRF elemental analysis	30
Table 2.8: Unit cell parameters of AlPO series catalysts.....	31
Table 2.9: Refined unit cell parameters for AlPO catalysts.....	32
Table 2.10: Surface area analysis results for AlPO series.....	37
Table 2.11: EDX results for AlPO catalysts	39
Table 2.12: IR data for DJP016	44
Table 2.13: Unit cell parameters of α -ZrP catalyst.....	44
Table 2.14: Refined unit cell parameters for α -ZrP.....	44
Table 2.15: Surface area analysis results for α -ZrP	46
Table 2.16: EDX analysis of α -ZrP catalyst.....	46
Table 3.1: Processed data showing the mass and yields of glycerol carbonate	54
Table 3.2: Table comparing molar ratios of glycerol carbonate and ammonia	55
Table 4.1: Potential unknown compounds found in reaction mixtures	59
Table 5.1: Ammonia capture data for DJP011	66
Table 5.2: Ammonia capture data for DJP015	66
Table 5.3: Ammonia capture data for DJP016	67
Table 5.4: Ammonia capture data for DJP017	67
Table 5.5: Ammonia capture data for DJP018	68
Table 5.6: Ammonia capture data for DJP019	68
Table 5.7: Ammonia capture data for un-catalysed reaction	69
Table 5.8: Refined lattice parameters for DJP011	100
Table 5.9: Refined lattice parameters for DJP015	101
Table 5.10: Refined lattice parameters for DJP016	102
Table 5.11: Refined lattice parameters for DJP017	103
Table 5.12: Refined lattice parameters for DJP018	104
Table 5.13: Refined lattice parameters for DJP019	105

Chapter 1: Introduction

1.1: Glycerol, waste product or valuable raw material?

Glycerol is a relatively cheap waste product from many industrial processes including the production of biofuels, fermentations and reactions used to synthesise alkenes. The rising cost of safely disposing of chemical waste is forcing companies to find new and innovative ways of either reusing their waste products or ways to minimise the amount of waste produced.

In the short term, biodiesel is being increasingly seen as an alternative fuel source to combat the dependence most countries have on petroleum based economies. Biodiesel requires little or no modification to existing vehicles and infrastructure. The synthesis of biodiesel produces approximately 10%, with respect to weight, crude glycerol as one of the main side-products. The price of crude glycerol is valued at around \$0.05 per lb (at 2007 prices) [1]. It is anticipated that by the end of 2013 the United States alone will produce over 1 billion gallons of biodiesel [2], this potentially means a stockpile of over 100 million gallons of crude glycerol suitable for refining and converting into value-added products.

Table 1.1: Glycerol market breakdown [3]

Use	Size of market	Use	Size of market
Drugs / Pharmaceuticals	18%	Alkyd resins	6%
Personal Care	16%	Tobacco	2%
Polyether / Polyols	14%	Detergents	2%
Food	11%	Cellophane	2%
Others	11%	Explosives	2%
Triacetin	10%		

The Table 1.1 shows the market breakdown for refined glycerol. As can be seen from the table above there are many different products that require glycerol for their manufacture. Shown in Figure 1.1 is a pathway of currently known reactions and products involving glycerol as the main starting material. As discussed by Behr *et al.* [4] all chemical products derived from glycerol are a result of following one of eight

processes. These processes include synthesis of glycerol esters, ethers, acetals and ketals, propanediols, epoxides, the oxidation and dehydration products of glycerol and production of synthesis gas.

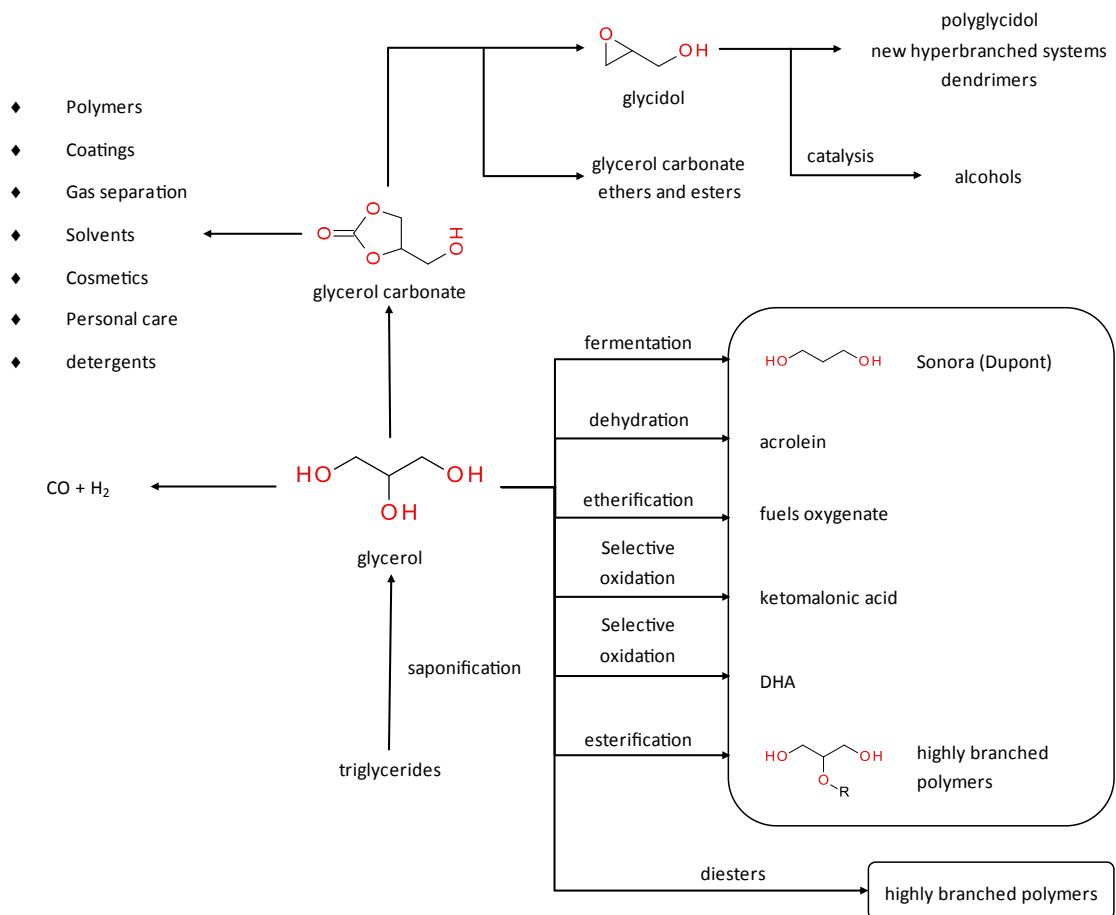


Figure 1.1: Derivatives of glycerol, chemical pathway [3]

As shown in Figure 1.1 glycerol can be used as a starting material for many fine chemical derivatives (Figure 1.2), including tertiary butyl ethers, 1,3-propanediol and glyceric acid, to name but a few. There are currently several competing and very different methods for synthesising glyceric acid. One method, as investigated by Habe *et al.* [5], is to use bacteria to process crude glycerol into glyceric acid. The advantage in using bacteria for the synthesis of fine chemicals is that they can be highly specific in synthesising particular enantiomers of a product, as shown in the results of Habe *et al.* where several of the bacteria selected could produce glyceric acid with an enantiomeric excess of 90-99% [5].

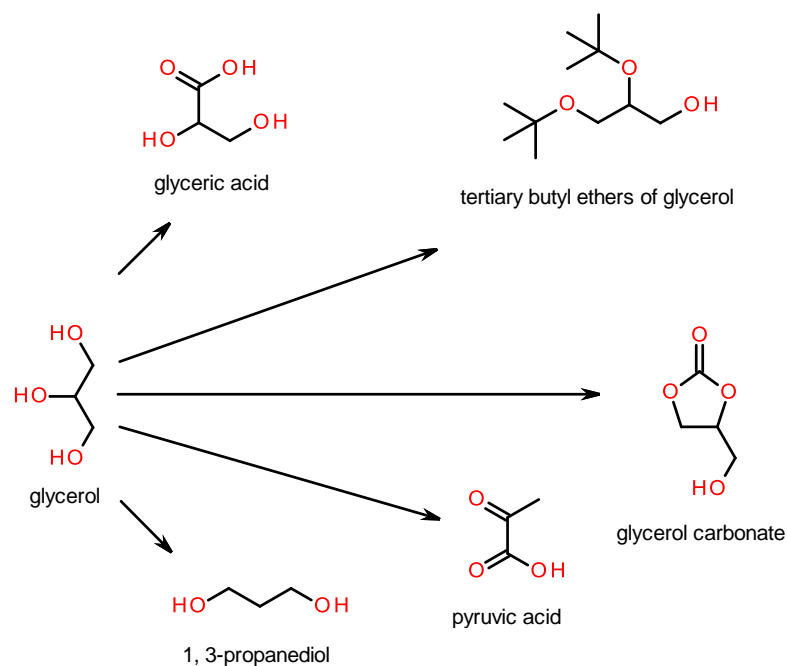


Figure 1.2: Fine chemical derivatives of glycerol

However, only one strain of bacteria (*Gluconobacter frateurii* NBRC103471), was able to produce a relatively good yield of 30g – 40g per litre with a high enantiomeric excess. If enantiomeric purity is not required then the number of suitable candidate bacteria rises to 9.

Another method to synthesise glyceric acid from glycerol is to perform a selective oxidation using a catalyst. Carrettin *et al.* have studied the use of gold catalysts in mild reaction conditions to produce 100% selectivity [6]. As with the bacterial method of synthesis, if higher selectivity is required the amount of glycerol converted decreases. It was found that a 1% gold/carbon or 1% gold/graphite catalyst compares favourably with that of *Gluconobacter frateurii* in the synthesis of glyceric acid, whereas the gold catalysts not only produce 100% glyceric acid with no side-products, but also a 56% conversion of the glycerol starting material. However, it is not known whether the gold catalysts can also produce a high enantiomeric excess of glyceric acid, like *Gluconobacter frateurii*.

1,3-propanediol is another derivative of glycerol that can be synthesised either by catalytic or biological means. According to Zeng *et al.* [7] there are several suitable

bacteria that can be used in the synthesis of 1,3-propanediol, including *Klebsiella pneumonia*, *Citrobacter freundii* and *Clostridium butyricum*. However, the problem with using these bacteria is that the yield of 1,3-propanediol does not generally increase above that of 70% due to side-products, such as ethanol, being produced.

Hydrogenolysis of glycerol, using noble metal loaded catalysts, can also produce 1,3-propanediol. Kurosaka *et al.* [8] have researched the effect of various different noble metals loaded on to WO_3 supported ZrO_2 catalysts. These noble metals include platinum, palladium, ruthenium, rhodium and iridium. The results show that the most suitable noble metal for use in the catalyst is platinum, where it makes up approximately 2% (by weight) of the catalyst. The chosen Pt/ WO_3 / ZrO_2 catalyst reported a yield of 24.2% for 1,3-propanediol, but it is still not as efficient as the bacterial synthesis since approximately 14% of the glycerol is left unreacted and one of the main side-products is 1,2-propanediol. This shows that there are still problems with the enantiomeric selectivity of the catalysts towards 1,2-propanediol compared to bacterial synthesis.

Glycerol *tert*-butyl ethers (GTBE) can be used in the automotive fuel industry as either additives to both diesel and biodiesel fuels or as an octane booster for petroleum fuels. Work carried out by Di Serio *et al.* [9] studied the effects of using the acid support resin Amberlyst® 15 as a suitable catalyst for the etherification reaction. Multiple tests were conducted to find the optimum reaction conditions and maximise product yield. Under ideal conditions, approximately 90% of the glycerol is converted to either mono-, di- or tri-ether forms of GTBE with only approximately 5% of the glycerol left unreacted and the remainder as undesired side-products.

Alternatively, HY zeolite catalysts can be used in the etherification of glycerol. Xiao *et al.* [10] have studied the effects of pre-treating HY zeolites with different acids in an attempt to increase the catalytic properties and yield of GTBEs produced. Both citric acid and nitric acid were used to wash the HY zeolites. The results from their study

show that treating HY catalysts with either of the above mentioned acids increases the Brønsted acidity of the catalyst and also increases the surface area pore volume and pore size of the catalyst improving its catalytic efficiency. Their work also shows that acid treated HY zeolites are as active as SAC-13 catalysts and have an increased affinity to synthesise the desired GTBEs.

As reported by Soares *et al.* [11] glycerol can be used as a fuel source by converting it into synthesis gas using platinum supported catalysts. Soares *et al.* studied a wide variety of catalytic supports including carbon, ZrO₂, AlPO and both CeO₂/ZrO₂ and MgO/ZrO₂. All the catalysts showed deactivation during the reaction except for the carbon supported platinum catalyst (Pt/C) which lasted for at least 30 hours. It is apparent from the research that in the metal oxide catalysts, the higher the number of acid sites, the longer it takes for the deactivation of the catalysts to occur.

Platinum-rhenium carbon catalysts (Pt-Re/C) have also been analysed for their potential in the production of synthesis gas. Simonetti *et al.* [12] have been researching an improved method of increasing the yield of synthesis gas over that of the use of the traditional Pt/C catalyst. After optimising the reaction conditions for the new Pt-Re/C catalyst, it has been determined that the bimetallic Pt-Re/C catalyst is 5 times more efficient than the monometallic Pt/C catalyst as long as the atomic Pt:Re ratio is ≤ 1 . Also, stable catalytic performance can be achieved at low conversions by co-feeding a H₂ stream into the reaction.

However, glycerol carbonate is probably the most desirable chemical to be derived from glycerol because glycerol carbonate has a large variety of applications, low toxicity and good biodegradability. Some of these applications and future uses include use as a curing agent, use in cosmetics, as a starting product for forming chemical derivatives and many others [13].

1.2: Existing and new methods of glycerol carbonate synthesis

Currently, there are several different methods of synthesising glycerol carbonate. The two most common types are either phosgenation or the transesterification of glycerol, both of which are carried out in the presence of a catalyst. Recently, there has been a shift towards using cleaner, more energy efficient methods such as direct carboxylation and the glycerolysis of urea.

One of the newer methods of synthesising glycerol carbonate is to use the waste greenhouse gas carbon dioxide as a starting material along with crude glycerol. Currently there are several different methods under development using different catalysts to synthesis glycerol carbonate. These methods make use of either CO₂ or supercritical CO₂ and utilise both solid acid and organometallic catalysts.

Aresta *et al.* [14] have been studying the viability of using CO₂ at sub-supercritical levels in the presence of tin based organometallic catalysts. Three different tin based catalysts were trialled and either glycerol or tetraethylene glycerol dimethyl ether (TEGDME) were used as the starting material for the reaction. The reaction was conducted at 177°C at 50 bar pressure. It was determined that *n*-Bu₂Sn(OMe)₂ was the most active of the three catalysts tested and it is believed that the reaction proceeded by the following mechanism shown in Figure 1.3.

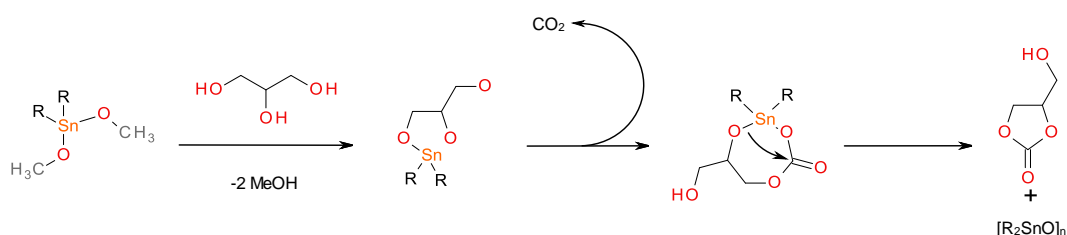


Figure 1.3: The direct carboxylation of glycerol via *n*-Bu₂Sn(OMe)₂ catalysis

Similarly, Vieville *et al.* [15] have been studying the use of supercritical CO₂ in the presence of different zeolites and ion exchange resins, such as Amberlyst® A26. Satisfactory yields of glycerol carbonate have been obtained using zeolite 13X and purosiv zeolite, as well as basic resins such as Amberlyst® A26. This work uncovered some interesting results. It has been shown that the yield of glycerol carbonate

synthesised depends on the ratio of Si/Al atoms present in the zeolite catalysts and that powdered forms of catalysts had a higher affinity in aiding the synthesis of glycerol carbonate compared with their macromolecular forms.

An alternative method of synthesising glycerol carbonate has been reported by Hammond *et al.* [16] using different metal supported heterogeneous catalysts, utilising different supporting media. After much testing, three metals (zinc, gold and gallium) were identified as actively promoting the catalytic process, supported on the zeolite ZSM-5. These metals were further tested on other catalytic supports, with gold supported on a magnesium oxide structure proving to be the most efficient catalyst for the reaction. The gold supported magnesium oxide catalyst managed to retain its full catalytic activity even after 10 re-cycles.

Another common catalyst type, used in the synthesis of glycerol carbonate, are metal oxides and their derivatives, with basic oxides such as magnesium and calcium oxide being the most commonly chosen. When using metal oxide catalysts glycerol is formed via transesterification of glycerol with a carbonate ester. Climent *et al.* [17] created various mixed and non-mixed metal oxides hydrotalcite catalysts and tested their catalytic efficiency towards the transesterification reaction. They determined that in order to prevent unwanted formation of side-products, the transesterification reaction must be conducted at as low a temperature as possible. Increasing the Lewis basicity of the mixed Al/Mg oxide allows the reaction to proceed at a much lower temperature. The lower Lewis basicity was achieved by substituting magnesium for lithium.

Similarly, Ochoa-Gómez *et al.* [18] focused on optimising their chosen catalysts and reaction conditions for a similar transesterification process to form glycerol carbonate, using dimethyl carbonate (DMC) instead of ethylene carbonate (as was used in the work of Climent *et al.*). They successfully obtained a greater than 95% yield of glycerol carbonate under their optimised conditions, running the reaction for 90 minutes at

95°C. The leaching of calcium from the CaO catalyst was kept to a minimum with a reported calcium content of less than 0.34% in all samples tested. It has been shown that calcining the CaO catalyst before use increases the yield by approximately 23%. Also Ochoa-Gómez *et al.* [18] proposed a very simple method to isolate and purify the glycerol carbonate. The CaO catalyst is removed via vacuum filtration and washed with more DMC, the filtrate is then evaporated under vacuum to remove DMC and methanol leaving the residual glycerol carbonate with a purity of approximately 95%.

1.3: Aluminium phosphates and derivatives

Aluminium phosphate can have several different morphologies and can be either naturally occurring or synthetically manufactured. Naturally occurring aluminium phosphate is found in the form of berlinite, which shares a similar crystal structure and appearance to quartz. Most synthetic aluminium phosphate structures are now known, the first being successfully synthesised and reported in 1982 [19]. Although there are several small pore and dense phase naturally occurring AlPOs (e.g. berlinite, see Figure 1.4), the vast majority are synthetically formed structures [20].

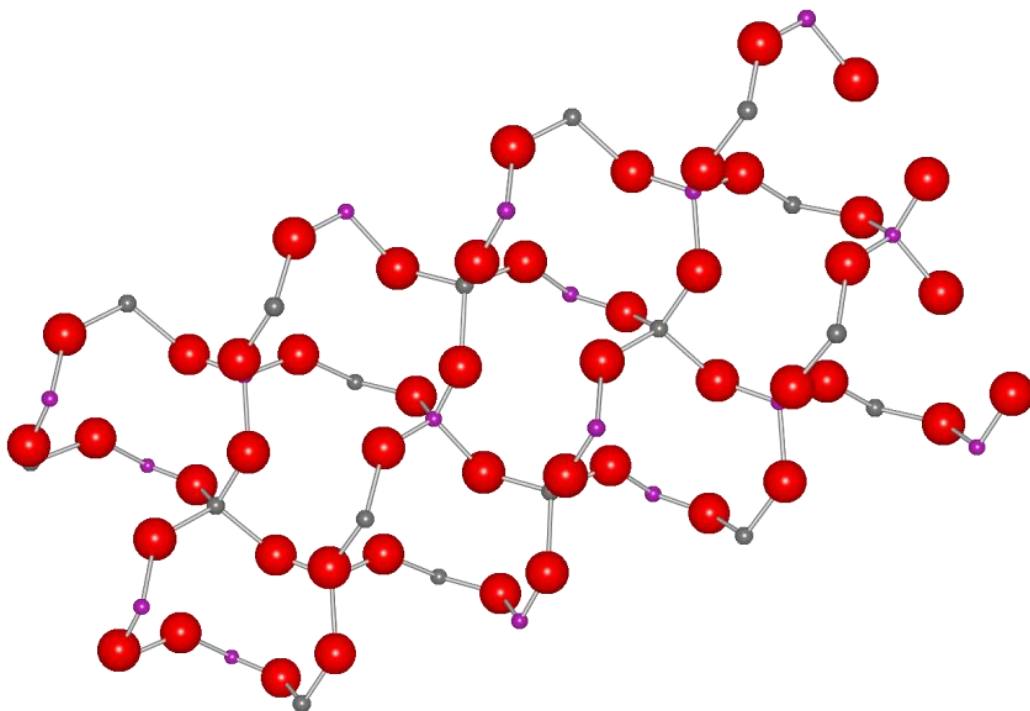


Figure 1.4: Crystal structure of berlinite [21]

Key: Aluminium – grey, Oxygen – red, Phosphorus – purple

There are several different methods used to synthesise aluminium phosphate and its derivatives. One synthesis method is to use hydrothermal techniques to form the desired AlPO or a doped metal derivative, since this method makes it relatively easy to substitute another metal into the AlPO structure by simply varying the amounts of reactants. Middelkoop *et al.* [22] used the hydrothermal method of synthesis to produce several germanium doped aluminium phosphates (Ge-AlPO). The method followed was one which was adapted from the work of Wilson *et al.* [23]. The reaction mixture was formed by combining boehmite and H₂O in a beaker with constant stirring, whilst orthophosphoric acid (H₃PO₄) is added slowly. To dope the required

amount of germanium into the AIPO structure, the equivalent percentage of germanium oxide (GeO_2) was added to the solution. Finally the structure directing agent (SDA), also known as the template, was added in the form of triethylamine. This mixture was stirred at room temperature until a homogenous gel was formed. The contents were then transferred to an autoclave cell and heated in an oven at 170°C for the desired amount of time.

Jones *et al.* [24] synthesised a unique large pore 3-dimensional AIPO ($[\text{Al}_5\text{P}_6\text{O}_{24}\text{H}]^{2-} 2[\text{N}(\text{C}_2\text{H}_5)_3\text{H}]^+ \cdot 2\text{H}_2\text{O}$) using triethylamine (TEA) as the templating agent and conducting the reaction in a non-aqueous reaction medium. Instead they chose the solvation method of synthesis using triethylene glycol (TEG) as the reaction medium. It is interesting to note that $\text{Al}_5\text{P}_6\text{O}_{24}\text{H}]^{2-} 2[\text{N}(\text{C}_2\text{H}_5)_3\text{H}]^+ \cdot 2\text{H}_2\text{O}$ (JDF-20) can only be obtained by using TEA as the template, whereas $\text{AlPO}_4\text{-5}$ can be synthesised using any one of around 23 amine containing templates [20]. Similarly Chippindale and Turner [25] used a non-aqueous solvent system containing butan-2-ol to synthesise the 1-dimensional AIPO: $[\text{C}_{10}\text{N}_2\text{H}_9] [\text{Al}(\text{PO}_4)(\text{PO}_2(\text{OH})_2)]$. Chippindale and Cowley [26] go on to state that in order for the solvation reaction to be successful the solvent of choice must meet certain criteria. For example the solvent must be viscous enough to help support the growing crystal particles to ensure that large crystals can be formed and that the phosphate being prepared should be slightly soluble in the chosen solvent otherwise there will be no crystal formation.

Alternatively, microwave assisted synthesis has been proposed for its ability to rapidly synthesise high purity single phase AIPOs. Using the ionothermal microwave synthesis technique, Wragg *et al.* [27] managed to successfully synthesise several AIPOs in as little as 20 minutes and after 1 hour the reactions were yielding high amounts of a single crystalline phase. This method of synthesis has several advantages over the more traditional hydrothermal method of synthesising AIPOs. First the reaction is simplified by using an ionic liquid as both the solvent for the reaction and as the SDA. Likewise compared to a typical hydrothermal reaction in an oven which might take several days (100+ hours) at continuous high temperatures ($>170^\circ\text{C}$), microwave

synthesis can accomplish the same results in a fraction of that time. This method has also been proven to work when synthesising doped metal AlPOs, such as cobalt doped aluminium phosphate (Co-AlPO) [28], allowing this technique to be used to synthesise solid acid catalysts or materials suitable for lightweight gas storage.

Aluminium phosphate and its derivatives are being extensively investigated for the catalytic properties afforded by their structures, along with other potential uses such as lightweight materials to store gases (e.g. hydrogen) cheaply and efficiently which would allow electric vehicles powered by hydrogen fuels cells to compete with traditional forms of transport powered by the internal combustion engine. However, in order to do this, materials with large surface area are required. Although AlPOs already exhibit some of these properties, Kannan *et al.* [29] have successfully synthesised a large pore thermally stable AlPO. The AlPO synthesised had a pore diameter 153Å and was thermally stable at temperatures greater than 1000°C, meaning that if this material is used in catalytic reactions it can be easily recycled as any residue on the used catalysts can be “burned off” and removed. The AlPO was also tested for its catalytic properties and as an absorbent to remove chemicals such as dyes from the environment. Through testing it was proven that this AlPO could potentially be a very useful catalyst for esterification reactions as it successfully managed to convert 70% of the *n*-butanol present with a selectivity as high as 97% in the optimum conditions. Similarly its absorbent properties were determined by testing its ability to remove the dye indigo carmine. At a dye concentration of 100 ppm it took only 10 minutes for the AlPO to remove 99% of the dye present. This presents the possibility that large pore AlPOs could have a significant use in environmental applications and replace other less environmentally friendly absorbents.

Both AlPO and Zn-AlPO have been studied by Sreenivasulu *et al.* [30] for their potential use in the hydroxylation of benzene to phenol. These catalysts were synthesised using a solvent free system and the templating agent, tetrapropylammonium bromide (TPABr), was employed. After synthesis the samples were collected, washed with a

large quantity of ethanol and calcined for 5 hours at 500°C. Although both catalysts exhibit similar surface areas, the formation and size of the pores present in the catalysts are remarkably different. The large difference could be explained by the uneven distribution of the templating agent in the mixture and/or its removal by calcination. The catalytic abilities of the AlPOs were tested in a reaction involving the hydroxylation of benzene to phenol using H₂O₂. Phenol is one of the major chemical precursors used in the chemical industry with applications in fine chemicals, pharmaceuticals, dyes and resins. Results from the catalytic testing are promising, the basic AlPO had a 100% selectivity towards phenol however its conversion rate was very low (approx. 13%). The results for the Zn-AlPO compare favourably to AlPO whereby it managed to convert in excess of 85% benzene present with a selectivity of around 85 - 88%, producing a small amount of 1,4-benzoquinone (a similarly useful chemical precursor). A reference experiment was conducted without any catalysts present, yielding no phenol or 1,4-benzoquinone confirming the need for a catalyst to be present in the reaction.

Iron doped aluminium phosphates (Fe-AlPO) have been proven to have numerous uses including catalytic applications and as a templating agent. Shiju *et al.* [31] have reported the use of an Fe doped AlPO-5 as a catalyst suitable for hydroxylation reactions. In their testing Shiju *et al.* used Fe-AlPOs to catalyse benzene to phenol via a hydroxylation reaction using nitrous oxide as the oxidant of choice. With 1% doping of Fe the catalyst converted 13.4% of the benzene present with a phenol yield of 13% indicating that Fe-AlPO catalysts have a high selectivity for this reaction. However, it is also reported that upon calcining Fe-AlPO to form an active FeMFI catalyst the yield of phenol increases to approximately 23%. Several Fe containing AlPOs have also been investigated as catalysts for the selective oxidation of cyclohexane to cyclohexanol and cyclohexanone by Zhou *et al.* [32]. The oxidation of cyclohexane is important to the chemical industry as it is a precursor stage to synthesising many man-made synthetic fibres such as nylon-6 and nylon-6, 6. Zhou *et al.* used the hydrothermal method of synthesising the various Fe containing catalysts, with the amount of Fe varied between 0.02% – 0.06% as a molar percentage of the overall catalyst. Reactivity of the Fe containing catalysts was good, with the FeCoMn-AlPO converting the highest amount

of cyclohexanone and the FeMn-AIPO converting 31.7% of the cyclohexane to cyclohexanol. As a templating agent Fe-AIPO has been used for the novel application of speeding up the synthesis of Y-shaped carbon nanotubes (Y-CNT) via chemical vapour deposition, as reported by ChadraKishore and Pandurangan [33].

1.4: Zirconium phosphates and derivatives

One of the leading authorities in this pioneering research was Abraham Clearfield who, in 1964 along with James Stynes, reported the synthesis of zirconium phosphate [34], which is now known as the alpha form of zirconium phosphate (α -ZrP). Clearfield and Stynes synthesised α -ZrP by refluxing zirconium phosphate gel in phosphoric acid, obtaining crystalline α -ZrP which could be readily and accurately characterised. However, this method is rather cumbersome and time consuming and therefore the process is now accelerated by the use of hydrothermal methods [35]. Today zirconium phosphate and its derivatives can be synthesized in a variety of different ways and have a wide range of applications.

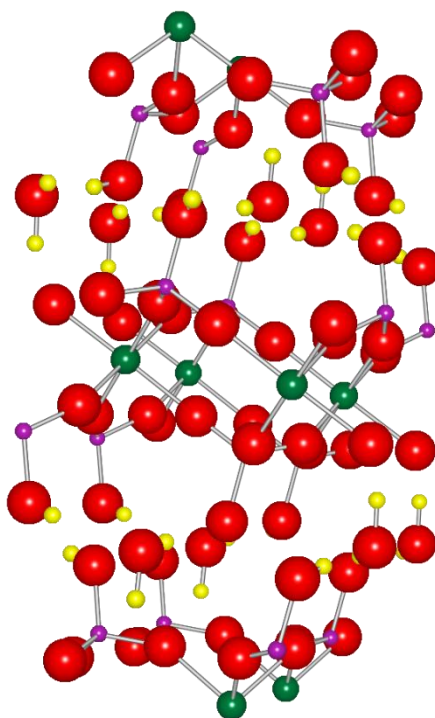


Figure 1.5: Crystal structure of α -zirconium phosphate [36]

Key: Zirconium – green, Oxygen – red, Phosphorus – purple, Hydrogen – yellow

One method of obtaining both α -ZrP and crystalline α -ZrP is reported by Trobajo *et al.* [37] in which they first form crude ZrP before converting it to its crystalline form. The crude ZrP was formed by the traditional method of reacting zirconyl chloride, dissolved in hydrochloric acid, with phosphoric acid and stirred until a precipitate forms. This precipitate is centrifuged and washed with phosphoric acid to remove any remaining chloride ions. The remaining solid is air dried at room temperature, giving crude ZrP.

To form crystalline ZrP the crude ZrP is refluxed for 48 hours with 10M phosphoric acid, then filtered and the precipitate is left to dry.

Similar to the traditional reflux method, hydrothermal synthesis can be used to synthesise crystalline α -ZrP. However, unlike the traditional reflux method, hydrothermal synthesis requires a much shorter reaction time. Sun *et al.* [38] reported that α -ZrP can be synthesised via the hydrothermal method by combining zirconyl chloride octahydrate with phosphoric acid in a sealed Teflon[®] lined pressure vessel which is then heated for 24 hours at 200°C.

Alternatively, new more novel techniques (such as microwave assisted synthesis) are being investigated. With the advent of green chemistry and the drive to lower manufacturing costs (for synthesising chemicals in both industry and for research purposes) chemists are increasingly turning to microwave synthesis as a method for quickly synthesising compounds that require large amounts of energy in order for the reaction to progress. Naik *et al.* [39] have studied the effects of microwave assisted synthesis of sodium zirconium phosphate (Na/ZrP) at varying temperatures. Heating the reaction mixture in a standard resistance furnace for 1 hour at 450°C yielded poorly crystalline Na/ZrP and only achieved a suitably crystalline product at 650°C, whereas heating the same reaction mixture for 1 hour in a microwave at 450°C yielded the largest amount of crystalline Na/ZrP. This indicates that microwave assisted synthesis could help rapidly produce different zirconium phosphates much more quickly than traditional methods, with a potentially higher crystallinity.

There have also been a large number of studies into synthesising doped zirconium phosphates, as they could potentially have enhanced catalytic properties. Burnell *et al.* [40] synthesised a mixed layer titanium-zirconium phosphate (Ti/ZrP). The method of synthesis was based on the work reported by Clearfield and Frianeza [41], in which a crude gel is first formed by combining 4M H₃PO₄ with the desired ratios of TiCl₄/ZrOCl₂ and left to stir overnight. The resultant crude gel is washed with deionised water,

collected by filtration and reslurried with 12M H₃PO₄. The gel was then sealed in a 23 ml stainless steel autoclave and heated for 1 week at 150°C. The resultant solid precipitate was collected via centrifugation and washed with deionised water. This washing process was repeated until the supernatant had reached a pH of 4. Kapoor *et al.* [42] have reported the use of a novel Ti/ZrP for aiding hydrogen production from the splitting of water. This novel catalyst shows a great efficiency towards the photocatalytic splitting of water and therefore could be potentially useful in the production of hydrogen as a clean fuel source.

Zirconium phosphate and its derivatives can also be used as molecular sieves. Scheetz *et al.* [43] have studied Na/ZrP with the aim of using it as a way of immobilising radioactive nuclei from commercial radioactive waste by way of an ion-exchange substitution. Several different methods of synthesising Na/ZrP were employed including, both sol-gel and hydrothermal methods. Results show that Na/ZrP could potentially be very useful in the use of nuclear waste remediation as its structure will accept approximately two thirds of all potential cations from the periodic table, including those that are found in radioactive waste. In addition, its long lifetime (before starting to decompose) means that it could be suitable as a long term storage medium.

Tungsten oxide supported ZrP catalysts with various tungsten loadings have been synthesised and tested by Rao *et al.* [44] for their potential use in the esterification of palmitic acid. ZrP catalysts were synthesised using the hydrothermal method, then a method of wet impregnation was used to add the designed percentage of tungsten oxide to the catalysts. The samples were stored in air before being analysed and tested. It was proven that the tungsten supported ZrP catalysts contained a greater number of acid sites and therefore possessed a greater acidity to that of normal ZrP. All catalysts were highly active in increasing the esterification of palmitic acid, were resistant to the leaching of tungsten into the reaction mixture and because of the heterogeneous nature of the catalyst it was easy to recover and re-use the catalysts.

This shows that there is future potential in using tungsten or other metal oxide supported catalysts in esterification reactions.

1.5: Aims of research

The main aim of this thesis is to synthesise several aluminium substituted layered phosphate catalysts and analyse their potential as novel heterogeneous catalysts for the glycerolysis of urea. In order to accomplish this, a library of doped and un-doped AlPOs will be synthesised along with α -ZrP as a control and comparison since its catalytic properties have already been extensively reported. In the glycerolysis method of synthesis, glycerol and urea are combined in the presence of a doped or un-doped metal phosphate catalyst and then reacted under vacuum at 140°C for three hours. The synthesis proceeds via a simple two-step reaction. Firstly the carbamate is formed, evolving ammonia. Then the carbamate cyclises to form glycerol carbonate, evolving another molecule of ammonia (shown in Figure 1.6).

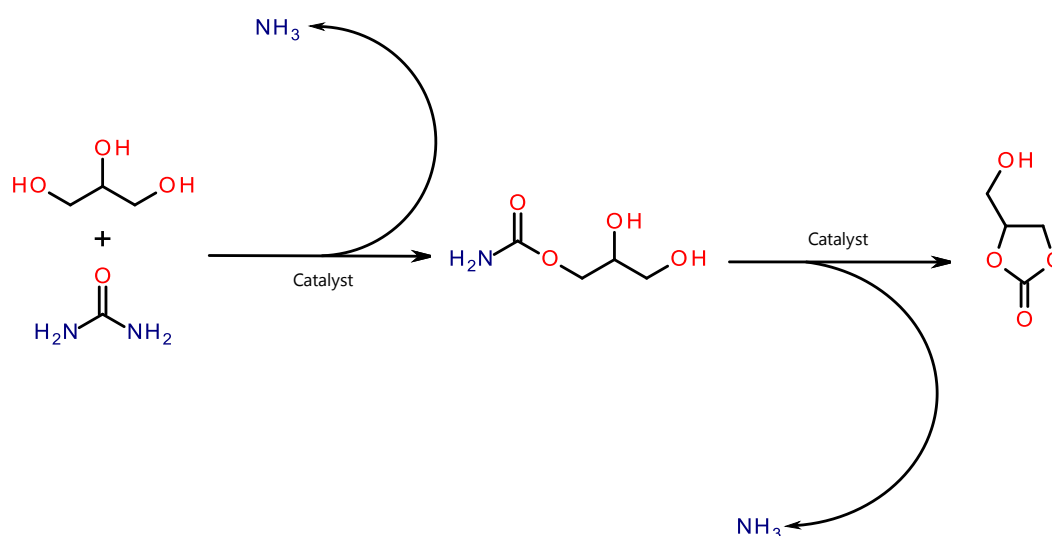


Figure 1.6: The glycerolysis of urea via catalytic reaction

To quantify results and to characterise the catalysts synthesised, a range of analytic techniques and computational methods will be employed. This project will build upon the research and findings of Aresta *et al.* [45] into using zirconium phosphate (both doped and α forms) as catalysts for the glycerolysis of urea and the work of Readman [46] into synthesising different forms of layered doped AlPOs for catalytic applications.

Chapter 2: The synthesis and characterisation of doped metal phosphates

2.1: Introduction

All the aluminium phosphates and zirconium phosphates were prepared by modified hydrothermal methods of synthesis. The method chosen for synthesising the zirconium phosphates is very similar to a method used by Poojary *et al.* [35] for the synthesis of metal substituted α -ZrP and γ -ZrP forms of the catalysts. As reported in the literature of Chippindale and Walton [47] and Bond *et al.* [48], the synthesis of aluminium or substituted gallium phosphate(s) via the hydrothermal/solvothermal process is an almost identical approach and will be used to synthesise the metal substituted aluminium phosphate catalysts for this project. The synthesised metal substituted catalysts will be characterised using various analytical techniques including Scanning Electron Microscopy (SEM), powder X-Ray Diffraction (XRD), X-Ray Fluorescence (XRF) and both ^{31}P and ^{27}Al Nuclear Magnetic Resonance (NMR) analysis.

2.2: Synthesis of catalysts

Aluminium phosphate [$\text{Al}_3\text{P}_4\text{O}_{16}$] was synthesised via the following method [46]. 2.0 g of aluminium isopropoxide ($\text{C}_9\text{H}_{21}\text{O}_3\text{Al}$), 3.0 ml ethylenediamine ($\text{C}_2\text{H}_8\text{N}_2$), 1.75 ml 85% orthophosphoric acid (H_3PO_4) and 20.0 ml of deionised water were combined in the PTFE liner of the hydrothermal stainless steel autoclave and left to stir for several hours until a white gel had formed. The crude gel was then sealed in a hydrothermal stainless steel autoclave and heated for 120 hours at 195°C. The precipitate was then washed with deionised water, filtered under vacuum and left to dry.

Synthesis of the doped aluminium catalysts was achieved using a similar method to that employed to synthesise aluminium phosphate. However, the appropriate metal salt was added to the reaction mixture so as to give a dopant metal to aluminium ratio of 1:5. The molar ratios used in the reactions are shown in Table 2.1.

The zirconium phosphate $[\text{Zr}(\text{HPO}_4)_2 \cdot \text{H}_2\text{O}]$ was synthesised in a similar manner to the aluminium phosphate. The method of synthesis was derived from the work of Burnell *et al.* [40]. Crude zirconium phosphate gel was prepared by combining 2.5 ml of 1M zirconyl chloride (ZrCl_4) solution and 20.0 ml of 4M H_3PO_4 in a beaker. The resulting solution was stirred for several hours at room temperature. The crude gel was then collected by centrifugation, reslurried with 20.0 ml of 12M H_3PO_4 and heated to 150°C in a 25.0 ml hydrothermal stainless steel autoclave for 126 hours. The product was collected by centrifugation and washed with deionised water and re-centrifuged. The process was repeated until the pH of the supernatant reached approximately 4.

2.3: Materials

A summary of the starting materials, molar ratios and reaction conditions used to synthesis the catalysts produced is shown in Table 2.1. Experiments DJP001 to DJP004 and DJP010 were excluded from the table as these reaction did not yield the correct product. All chemicals were obtained from either Sigma Aldrich or Alfa Aesar. All chemicals were of analytical grade quality and used as supplied.

Table 2.1: Summary of starting materials and reaction conditions

Catalyst	Template (T)	Gel Composition (molar ratio)	Time (hours)	Temperature	Used in catalytic testing
DJP005	Ethylenediamine	Al(O-i-Pr) ₃ : H ₂ O : H ₃ PO ₄ : T 1 : 113.40 : 3.43 : 4.60	160	160°C	✓
DJP006	Ethylenediamine	Al(O-i-Pr) ₃ : VOSO ₄ : H ₂ O : H ₃ PO ₄ : T 1 : 0.33 : 152.18 : 4.60 : 6.17	160	160°C	✗
DJP007	Ethylenediamine	Al(O-i-Pr) ₃ : Zn(NO ₃) ₂ : H ₂ O : H ₃ PO ₄ : T 1 : 0.34 : 152.18 : 4.60 : 6.17	120	195°C	✓
DJP008	Ethylenediamine	Al(O-i-Pr) ₃ : Ga(NO ₃) ₂ : H ₂ O : H ₃ PO ₄ : T 1 : 0.34 : 152.18 : 4.60 : 6.17	120	195°C	✓
DJP009	Ethylenediamine	Al(O-i-Pr) ₃ : Co(NO ₃) ₂ : H ₂ O : H ₃ PO ₄ : T 1 : 0.33 : 152.18 : 4.60 : 6.17	120	195°C	✓
DJP0011	Ethylenediamine	Al(O-i-Pr) ₃ : Ti[OCH(CH ₃) ₂] ₄ : H ₂ O : H ₃ PO ₄ : T 1 : 0.34 : 152.18 : 4.60 : 6.17	120	195°C	✓
DJP012	Ethylenediamine	Al(O-i-Pr) ₃ : Cr(NO ₃) ₃ : H ₂ O : H ₃ PO ₄ : T 1 : 0.34 : 152.18 : 4.60 : 6.17	120	195°C	✗
DJP013	Ethylenediamine	Al(O-i-Pr) ₃ : HAuCl ₄ : H ₂ O : H ₃ PO ₄ : T 1 : 0.15 : 126.69 : 3.83 : 5.13	120	195°C	✗
DJP014	Ethylenediamine	Al(O-i-Pr) ₃ : Pr(NO ₃) ₃ : H ₂ O : H ₃ PO ₄ : T 1 : 0.11 : 126.69 : 3.83 : 5.13	120	195°C	✗
DJP015	Ethylenediamine	Al(O-i-Pr) ₃ : H ₂ O : H ₃ PO ₄ : T 1 : 113.40 : 3.43 : 4.60	120	195°C	✓
DJP016	-----	ZrOCl ₂ : HCl : H ₂ O : H ₃ PO ₄ 1 : 5.25 : 675.41 : 705.64	112	195°C	✓
DJP017	Ethylenediamine	Al(O-i-Pr) ₃ : Zn(NO ₃) ₂ : H ₂ O : H ₃ PO ₄ : T 1 : 0.34 : 152.18 : 4.60 : 6.17	120	195°C	✓
DJP018	Ethylenediamine	Al(O-i-Pr) ₃ : Ga(NO ₃) ₂ : H ₂ O : H ₃ PO ₄ : T 1 : 0.34 : 152.18 : 4.60 : 6.17	120	195°C	✓
DJP019	Ethylenediamine	Al(O-i-Pr) ₃ : Co(NO ₃) ₂ : H ₂ O : H ₃ PO ₄ : T 1 : 0.33 : 152.18 : 4.60 : 6.17	120	195°C	✓

2.4: Methods of characterisation and analysis

This project can be divided into two distinct but complementary parts. First a series of AlPO and α -ZrP catalysts were synthesised and then characterised using standard procedures. The main methods of characterising the catalysts were XRD, XRF, SEM, EDX, TGA, physisorption analysis (BET), FT-IR and solid state NMR. The second part of the project involved analysing the catalytic reactions, determining products and yields. Both GC-MS and NMR techniques were employed.

Powder X-Ray Diffraction

Powder X-ray diffraction patterns were collected using a Bruker D2 PHASER diffractometer using CuK α radiation source ($\alpha_1 = 1.54060\text{\AA}$, $\alpha_2 = 1.54439\text{\AA}$). A small amount of a finely powdered sample was affixed to a Si low background sample holder using a very small quantity of petroleum jelly. A customised experimental set-up file was created using the DiFFRAC.SUITE™ measurement software [49], setting the sample to rotate at 30 rpm and setting the detector 2θ range between 3.0° and 80.0° .

X-Ray Fluorescence

X-ray fluorescence data was collected using a Bruker TRACER IV-SD using a rhodium radiation source. Sample data was collected using the following parameters: no filter, 15.00 kV, 55.00 μA and 15 second acquisition time. Sample holders were prepared with Mylar® film. The XRF was primarily used to quickly determine the structural composition of the catalysts and to assess whether there were any impurities, as this could not only effect the ability of the catalyst to work but it could also affect the ability to correctly categorise and characterise the catalysts synthesised.

Scanning Electron Microscopy

Scanning electron microscopy was used in two different ways. First the FEI Quanta™ 200 SEM was used to obtain high resolution micrographs to visually study and compare the catalysts respective surface structures. Secondly, using the attached EDX

equipment it was possible to determine the elemental composition of the catalysts. Samples were prepared by placing a small amount of finely powdered sample onto a sample stub coated with a self-adhesive carbon pad. Excess sample was removed by blowing nitrogen across the sample stub and then the samples were coated with a fine gold film. The accelerating voltage used was 20 kV.

Thermogravimetric Analysis

Thermogravimetric Analysis (TGA) was carried out using Mettler-Toledo TGA/sDTA851e. The samples were run in a 70 μ L aluminium oxide crucible, between 25°C and 700°C with a ramp rate of 5°C per minute. All experiments were conducted in a nitrogen atmosphere. This technique was used to study the weight loss of the catalysts and in the case of the AlPO series to try and determine at what point the templating agent started to decompose.

Physisorption analysis

Surface area analysis was carried out using a Micrometrics ASAP 2010. Approximately 0.15 g of each catalyst was weighed, placed in a pre-weighed glass sample holder and attached to the ASAP 2010. The sample was then placed under vacuum, heated to 150°C and left overnight to fully remove all water from the sample. After the sample had been sufficiently dried, it was then connected to a nitrogen line and testing was undertaken. Samples were prepared and run with the assistance of Dr Runjie Mao. The data collected from the ASAP 2010 contained information about the surface area and porosity of the catalysts.

Infrared Spectroscopy

Fourier Transformed Infrared spectroscopy (FT-IR) was used predominately to analyse the phosphorus groups in the catalysts and the organic templating agent. Samples were placed on the IR neat and were recorded on a Thermo NICOLET IR200 FT-IR,

between 400 cm⁻¹ to 3800 cm⁻¹ using an attenuated total reflectance accessory for 16 scans.

Nuclear Magnetic Resonance

Both aluminium, phosphorus and MQMAS aluminium solid state experiments were conducted on all catalyst samples. Samples were prepared by tightly packing a 4 mm zirconia rotor with the desired catalyst. All samples were prepared and run by Mr Patrick Cookson. All solid state experiments were carried out on a Bruker Avance II+ 400 MHz spectrometer, with ammonium phosphate and yttrium aluminium garnet (YAG) being used to tune the NMR to the correct nuclei. Standard ²⁷Al experiments were single pulse excitation acquisitions without decoupling, with a recycle delay of 0.5 s and a spinning speed of 12 kHz. ³¹P experiments were single pulse excitation acquisitions using the Zg pulse program, with a recycle delay of 0.3 s and a spinning speed of either 6 kHz or 7 kHz. Aluminium triple quantum MAS experiments were carried out using pulses of 8.5 μs, 2.5 μs and 45 μs. The MAS rotational rate was 12 kHz and each sample was run for 2048 scans. All solid state experiments were carried out at room temperature.

Carbon solution experiments were conducted on the catalytic reaction mixtures. Samples were prepared by taking a 0.1 g sample and dissolving it in 500 μl of deuterated dimethyl sulfoxide (DMSO). Samples were analysed using a Bruker Fourier 300 (300 MHz) spectrometer. To ensure the best possible results, a custom ¹³C NMR experiment was set up using the pulse program ZgPg30, with a relaxation delay of 4 s and each sample being run for 512 scans. All solution experiments were carried out at room temperature.

Gas Chromatography – Mass Spectrometry

GCMS was used to analyse the catalytic reactions to aid in determination of products and side-products. Samples were prepared by taking a small quantity of the reaction solution and diluting it with methanol, this was then directly injected into the GCMS. All analysis was carried out on a Thermo Scientific Trace Ultra GC and DSQ II MS.

2.5: Characterisation of aluminium phosphate series catalysts

2.5.1: Infrared Spectroscopy

The five aluminium phosphate catalysts were analysed by FT-IR and as can be seen from Figures 2.1 – 2.5, all spectra indicate that similar structures have been formed with the same functional groups present. Out of the 5 AlPO based catalysts, both DJP011 (Figure 2.1) and DJP015 (Figure 2.2) have slightly different IR spectra compared to the other catalysts. In the case of DJP011 there is a very shallow change in intensity between 3200cm^{-1} and 2700cm^{-1} which could be masking a very small OH peak caused by the bridging hydroxyl group. This could be caused by either poor formation of the titanium doped catalyst or could be indicative of a more crystalline structure compared to the other doped AlPOs.

Unlike DJP011 (which has a very broad and shallow peak from 3200cm^{-1} to 2500cm^{-1}), the remaining AlPO catalysts show clearly a bridging hydroxyl group, with a peak at $>3150\text{cm}^{-1}$, however this is most clearly identifiable on the un-doped AlPO DJP015. The other noticeable difference when comparing the IR spectrum of DJP015 to any of the other doped AlPO catalysts is that the relative transmittance is higher and the peaks are better defined. This could be caused by the structure of DJP015. The XRD analysis (Section 2.5.2) shows that the structure is very well defined and is mostly a single phase unlike the majority of the doped metal AlPOs which appear to be multiphasic; the exception being DJP018, which also shows slightly better defined peaks in its IR spectra.

The assignment of the absorption bands have been made by using data taken from Nakamoto [50] and Socrates [51]. Shown in Tables 2.2 – 2.6.

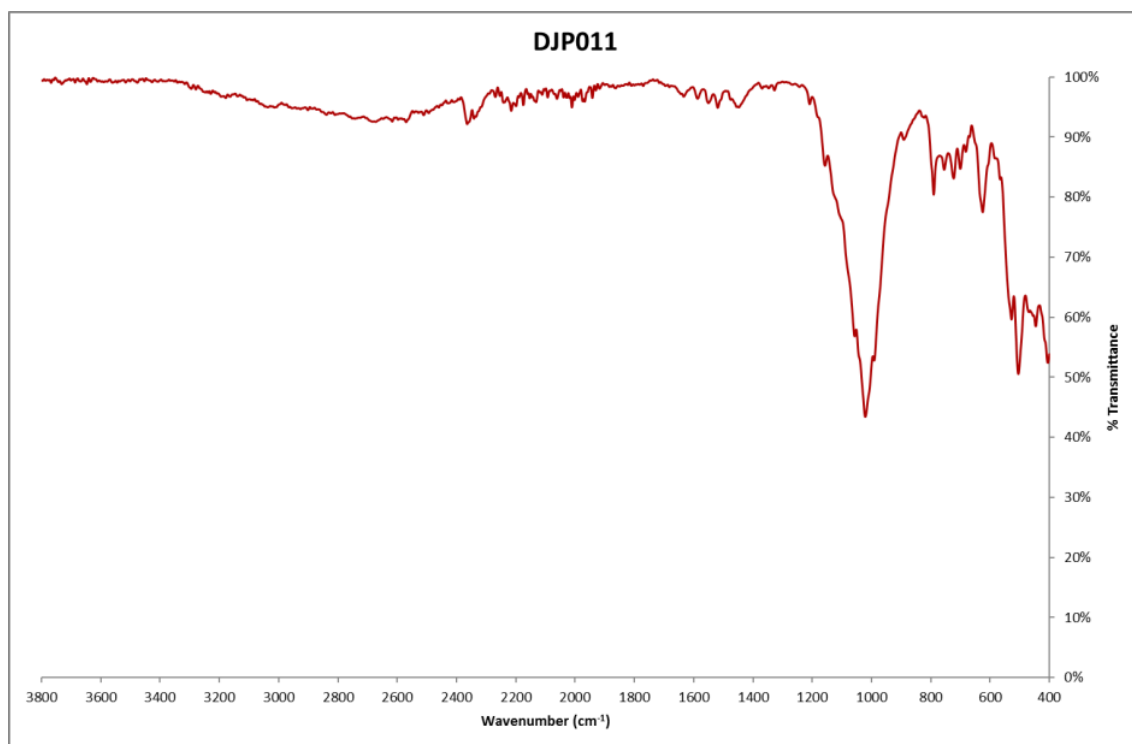


Figure 2.1: IR spectrum of DJP011 (Ti doped)

Table 2.2: IR data for DJP011

Wavenumbers (cm ⁻¹)	Intensity (%T)	Assignment
2570.36	92.491	C – H stretching
2364.16	92.169	CO ₂ stretching
2215.51	94.374	NH ₂ stretching
2131.88	95.784	N – H stretching
1519.20	94.876	N – H deformation
1448.18	94.960	-CH ₂ - scissoring
1021.35	43.390	P – O vibrational
790.54	80.432	NH ₃ ⁺ rocking
755.21	84.558	CH ₂ rocking
723.35	83.108	CH ₂ rocking
700.96	84.694	C – C stretching
625.50	84.694	Al – O stretching
528.23	59.642	P – O bending
505.03	50.555	Al – O vibrational
446.54	58.457	P – O bending

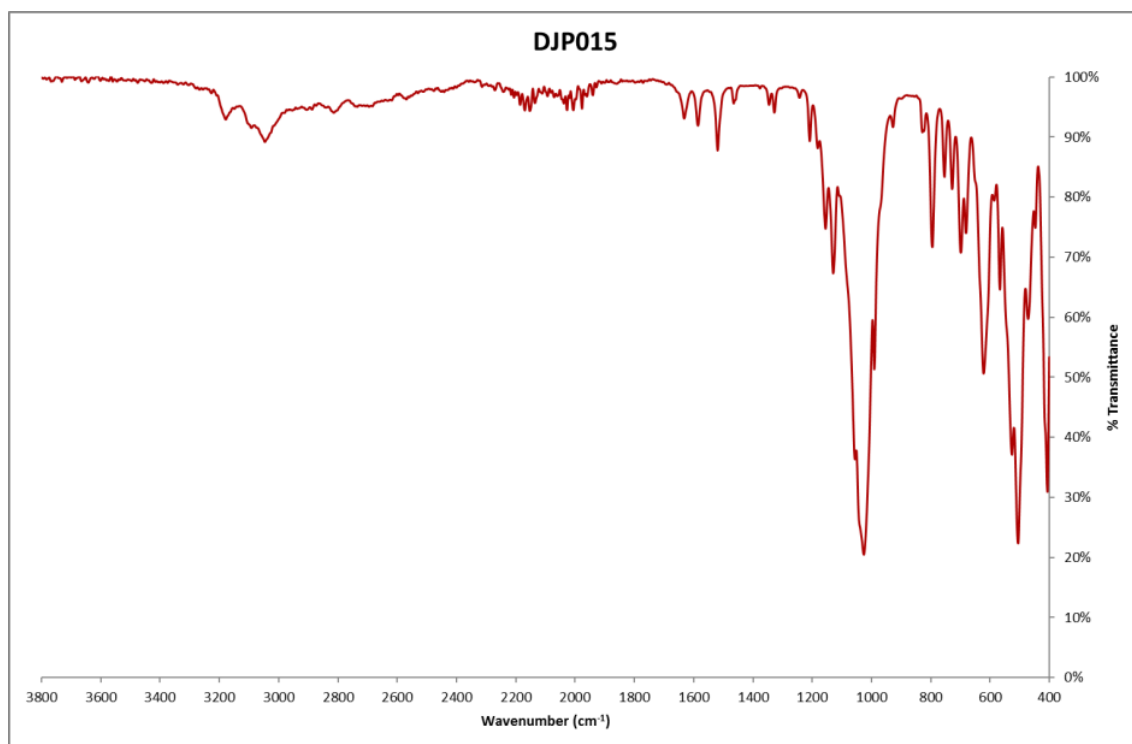


Figure 2.2: IR spectrum of DJP015

Table 2.3: IR data for DJP015

Wavenumbers (cm ⁻¹)	Intensity (%T)	Assignment
3170	94.551	<i>O – H stretching (bridging hydroxyl)</i>
3046	90.094	<i>N – H stretching</i>
2153	95.294	<i>N – H stretching</i>
2027	95.336	<i>P = O stretching</i>
1632	94.009	<i>NH₃⁺ bending</i>
1585	92.818	<i>NH₃⁺ deformation</i>
1519	88.643	<i>N – H deformation</i>
1328	94.981	<i>CH₂ twisting</i>
1208	90.185	<i>P = O stretching</i>
1155	75.463	<i>-CH₂ – CH₂- (C-C doublet)</i>
1129	67.922	<i>-CH₂ – CH₂- (C-C doublet)</i>
990	51.807	<i>O – H bending (bridging hydroxyl)</i>
828	91.687	<i>-CH₂-NH₂</i>
795	72.190	<i>NH₃⁺ rocking</i>
754	84.172	<i>CH₂ rocking</i>
728	82.057	<i>CH₂ rocking</i>
699	71.325	<i>C – C stretching</i>
622	51.063	<i>Al – O stretching</i>
567	65.243	<i>C – N bending</i>
526	37.456	<i>P – O bending</i>
506	22.405	<i>Al – O vibrational</i>
472	31.131	<i>P – O bending</i>

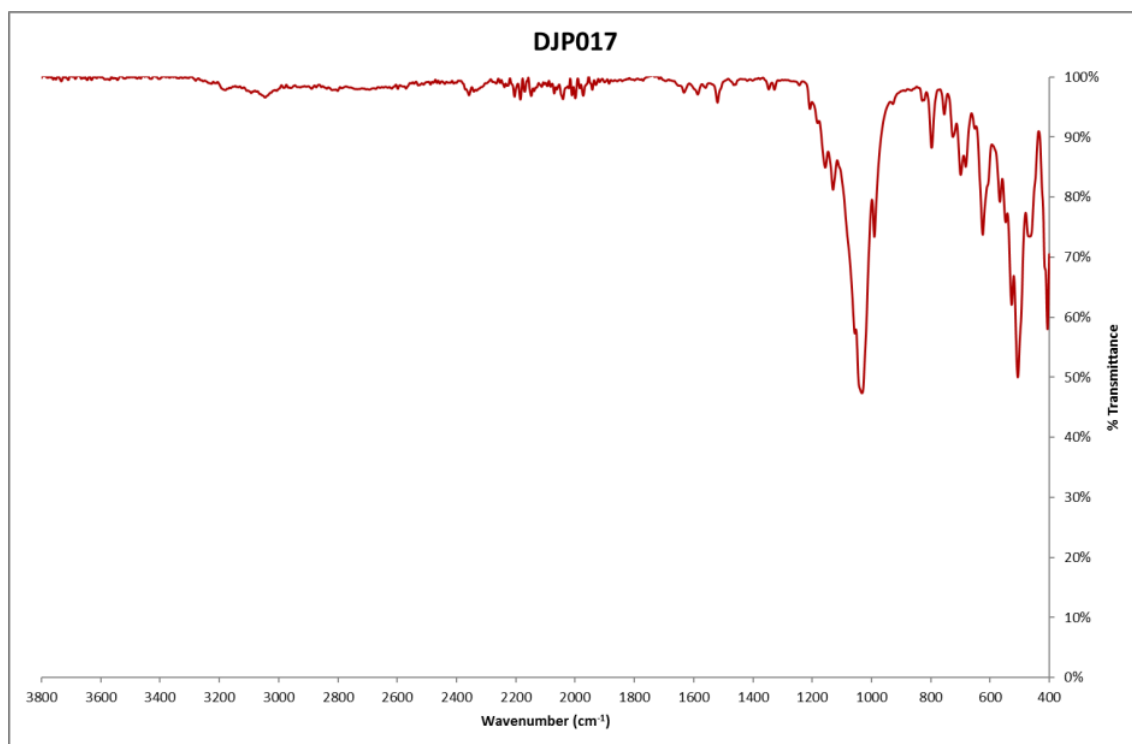


Figure 2.3: IR Spectrum of DJP017 (Zn doped)

Table 2.4: IR data for DJP017

Wavenumbers (cm ⁻¹)	Intensity (%T)	Assignment
3046	97.552	<i>N – H stretching</i>
2358	97.943	<i>CO₂ stretching</i>
2184	97.215	<i>N – H stretching</i>
2041	97.249	<i>P = O stretching</i>
1999	97.426	<i>NH₃⁺ deformation</i>
1519	96.697	<i>N – H deformation</i>
1156	85.756	<i>-CH₂ – CH₂- (C-C doublet)</i>
1130	82.062	<i>-CH₂ – CH₂- (C-C doublet)</i>
1032	47.834	<i>P – O vibrational</i>
990	74.052	<i>O – H bending (bridging hydroxyl)</i>
797	89.010	<i>NH₃⁺ rocking</i>
754	94.671	<i>CH₂ rocking</i>
725	90.934	<i>CH₂ rocking</i>
699	84.520	<i>C – C stretching</i>
625	74.438	<i>Al – O stretching</i>
567	79.984	<i>C – N bending</i>
527	62.588	<i>P – O bending</i>
506	50.487	<i>Al – O vibrational</i>
467	74.190	<i>P – O bending</i>

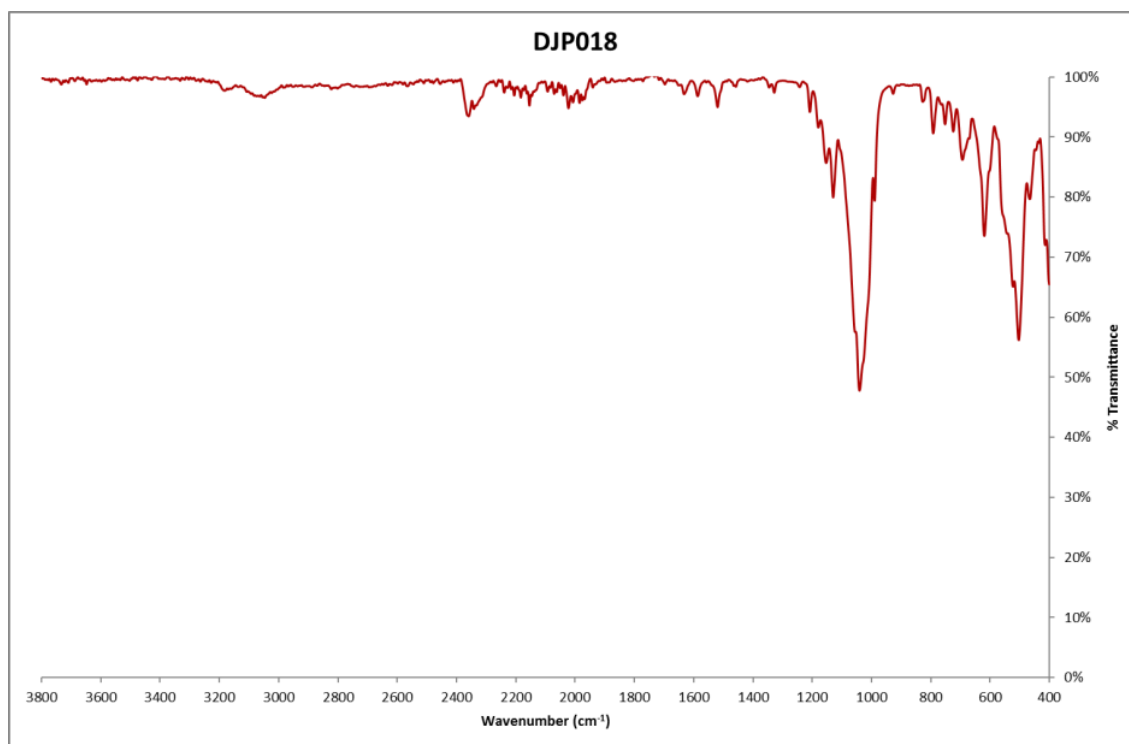


Figure 2.4: IR Spectrum of DJP018 (Ga doped)

Table 2.5: IR data for DJP018

Wavenumbers (cm ⁻¹)	Intensity (%T)	Assignment
3176	98.964	<i>O – H stretching (bridging hydroxyl)</i>
3047	97.500	<i>N – H stretching</i>
2359	94.381	<i>CO₂ stretching</i>
2183	97.544	<i>N – H stretching</i>
2022	95.748	<i>P = O stretching</i>
1632	98.120	<i>NH₃⁺ bending</i>
1586	97.778	<i>NH₃⁺ deformation</i>
1519	95.950	<i>N – H deformation</i>
1208	95.076	<i>P = O stretching</i>
1153	86.542	<i>-CH₂ – CH₂- (C-C doublet)</i>
1129	80.738	<i>-CH₂ – CH₂- (C-C doublet)</i>
1040	48.247	<i>P – O vibrational</i>
990	79.992	<i>O – H bending (bridging hydroxyl)</i>
827	96.830	<i>-CH₂-NH₂</i>
792	91.520	<i>NH₃⁺ rocking</i>
752	93.052	<i>CH₂ rocking</i>
724	91.821	<i>CH₂ rocking</i>
693	87.072	<i>C – C stretching</i>
619	74.207	<i>Al – O stretching</i>
503	56.725	<i>Al – O vibrational</i>
466	80.459	<i>P – O bending</i>

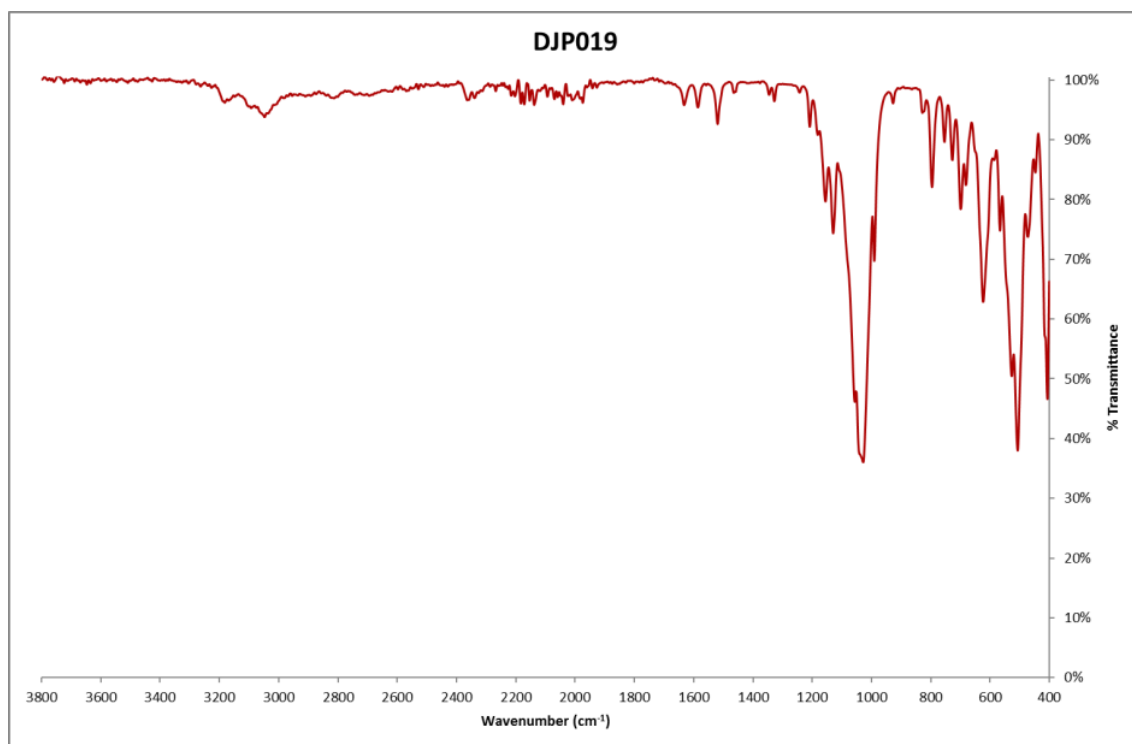


Figure 2.5: IR spectrum of DJP019 (Co doped)

Table 2.6: IR data for DJP019

Wavenumbers (cm ⁻¹)	Intensity (%T)	Assignment
3182	97.186	<i>O – H stretching (bridging hydroxyl)</i>
3047	94.740	<i>N – H stretching</i>
2364	97.591	<i>CO₂ stretching</i>
2171	96.876	<i>N – H stretching</i>
2040	96.900	<i>P = O stretching</i>
1632	96.760	<i>NH₃⁺ bending</i>
1585	96.358	<i>NH₃⁺ deformation</i>
1519	93.568	<i>N – H deformation</i>
1328	97.403	<i>CH₂ twisting</i>
1208	93.072	<i>P = O stretching</i>
1155	80.423	<i>-CH₂ – CH₂- (C-C doublet)</i>
1129	75.067	<i>-CH₂ – CH₂- (C-C doublet)</i>
1028	36.338	<i>P – O vibrational</i>
990	70.395	<i>O – H bending (bridging hydroxyl)</i>
796	82.891	<i>NH₃⁺ rocking</i>
754	90.516	<i>CH₂ rocking</i>
727	87.356	<i>CH₂ rocking</i>
623	63.368	<i>Al – O stretching</i>
527	50.828	<i>P – O bending</i>
507	38.364	<i>Al – O vibrational</i>
473	74.469	<i>P – O bending</i>

2.5.2: X-Ray Diffraction and X-Ray Fluorescence analysis

All five AlPO derived catalysts were characterised using both X-Ray Diffraction (XRD) and X-Ray Fluorescence (XRF) analysis. The data gathered from using XRD is useful in two respects; first the raw data (intensity and 2θ) can be plotted to form an XRD pattern which can be visually compared to others. Secondly, XRD was used to determine the crystallinity of the sample and its phase purity. If the diffraction pattern is unknown then indexing must be conducted to determine the properties of the sample, such as its unit cell parameters. Auto indexing programs calculate potential unit cell parameters from peak lists, which if need be can be further refined until the correct unit cell is found. Several autoindexing programs were used to process the collected data, they were; ITO [52], TREOR [53] and DICVOL [54]. Three autoindexing programs were used, as alluded to by David *et al.* [55], because each one processes the data in a different way and therefore if one program cannot find a correct indexing solution another may.

The XRF results show (Appendix 5.2) that there are no major impurities in the samples and that chosen metal dopants had been incorporated into their respective catalysts (Table 2.7).

Table 2.7: XRF elemental analysis

Catalyst	XRF element peak (radiation band)
DJP011	Aluminium ($K\alpha$), Phosphorous ($K\alpha$), Titanium ($K\alpha$), Rhodium ($L\alpha$)
DJP015	Aluminium ($K\alpha$), Phosphorous ($K\alpha$), Rhodium ($L\alpha$)
DJP017	Aluminium ($K\alpha$), Phosphorous ($K\alpha$), Zinc ($K\alpha$), Rhodium ($L\alpha$)
DJP018	Aluminium ($K\alpha$), Phosphorous ($K\alpha$), Gallium ($K\alpha$), Rhodium ($L\alpha$)
DJP019	Aluminium ($K\alpha$), Phosphorous ($K\alpha$), Cobalt ($K\alpha$), Rhodium ($L\alpha$)

From a visual comparison of the XRD patterns Figure 2.6, it can be seen that there are many similarities between the respective structures of all five AlPO catalysts. All five XRD patterns were searched against both the Crystallographic Open Database (COD) and the PDF-4+ database provided by The International Centre for Diffraction Data (ICDD) however, no exact matches were found indicating that these materials could be novel. It is worth noting that there are several extra peaks in samples DJP011 and DJP017. This could indicate that the material is multi-phasic as opposed to being a

more uniform singular phase or that some unwanted side-product is present in the crystal structure, which formed during the synthesis. Alternatively, it could show that both catalysts have different crystal structures when compared with the other catalysts synthesised. Both DJP011 and DJP017 have been doped with titanium and zinc respectively.

Indexing was also performed on all recorded XRD data from the five catalysts, with results shown in Table 2.8. Again the trend, highlighted by a visual comparison of the XRD patterns, is shown in the results of the autoindexing with both DJP011 and DJP017 providing different results when compared with the other catalysts in the series. All AlPO series catalysts bar DJP011 and DJP017 have high Figures of Merit (FoM), greater than 20, and have very similar unit cell parameters as well as sharing similar space groups.

Table 2.8: Unit cell parameters of AlPO series catalysts

Catalyst	Unit Cell Parameters						Crystal System	Figure of Merit	Space Group
	A (Å)	B (Å)	C (Å)	α	β	γ			
DJP011	19.395	10.705	17.545	90.000	102.108	90.000	Monoclinic	8.0	P2 ₁ /n
DJP015	14.527	9.417	9.607	90.000	98.286	90.000	Monoclinic	39.0	P2 ₁ /c
DJP017	13.891	14.546	8.573	100.638	104.257	81.537	Triclinic	6.0	P1
DJP018	14.554	9.445	9.615	90.000	98.331	90.000	Monoclinic	42.0	P2/c
DJP019	14.517	9.411	9.596	90.000	98.193	90.000	Monoclinic	45.0	P2 ₁ /c

A high FoM is important as it is used to determine the accuracy of the autoindexing process. If the material being analysed contains more than one phase then this can show “erroneous” peaks in the XRD pattern, which in turn makes it impossible to index the material correctly. If a sample contains either a single phase or is only slightly multi-phasic then it will have a high FoM. However the more multi-phasic it becomes the lower the FoM. According to Blake *et al.* [56] FoMs can be calculated quickly and give an indication of quality, therefore correlating with the confidence and accuracy of the results.

The estimated unit cell parameters were then refined using Celref V3 in order to determine how accurate the initial refinement process was and if need be to identify any erroneous peaks. If any erroneous peaks were identified whilst refining the data,

this information would then be used to generate a new set of initial unit cell parameters and the process would be repeated. As can be seen from Table 2.9, the initial unit cell parameters were relatively accurate (estimated standard deviations in parenthesis) and no erroneous peaks were identified during the refinement process. A list of the full refined unit cell and lattice parameters can be found for each catalyst in Appendix 5.6

Table 2.9: Refined unit cell parameters for AlPO catalysts

Catalyst	Refined Unit Cell Parameters					
	A (Å)	B (Å)	C (Å)	α	β	γ
DJP011	19.4021 (0.0413)	10.6952 (0.0064)	17.5564 (0.0336)	90.000	102.06 (0.357)	90.000
DJP015	14.5338 (0.0051)	9.4145 (0.0030)	9.6076 (0.0029)	90.000	98.290	90.000
DJP017	13.8877 (0.0179)	14.5656 (0.0191)	8.5739 (0.0096)	100.670 (0.084)	104.240 (0.080)	81.490 (0.082)
DJP018	14.5611 (0.0083)	9.4475 (0.0035)	9.6135 (0.0042)	90.000	92.260 (0.066)	90.000
DJP019	14.5294 (0.0117)	9.4133 (0.0038)	9.6018 (0.007)	90.000	98.230 (0.121)	90.000

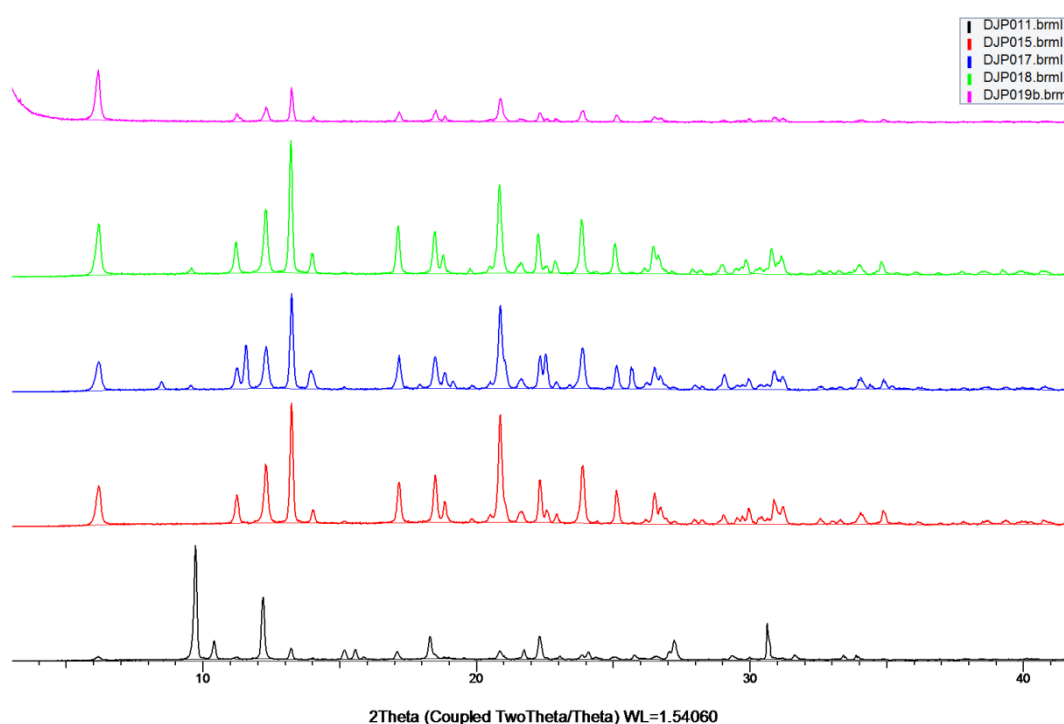


Figure 2.6: XRD patterns for aluminium phosphate series catalysts

2.5.3: Solid-state NMR

Both ^{27}Al and ^{31}P solid-state NMR were used to analyse all samples. Figure 2.7 to Figure 2.11 show the ^{31}P NMR spectra of each AIPO based catalyst and the ^{27}Al spectra are shown in Appendix 5.3. From the ^{27}Al NMR spectra, it can be determined that there are multiple aluminium environments in all the AIPO series catalysts synthesised, although one environment is much more clearly visible than the others, as there is a single well defined peak with associated spinning side-bands and then there are potentially two other peaks hidden in the broad peak present around 15ppm.

However this is not the case when analysing the ^{31}P NMRs for all of the AIPO series catalysts. Here multiple main peaks are present, indicating the presence of more than one phosphorus environment. By overlaying the spectra collected at different frequencies, it is clear that there are at least two different environments. On several of the ^{31}P NMRs at least four main peaks are present; but on the NMRs which only show 2 peaks, the peaks are quite broad. These multiple peaks have most likely been caused by chemical shift anisotropy (CSA), which happens when a polycrystalline sample is analysed. Therefore it is probable that only two phosphorous environments are present in the AIPO series catalysts, despite there being multiple peaks.

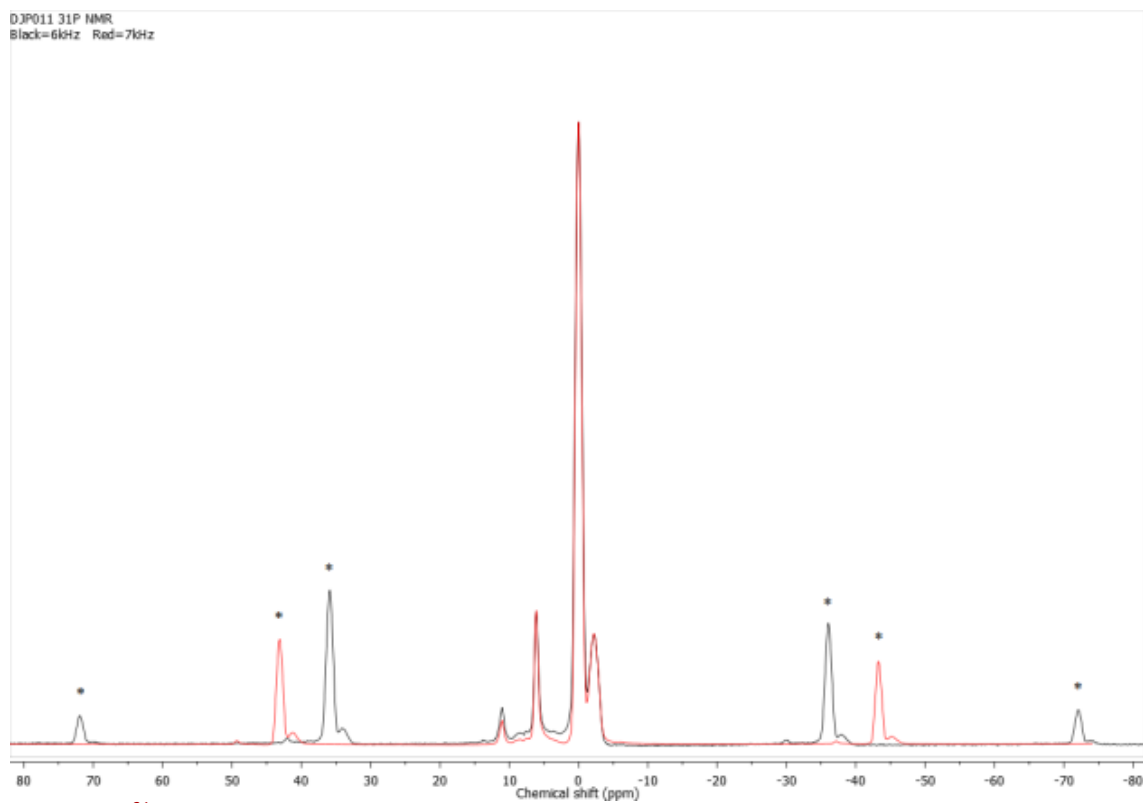


Figure 2.7: ^{31}P NMR spectrum of DJP011 (Ti doped)

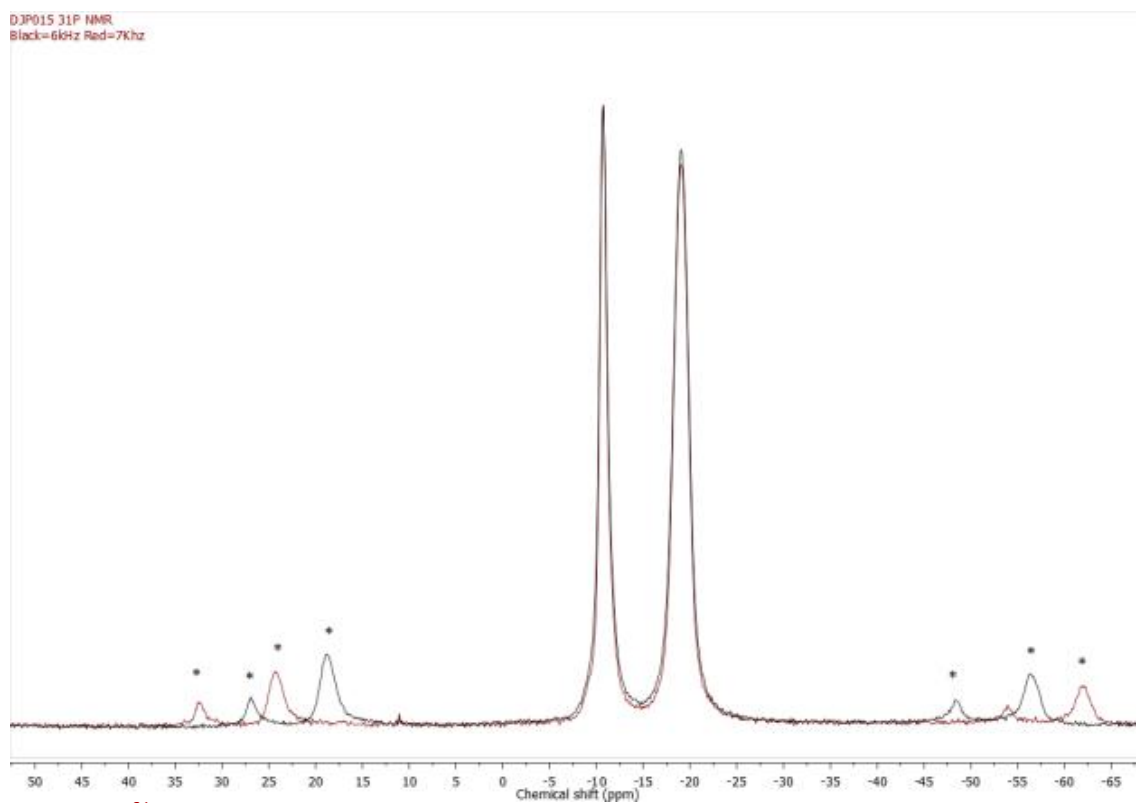


Figure 2.8: ^{31}P NMR spectrum of DJP015

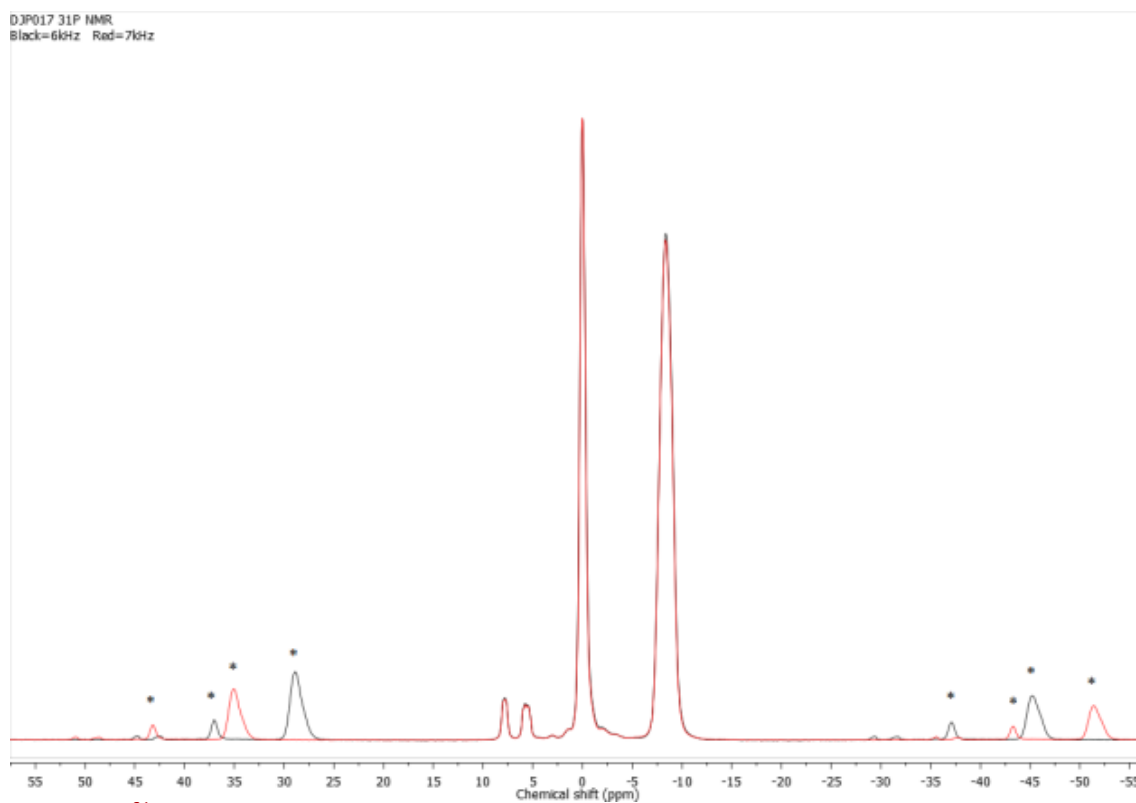


Figure 2.9: ^{31}P NMR spectrum of DJP017 (Zn doped)

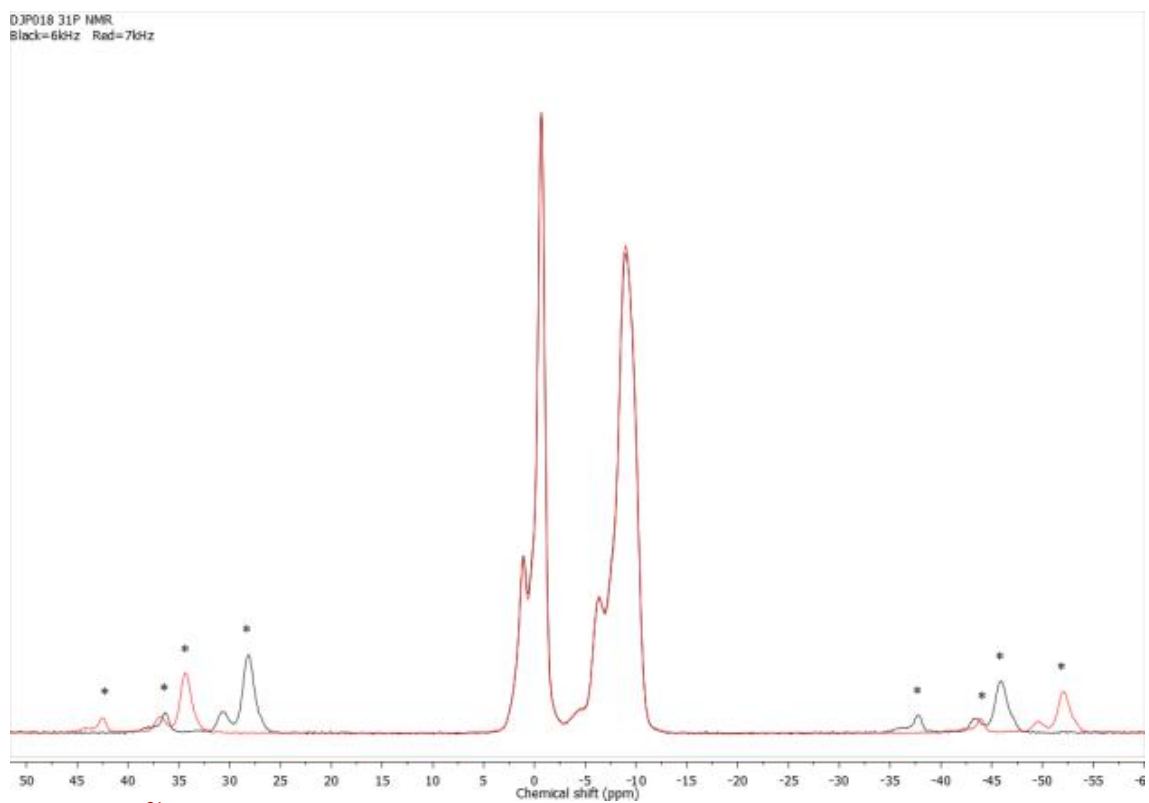


Figure 2.10: ^{31}P NMR spectrum of DJP018 (Ga doped)

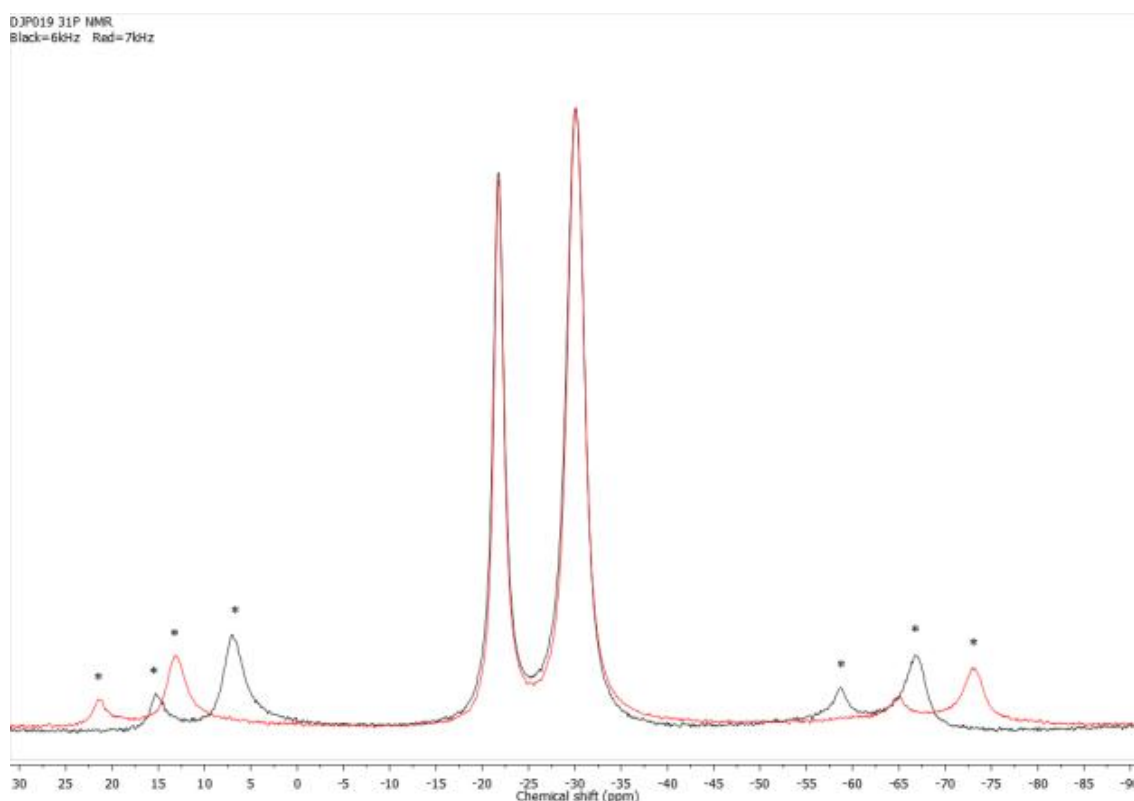


Figure 2.11: ³¹P NMR spectrum of DJP019 (Co doped)

Since ²⁷Al is a quadrupolar nucleus, ²⁷Al Multiple Quantum Magic Angle Spinning (MQMAS) NMR spectroscopy was also conducted on all AIPO series catalysts. Although 1D-MQMAS NMR provides a similar function to that of a standard ²⁷Al experiment (although both experiments have different acquisition programs) 1D-MQMAS can be combined with 2D-MQMAS NMR techniques to provide much more useful data. Should more than one peak be found in a 1D-MQMAS spectrum, 2D-MQMAS can be used to view spectra without 2nd order quadrupolar effects. The 1-D MQMAS NMRs collected can be seen in Appendix 5.4. From the MQMAS NMRs it can be confirmed that there is only a single aluminium environment in all AIPO series catalysts analysed except for the 1D-MQMAS spectra of DJP011, where the single peak appears to be splitting into two different peaks. However, this could only be confirmed by conducting a 2D-MQMAS experiment on the sample.

2.5.4: Surface properties and decomposition analysis

Surface area analysis was carried out using a Micrometrics ASAP 2010. There are two different types of calculation used to work out the surface area of a material, either using the Langmuir isotherm or the Brunauer Emmett Teller (BET) equation. The Langmuir isotherm bases its calculations on a single layer of gas absorbed on to the surface of the material being analysed. Although it is a useful result to obtain, it has largely been superseded by the BET equation. The BET equation is largely an extension of the Langmuir isotherm. The BET isotherm differs in three key assumptions: gas molecules can absorb on to an infinite number of layers in a material, there are no interactions between layers, as there are no interaction between the layers the Langmuir isotherm can be applied to each layer. Shown below (Table 2.10) are the results of the surface area analysis of the AlPO series catalysts.

Table 2.10: Surface area analysis results for AlPO series

Catalyst	BET surface area (m ² /g)	Total pore volume (cm ³ /g)	Average pore diameter (Å)
DJP011	2.528	0.0039	62.52
DJP015	6.193	0.0096	62.27
DJP017	6.073	0.0093	61.47
DJP018	9.222	0.0157	68.33
DJP019	10.699	0.0186	69.55

From the surface area results, some interesting conclusions can be drawn about the AlPO series catalysts. All catalysts share similar pore diameters (approx. average 65Å), yet the surface areas are, in some cases, several times larger. This in part can be explained by examining the scanning electron micrographs obtained of the catalysts synthesised. Although all the catalysts appear to be similarly porous, the physical structure and the orientation of the crystals within the structures differ greatly.

DJP011 exhibits a very disorganised structure with varying crystal shapes and sizes, much more so than any of the other AlPO series catalysts. Not surprisingly the scanning electron micrograph for DJP015 showed a very regular structure with clearly defined fairly uniform crystals (Figure 2.12). DJP018 was visually similar (not unsurprising as the gallium doped into the structure is very similar to aluminium)

however the structure was slightly less well ordered and the crystal size was slightly less uniform. This contrasts with both of the structures of DJP017 (Figure 2.12) and DJP019 which seem to exhibit crystals which are, in some cases, more of an elongated cube/needle like structure with differencing sizes and orientation. Although they are more structurally organised than that of DJP011 they are not as uniform as DJP015 and DJP018.

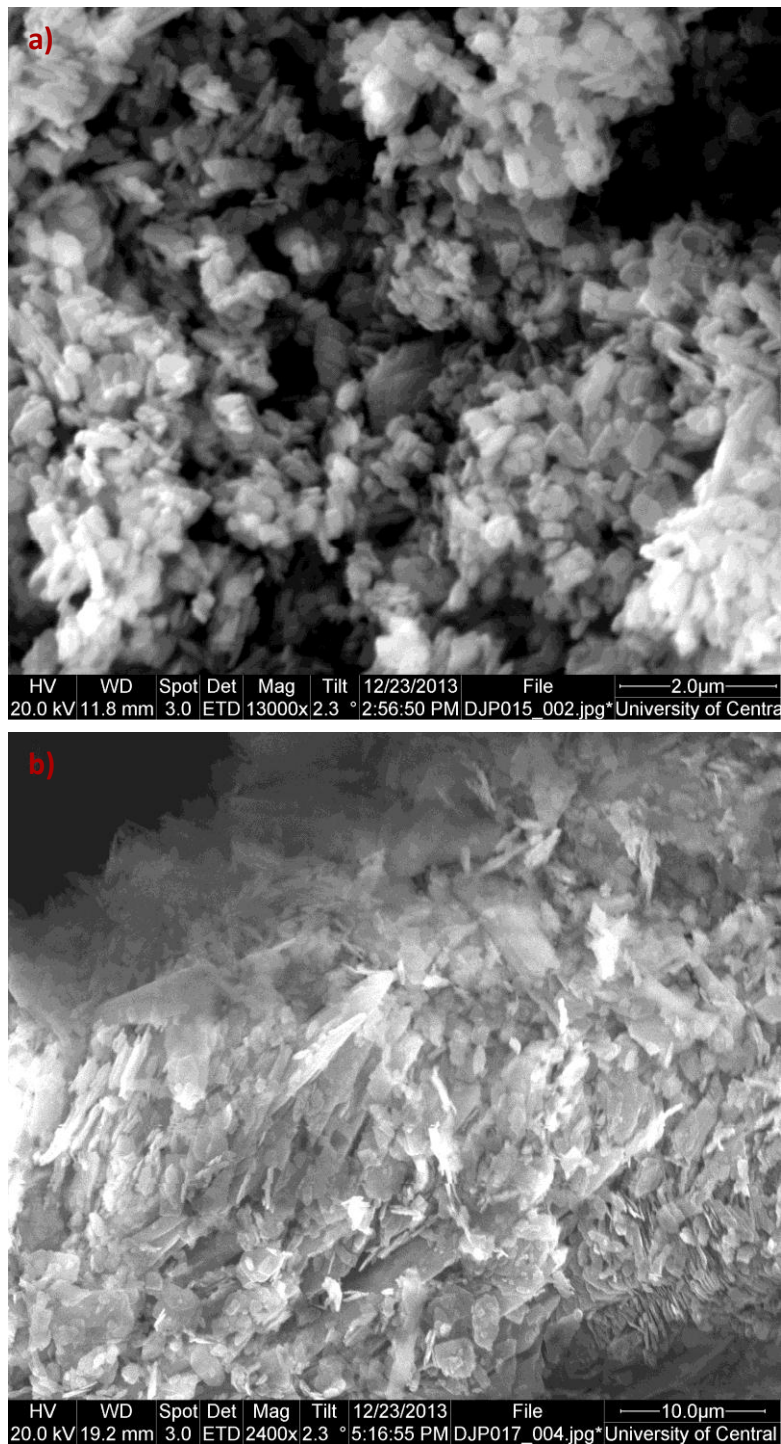


Figure 2.12: Scanning electron micrographs of DJP015(a) and DJP017(b)

The EDX results collected are shown in Table 2.11. These results confirm that the chosen metals were successfully doped into the AlPO structure, however there are two interesting observations to make from the data obtained. First there appears to be no correlation between the amounts of aluminium substituted for the doped metals, with only DJP017 being the closest to reaching the 25% doped content (approx. 22% gallium doped). Therefore it is also interesting to note that despite the varying amounts of doped metals in the AlPO structures the ratio between oxygen, phosphorus and metals in the doped AlPOs is very similar to that of the undoped AlPO (O:4, P:1, Al:1). Although there is a slight increase in the amount of phosphorus found in the doped catalysts leading to an approximate ratio of O:4, P:1.05 and M:0.95.

Table 2.11: EDX results for AlPO catalysts

Catalyst	EDX results for AlPO catalysts, weight % (Atom %)						
	O	Al	P	Ti	Zn	Ga	Co
DJP011	38.80% (56.38%)	15.31% (13.19%)	30.79% (23.11%)	15.11% (7.33%)	-----	-----	-----
DJP015	53.01% (67.19%)	21.12% (15.87%)	25.87% (16.94%)	-----	-----	-----	-----
DJP017	38.62% (59.09%)	12.41% (11.26%)	27.21% (21.51%)	-----	21.76% (8.15%)	-----	-----
DJP018	38.02% (56.34%)	19.67% (17.29%)	28.19% (21.58%)	-----	-----	14.12% (4.80%)	-----
DJP019	39.02% (54.44%)	24.71% (20.44%)	33.31% (24.00%)	-----	-----	-----	2.96% (1.12%)

As shown in the TGA plots below (Figure 2.13 - Figure 2.17), all AlPO catalysts behave similarly (apart from DJP011) and started to decompose at approximately the same temperature despite there being differences in their crystal structures and compositions. All AlPOs lost approximately 16% of their mass during the experiment, except for DJP011, which lost approximately 22% of its mass. It is also important to note that, when compared to the other AlPO catalysts synthesised, DJP011 shows two distinct mass losses occurring in quick succession suggesting a multi-stage decomposition. This is not unexpected as the AlPOs contain a templating agent that was not removed after synthesis and all the samples were not kept in a dry atmosphere, therefore the samples will contain trace amount of water as well.

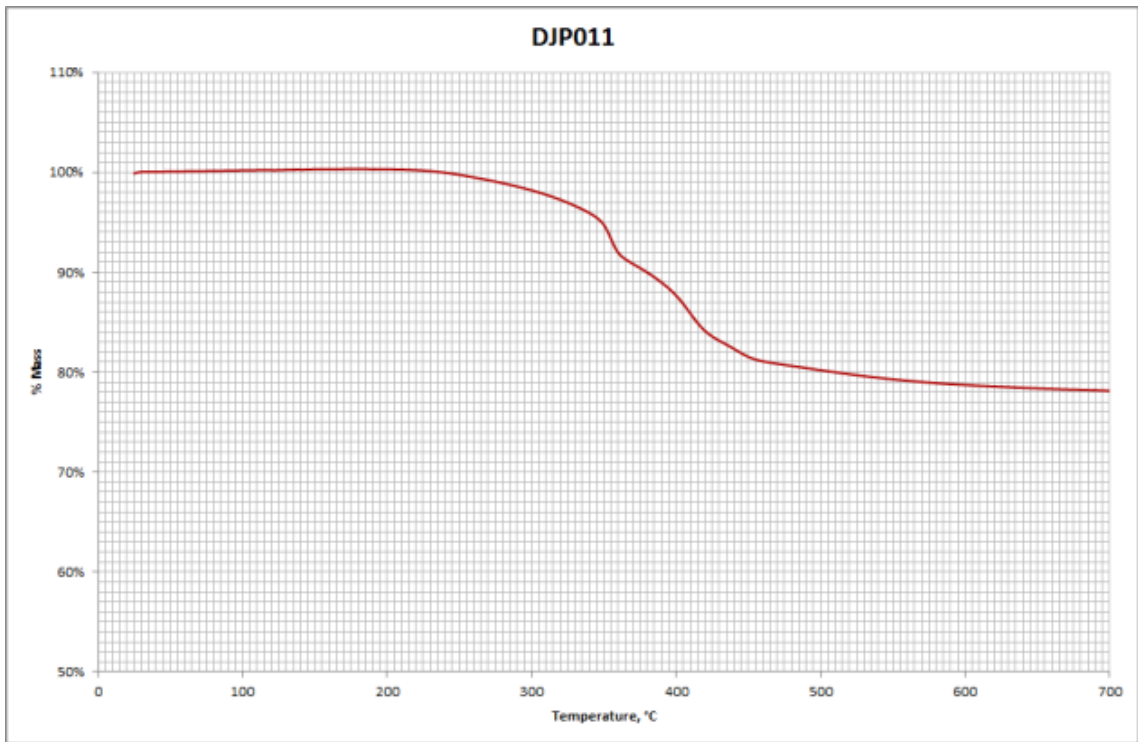


Figure 2.13: TGA curve of DJP011 (Ti doped)

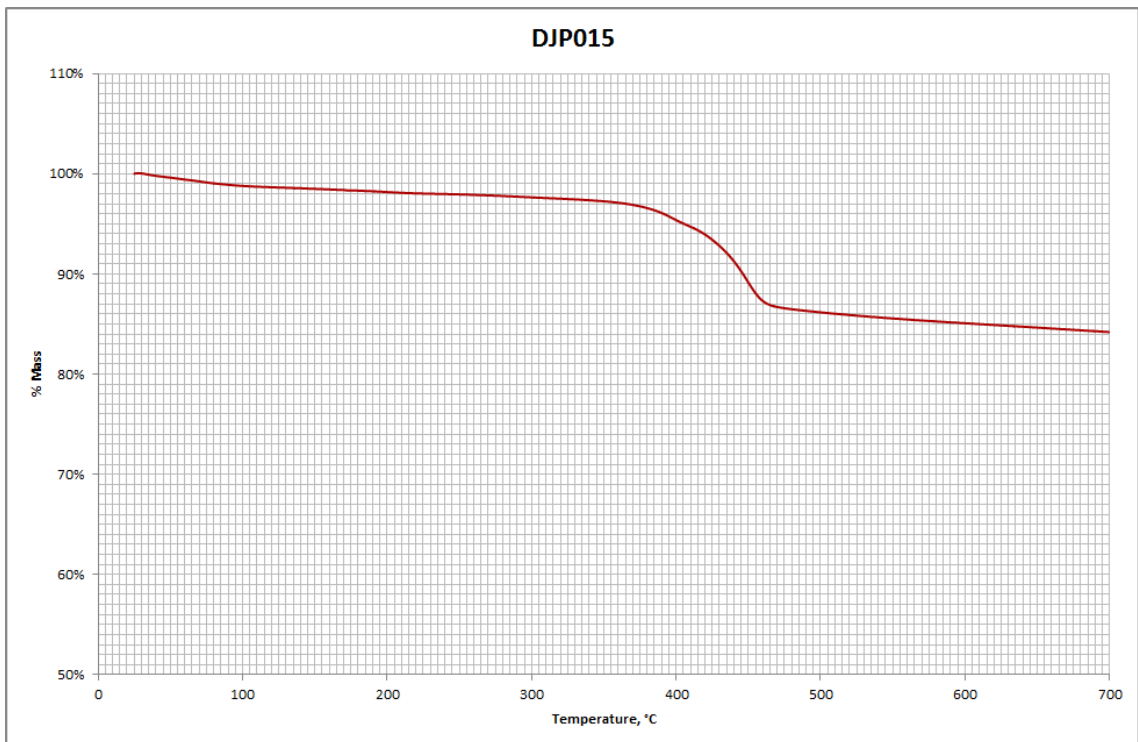


Figure 2.14: TGA curve of DJP015

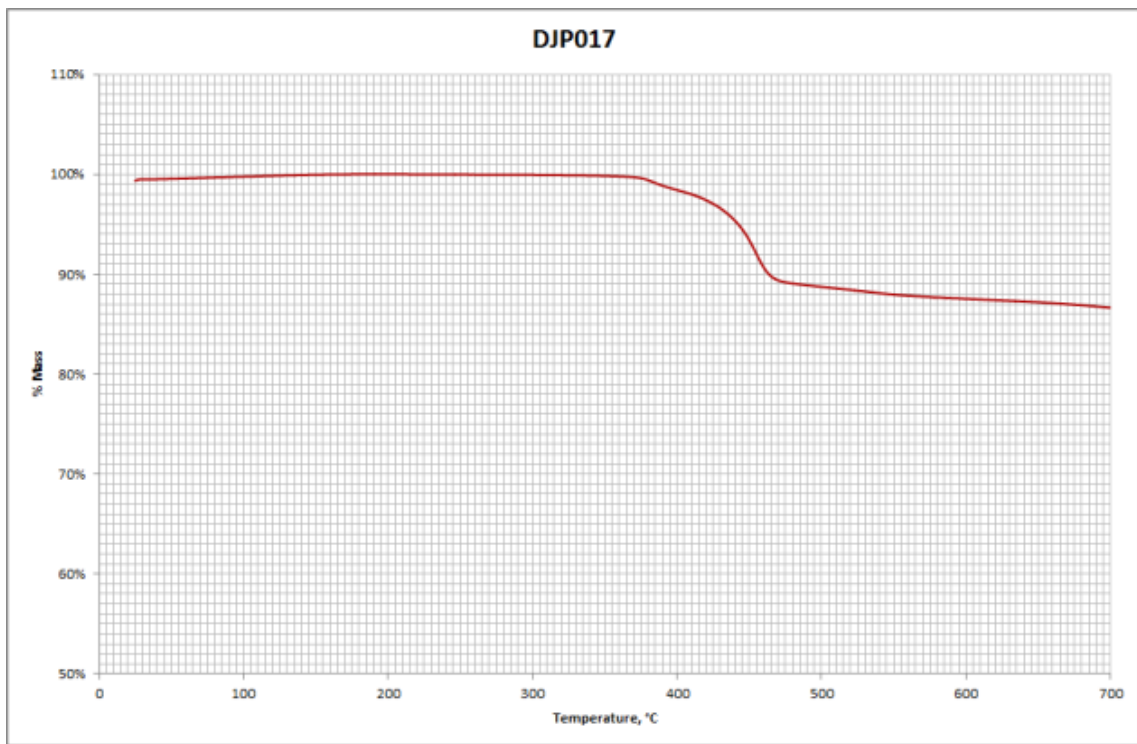


Figure 2.15: TGA curve of DJP017 (Zn doped)

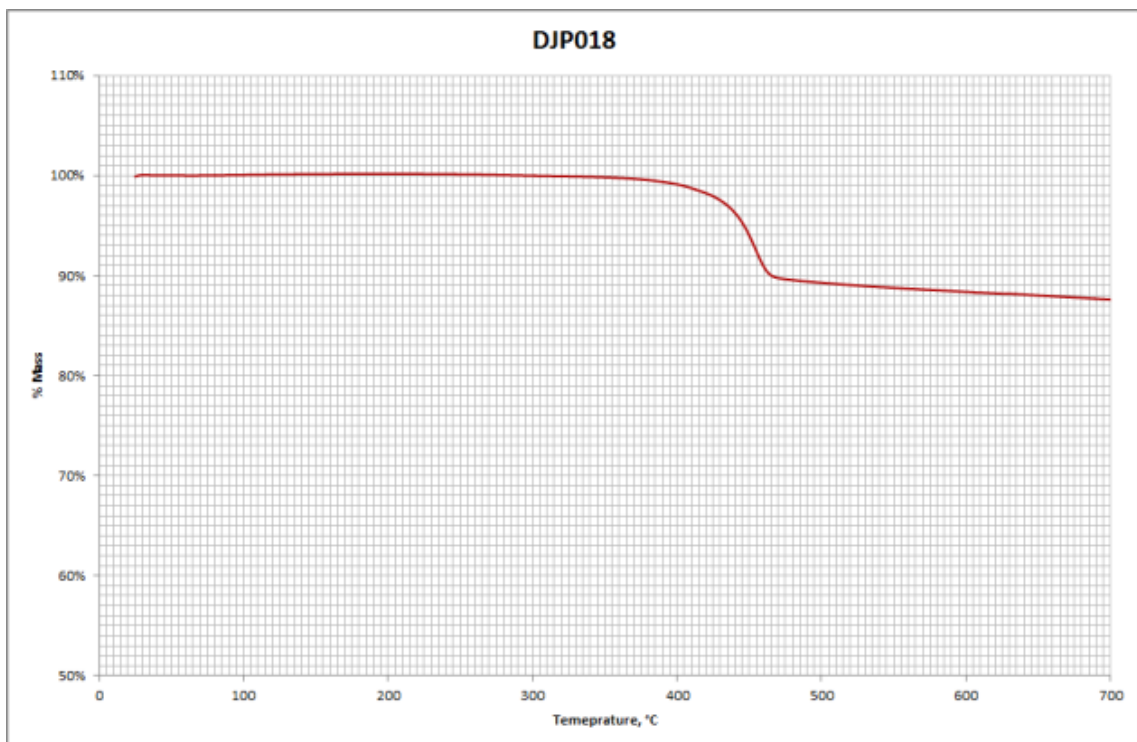


Figure 2.16: TGA curve of DJP018 (Ga doped)

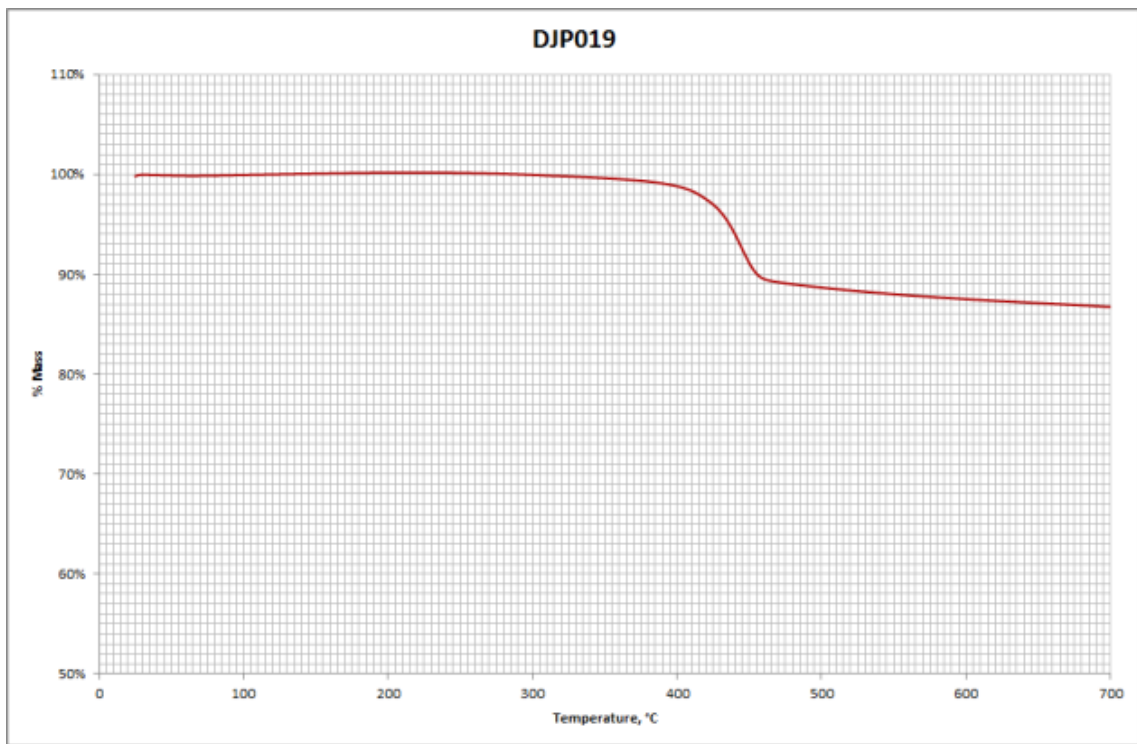


Figure 2.17: TGA curve of DJP019 (Co doped)

2.6: Characterisation of α -zirconium phosphate catalyst

2.6.1: Infrared Spectroscopy

The α -zirconium phosphate IR spectrum differs greatly from that of the aluminium phosphate based catalysts (Figure 2.1 - Figure 2.5, see pages 25 - 29). This is mainly due to the fact that α -zirconium phosphate is synthesised without the need for an organic template. As can be seen from the data below, there are clearly defined hydroxyl peaks at 3589 cm^{-1} and 3509 cm^{-1} , confirming the presence of the P – OH in the inter region area.

The assignment of the absorption bands have been made by using data taken from Horsley *et al.* [57] and Nakamoto [50].

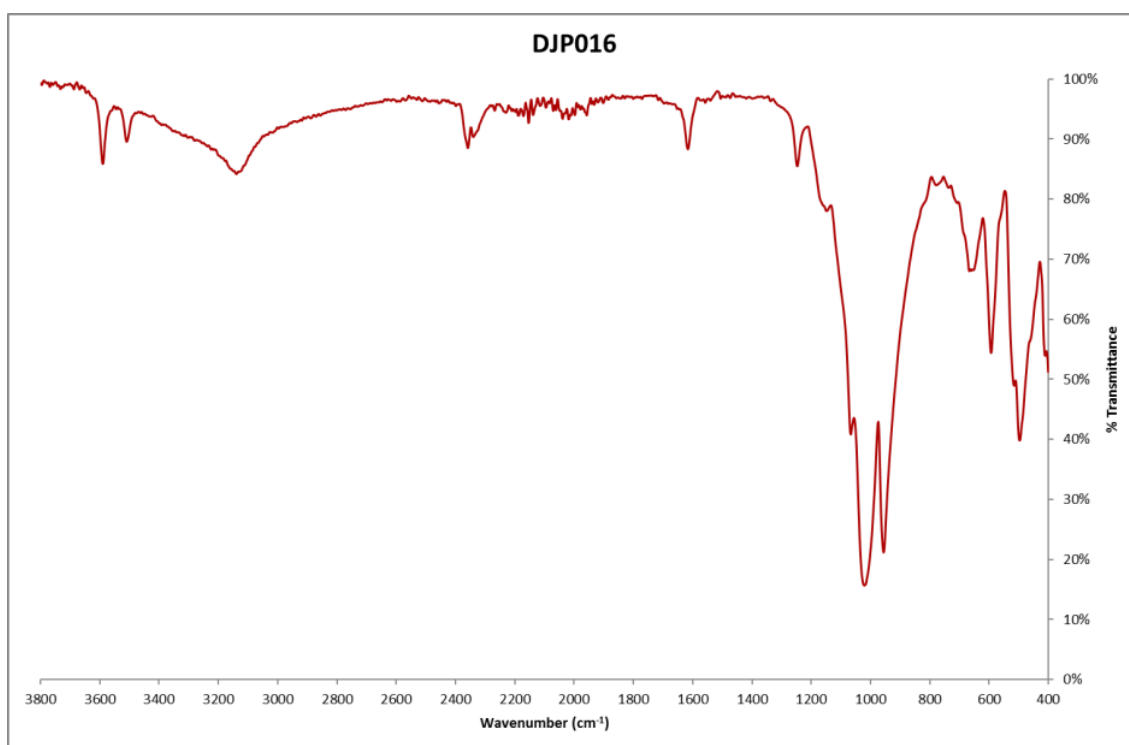


Figure 2.18: IR spectrum of DJP016

Correlation table shown on next page.

Table 2.12: IR data for DJP016

Wavenumbers (cm ⁻¹)	Intensity (%T)	Assignment
3589	85.841	<i>O – H bridging hydroxyl</i>
3509	89.546	<i>O – H bridging hydroxyl</i>
3139	84.191	<i>H – O – H vibrational (lattice water)</i>
2358	88.515	<i>CO₂ stretching</i>
2153	92.641	<i>P – OH stretching</i>
2018	93.261	<i>P = O stretching</i>
1616	88.315	<i>H – O – H vibrational (lattice water)</i>
1247	85.473	<i>P – OH deformation</i>
1021	15.669	<i>P – O vibrational</i>
956	21.180	<i>P – O vibrational</i>
593	54.378	<i>P – O bending</i>
497	39.806	<i>P – O bending</i>

2.6.2: X-Ray Diffraction and X-Ray Fluorescence analysis

The XRF and XRD data collected for DJP016, show that there were no chemical impurities detected by XRF (Appendix 5.2) analysis. This is confirmed by the unit cell parameter data shown in Table 2.13. Since the FoM is 24, it is reasonable to assume that the unit cell data is accurate and confirms the structure of DJP016 as α -ZrP. When comparing the unit cell parameters to that of the α -zirconium phosphate synthesised by Troup and Clearfield [36], the A, B, C and β parameters are concordant to 1 decimal place and both samples share the same space group (P2₁/n). These results confirm that DJP016 is α -zirconium phosphate. The refined unit cell and lattice parameters can be found in Appendix 5.6.

Table 2.13: Unit cell parameters of α -ZrP catalyst

Catalyst	Unit Cell Parameters						Crystal System	Figure of Merit	Space Group
	A (Å)	B (Å)	C (Å)	α	β	γ			
DJP016	15.422	5.288	9.038	90.000	101.747	90.000	Monoclinic	24.0	P2 ₁ /n

Table 2.14: Refined unit cell parameters for α -ZrP

Catalyst	Refined Unit Cell Parameters					
	A (Å)	B (Å)	C (Å)	α	β	γ
DJP016	15.425 (0.0057)	5.2894 (0.0015)	9.032 (0.0046)	90.000	101.750	90.000

2.6.3: Solid-state NMR

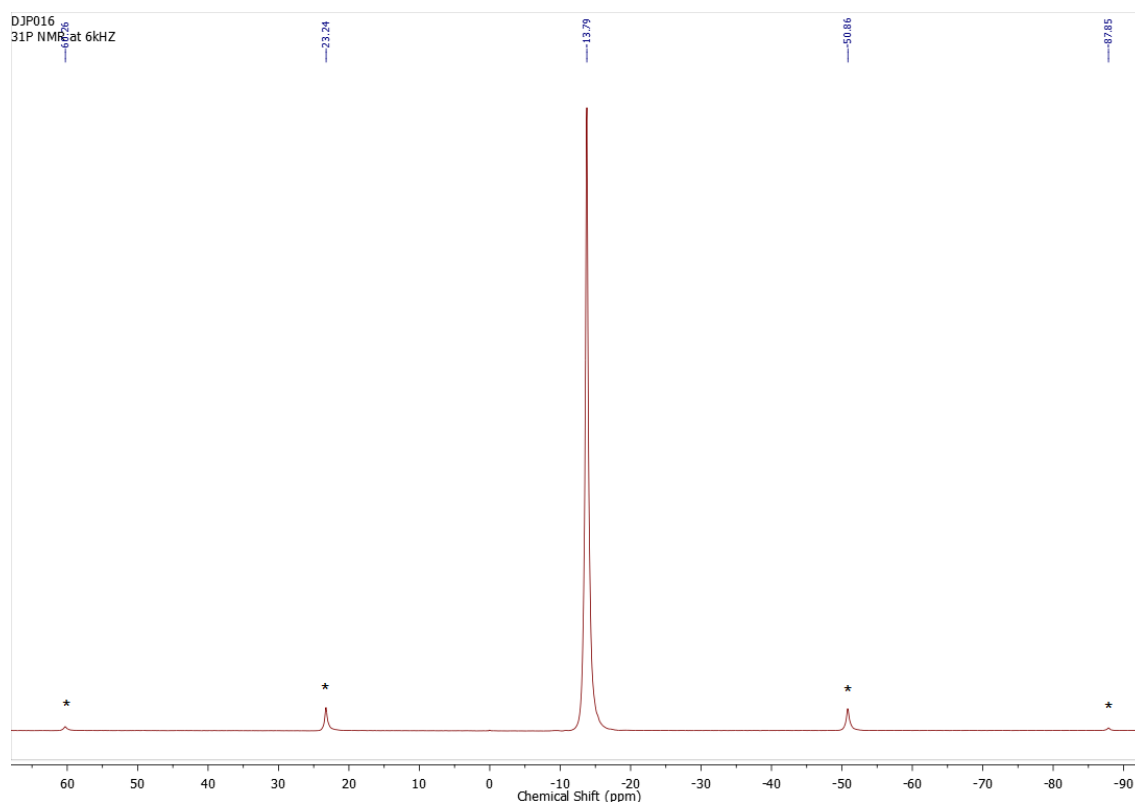


Figure 2.19: ^{31}P NMR spectrum of α -ZrP catalyst

Only ^{31}P solid-state NMR was used to analyse the α -zirconium phosphate catalyst. There was no zirconium based NMR study as the sample holders (rotors) are made out of zirconia therefore preventing the experiment to run as it would be impossible to analyse the spectra produced. Similarly there were no MQMAS NMRs performed on the catalyst. Figure 2.19 shows the ^{31}P NMR spectra of DJP016, run at 6 kHz. Present in the spectra is the single main peak (-13.79 ppm) and two pairs of spinning side bands (indicated by asterix). With only one main peak showing, it is confirmed that the phosphorus atoms in this particular α -zirconium phosphate structure are all in the same environment. Furthermore this suggests that the material contains only one phase.

2.6.4: Surface properties and decomposition analysis

Compared with the surface area results obtained from the AlPO catalysts (Table 2.10), DJP016 shows markedly different properties. As shown in Table 2.15, α -ZrP has a similar surface area compared to the AlPO series, however average pore diameter is

approximately a third the size of the AlPO catalysts, at only 41.9Å. From analysing the scanning electron micrograph of DJP016 (Figure 2.20), it shows that the catalyst has a fairly uniform structure and all the crystals are all of a relatively similar size and shape (it is interesting to note that it is visually very similar to DJP015). This similar visual appearance to some of the AlPO catalysts may also explain why it has a comparable total pore volume to some of the AlPO catalysts. The EDX analysis of the catalyst confirms the results obtained from the XRF and that the correct ratios of Zr, P and O are present in the sample, Table 2.16.

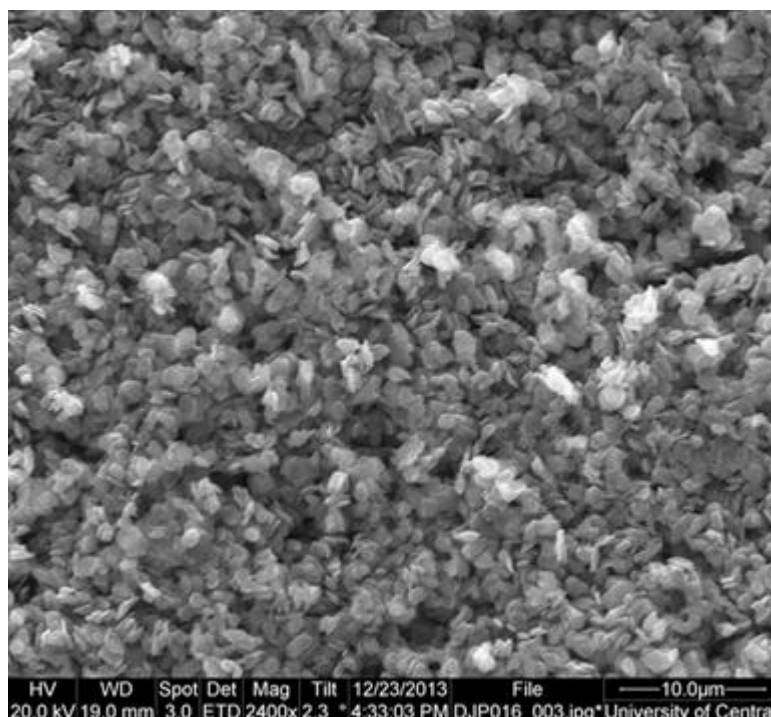


Figure 2.20: Scanning electron micrograph of DJP016

Table 2.15: Surface area analysis results for α -ZrP

Catalyst	BET surface area (m ² /g)	Total pore volume (cm ³ /g)	Average pore diameter (Å)
DJP016	4.532	0.0048	41.88

Table 2.16: EDX analysis of α -ZrP catalyst

Catalyst	EDX results for α -ZrP catalyst, weight % (Atom %)		
	O	Zr	P
DJP016	40.62 (70.12)	39.47 (12.03)	19.91 (17.85)

Compared to the TGA plots of the AlPO series catalysts (Figure 2.13 - Figure 2.17), the TGA plot obtained for α -ZrP shows that it starts to decompose at a much lower temperature than that of the AlPOs, this is most likely due to the loss of water from the interlayer spaces whereas the AlPOs contain ethylenediamine which would have to decompose as well. Despite the decomposition starting sooner than in the AlPO catalysts, approximately the same percentage weight loss occurred between the different types.

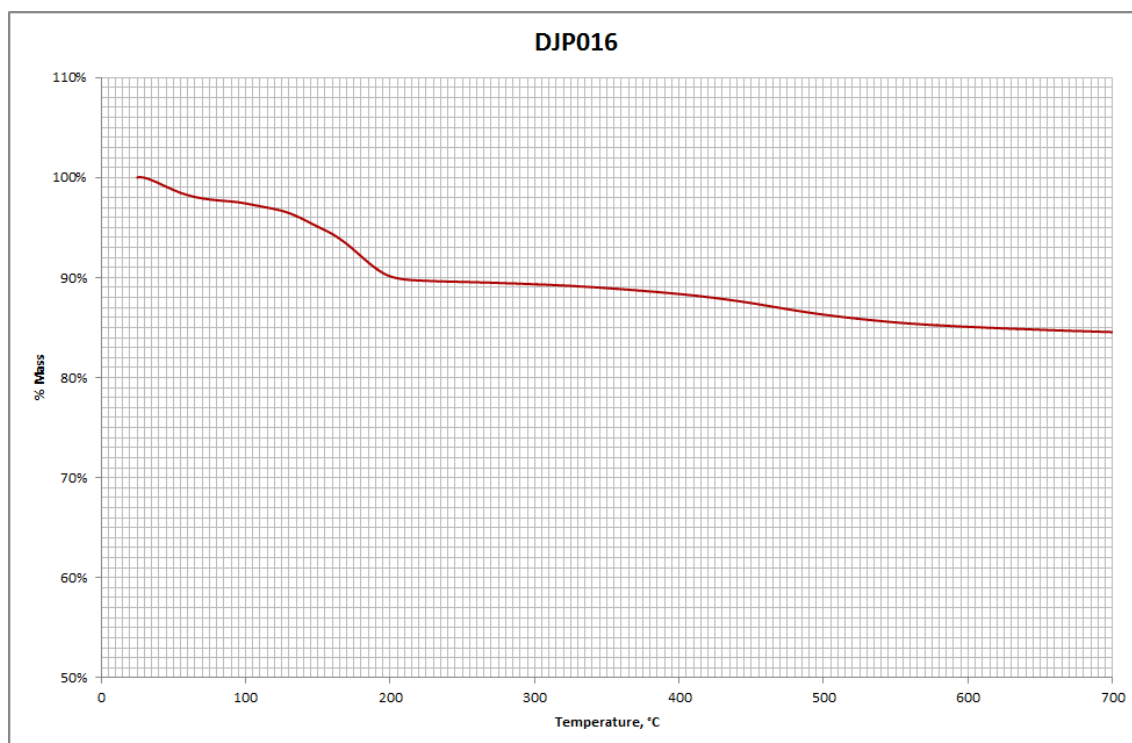


Figure 2.21: TGA curve of DJP016

2.7: Summary

In summary, whilst there are some definite similarities between AIPO series catalysts and the α -zirconium phosphate catalyst, there are also several key differences. Even though all but one of the catalysts (DJP017) exhibit similar monoclinic crystal structure, the AIPO catalysts contain multiple phosphorous environments which are not present in α -ZrP. In addition α -ZrP does not contain an organic template, which could affect its ability as a catalyst. The structural differences shown in the IR spectra of the AIPO catalysts confirm that, in terms of structure, the catalysts differ slightly from one another despite having the same theoretical crystal structure and sharing the same space group.

It is also interesting to note the correlation between the “phasic purity” of the catalysts’ structures and the metals doped into them. Both the un-doped catalysts (α -ZrP and AIPO) retained their correct crystal structures and had high FoMs, as did the gallium (+3) doped AIPO since it has the same oxidation state as aluminium and has a similar ionic radius. Conversely the cobalt doped AIPO also has a high FoM and the highest surface area of all the AIPO catalysts tested but its visual appearance is very disorganised and XRD differs slightly from the other high FoM AIPOs. This contrasts with the titanium (+4) and zinc (+2) doped AIPO catalysts, which have oxidation states that differ from that of aluminium, have slightly different crystal structures and low FoMs, indicating that they contained more than one phase.

Chapter 3: Catalytic testing and results

3.1: Introduction

It was decided that two methods of analysis should be used to determine the catalytic efficiency of the selected catalysts. The first method was by measuring the amount of glycerol carbonate synthesised at the end of the reaction. This could be regarded as a normal method of determining catalytic efficiency, however it does not provide a very effective picture of the overall reaction as it only provides data for the chosen endpoint of the reaction.

The second method was to measure the amount of ammonia released over the duration of the reaction. The results generated from this method are, by themselves, less useful than the absolute yield of glycerol carbonate produced. However, when this data is combined with the yields synthesised, a more complete picture is built up. As previously stated, when the reaction proceeds, 2 moles of ammonia are evolved for every mole of glycerol carbonate synthesised. Therefore by correlating the moles of ammonia and glycerol carbonate it appears possible to determine how efficient the catalyst is in aiding the synthesis of glycerol carbonate. Any difference between the 2:1 molar ratio could indicate that other side-products are being synthesised or that there are issues with the catalyst, such as a loss of efficiency through the reaction.

3.2: Method development and reaction set-up

A series of experiments was carried out, to find the optimum conditions to conduct the catalytic testing. The first series of experiments determined the type of reaction set-up to be used, while the second series of experiments determined the optimum reaction conditions to synthesise glycerol carbonate.

There were many variables to take into consideration when determining the reaction set-up. One method was to conduct the reaction at atmospheric pressure, with nitrogen bubbled through the reaction solution to remove the ammonia produced and to provide an inert environment. The second method involved conducting the reaction, with a similar set-up, under a reduced pressure of around 20 millibar. The reaction set-up comprised a round bottom flask, single-necked for the experiments conducted under vacuum and two-necked for the experiments conducted under nitrogen, connected to a jacketed water condenser. If the reaction was to be conducted at atmospheric pressure then a Dreschel bottle was attached, via tubing, to the top of the condenser. However if the reaction was to be carried out under reduced pressure then the top of the condenser was attached to a rotary-vane pump and the Dreschel bottle attached to the exhaust port of the vacuum pump.

The Dreschel bottle was filled with 500 ml of distilled water and used to trap the ammonia evolved from the reactions as ammonium hydroxide. This allowed for easy quantification of ammonia evolved as this could be calculated by using a simple titration. By titrating a 50 ml aliquot taken from the Dreschel bottle with 1M hydrochloric acid (HCl) the moles of ammonia can be calculated. From this, the mass of ammonia evolved was calculated and plotted against the amount of glycerol carbonate synthesised as shown in Figure 3.1. The red plots correlate to testing conducted at atmospheric pressure with a N₂ stream with black showing the experiments that were conducted under vacuum. The black trendline is the trend of the data set whilst the red trendline shows the ideal ammonia to glycerol carbonate ratio.

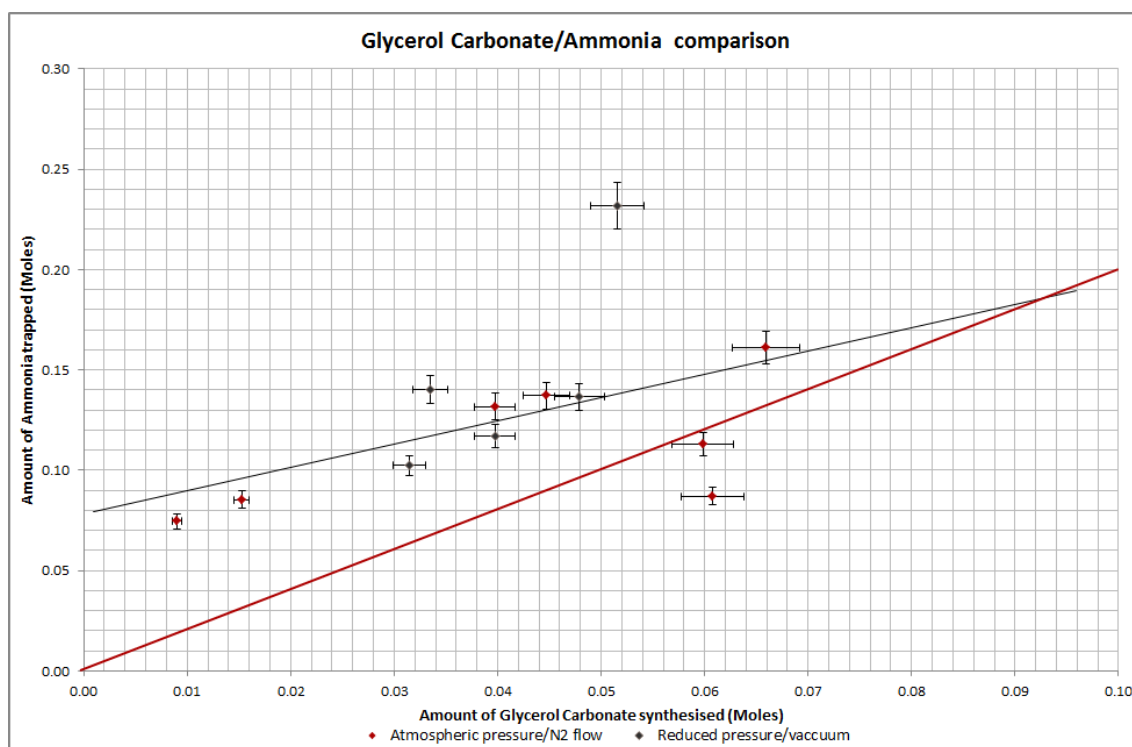


Figure 3.1: Correlation between glycerol carbonate and ammonia evolved

As can be seen in Figure 3.1 there is a strong correlation within the data set. However this does not entirely correlate with the anticipated ammonia:glycerol carbonate ratio of 2:1, with only one data point being within a 5% error of the ideal. Although this may in part be caused by the method of ammonia capture (with some of the ammonia lost in the vacuum pump for the reactions carried out under vacuum). Therefore, it was decided that the main catalytic testing would be carried out under vacuum as it was a simpler reaction set-up and reduced the risk of potential contaminants and leakages. The round bottom flask would be charged with 9.0g of urea, 20.7g of glycerol (a molar ratio of 1:1.5) and 0.1g of the chosen catalyst. The reaction would be heated to between 138 - 142°C for 3 hours.

3.3: Results

3.3.1: Ammonia capture results

As alluded to in section 3.2, the ammonia that is evolved during the reaction is “trapped” in a Dreschel bottle containing 500 ml of distilled water. For each catalytic test, the amount of ammonia produced was monitored every 30 minutes. For each data set, 3x 50 ml aliquots of ammonia hydroxide solution were removed from the Dreschel bottle and titrated against 1M HCl solution with phenolphthalein as the indicator.

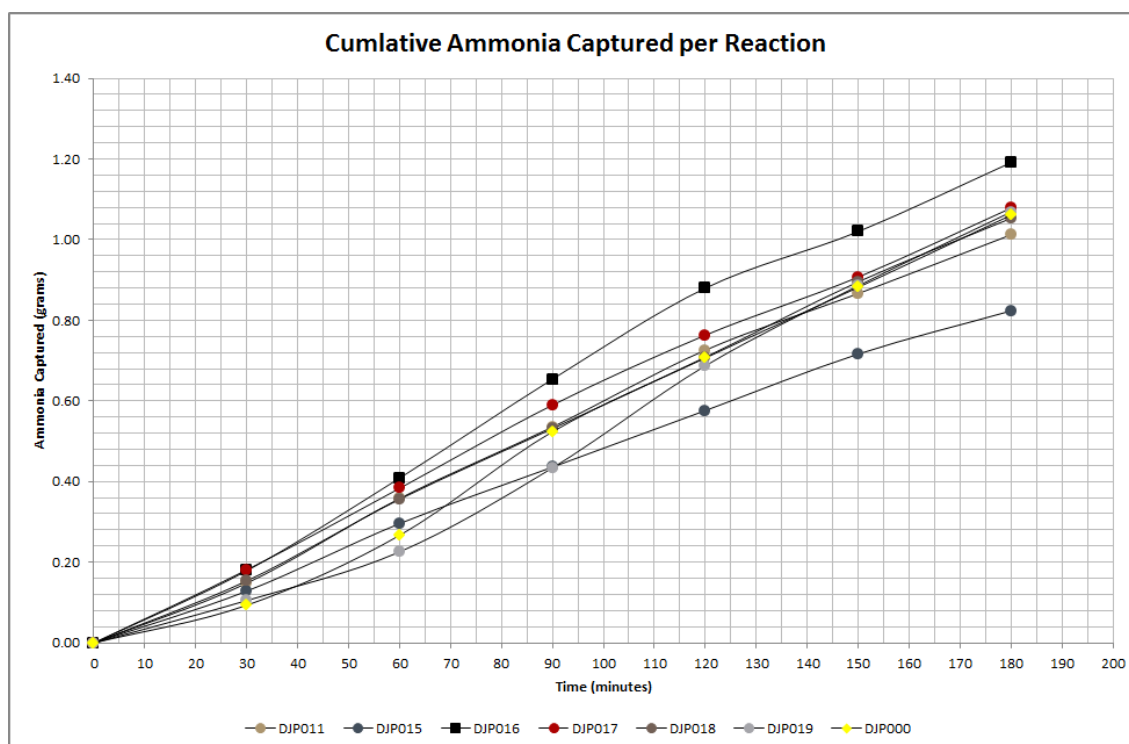


Figure 3.2: Graph showing the cumulative ammonia captured per reaction

These results were then recorded (Appendix 5.1) and plotted as a function of time (Figure 3.2). As can be seen from the figure above, all the reactions proceeded to release ammonia at similar rates with the exceptions of DJP016 and DJP015 which were above and below the group average respectively.

All but two of the reactions, the un-catalysed control (DJP000) and DJP019, show a steady rise in the amount of ammonia produced through the first 90-120 minutes and then a gradual levelling out/decrease in the amount of ammonia evolved. The un-catalysed reaction (DJP000) and DJP019 instead shows a gentle “S” curve plot. This is

interesting as it shows that when compared with the catalysed reactions, the initial release of ammonia is much slower in the first hour, however it then rapidly starts to increase over the next 30 to 60 minutes until it stabilises out.

3.3.2: Glycerol carbonate yields

Accurately determining the amount of glycerol carbonate synthesised during the catalytic reaction proved difficult, since the reaction mixture contained several different polyols and unreacted glycerol all of which have very high boiling points (>290°C at atmospheric pressure). To complicate matters further, glycerol, glycerol carbonate and the polyol side-products are all structurally similar and therefore their physical chemical properties such as polarity, viscosity and hygroscopy are similar. This means that classical methods of separation, such as organic extraction (as suggested and used by Aresta *et al.* [45], [58]) or column chromatography did not provide satisfactory results. The only other method of extraction which could be used was fraction distillation under vacuum. However since the amounts that were being used were small, this was not a practical set-up with regard to the equipment available. Therefore another method for quantifying the amount of glycerol carbonate synthesised was required.

The method that was instead chosen to quantify the amount of glycerol carbonate synthesised was ^{13}C NMR spectroscopy. It was felt that ^{13}C NMR offered the best balance between time taken to calculate the yield of glycerol carbonate and accuracy of results. In order to use ^{13}C NMR as a quantitative analytical technique, a method of correlating peak area to the amount of glycerol carbonate present in the sample was needed. To that effect, a range of standard samples comprising of different glycerol:glycerol carbonate ratios were prepared. Glycerol:glycerol carbonate standards with ratios between 90:10 and 30:70 were produced. From these NMR spectra, the four glycerol carbonate peaks were identified and their integrals plotted, to form calibration curves. It is believed this method of quantification should be accurate to within $\pm 10\%$ of the actual yield. From the results collected for each

reaction, the best two results were used to calculate the amount of glycerol carbonate synthesised per reaction and the yield with respect to urea. This is shown in Table 3.1.

Table 3.1: Processed data showing the mass and yields of glycerol carbonate

Catalyst	Reaction	Estimated GC (%w/w)	Estimated GC mass (g)	Estimated Average GC mass (g)	Estimated % yield for GC wrt Urea
DJP000	a	17.45%	4.276	3.750	21.21%
	b	12.57%	3.224		
DJP011	a	13.63%	3.223	3.201	18.11%
	b	13.03%	3.179		
DJP015	a	14.03%	3.524	3.193	18.06%
	b	11.26%	2.862		
DJP016	a	20.98%	5.181	4.771	26.98%
	b	16.28%	4.362		
DJP017	a	15.36%	3.887	3.734	21.12%
	b	13.70%	3.581		
DJP018	a	15.34%	3.930	3.739	21.15%
	b	13.77%	3.548		
DJP019	a	21.32%	5.897	5.658	32.00%
	b	19.80%	5.419		

As shown in the table above, most reactions produced a similar amount of glycerol carbonate with the exception of the reactions conducted with DJP016 and DJP019. The average yield is approximately 22.66%, the reaction catalysed by DJP015 produces a yield that is 25% lower than the average and DJP019 40% above average. These results raise two interesting points; the amount of glycerol carbonate synthesised is, for the most part, not affected by the choice of catalyst used and that the worst performing and best performing catalysts both share the same crystal structure.

3.4: Summary

Both the ammonia captured and glycerol carbonate synthesised seem to show similar trends, with the majority of the catalysts showing no change in yield or catalytic activity when compared to an un-catalysed reaction. Although the reaction containing DJP016 evolved the most ammonia, DJP019 produced the largest yield of glycerol carbonate. However these results are within the experimental error.

Theoretically the reaction to form glycerol carbonate, assuming the reaction favourably produces glycerol carbonate and not side-products, produces two moles of ammonia for every one mole of glycerol carbonate. Therefore there should be a strong correlation between moles produced, of both ammonia and glycerol carbonate, and catalytic performance. This correlation is shown in Table 3.2, where the average molar ratio is 1.9:1. However, with the exception of DJP019 all of the catalysts tested would fall within a 10% experimental error of each other potentially suggesting that DJP019 is the only catalyst exhibiting useful catalytic properties.

Table 3.2: Table comparing molar ratios of glycerol carbonate and ammonia

Catalyst	Mass of glycerol carbonate (g)	Molar ratio			Mass of ammonia (g)
		Glycerol carbonate	:	Ammonia	
DJP000	3.750	1.0	:	2.0	1.061
DJP011	3.201	1.0	:	2.3	1.012
DJP015	3.193	1.0	:	1.9	0.823
DJP016	4.771	1.0	:	1.8	1.191
DJP017	3.734	1.0	:	2.1	1.078
DJP018	3.739	1.0	:	2.1	1.053
DJP019	5.658	1.0	:	1.4	1.069

Chapter 4: Conclusions and future work

4.1: Conclusions

Surface area analysis of the catalysts has produced some interesting results, with all surface areas being less than 20m^2 . This is lower than expected when compared to traditional AlPOs and zeolites, especially for catalysts, where the greater surface area can allow a higher catalytic activity. Despite the low surface area, the catalytic activity has been satisfactory, with the average yield of glycerol carbonate being approximately 23% and the best catalyst yielding 32%. Similar work has been carried out by Aresta *et al.* [45], in which the gamma form of zirconium phosphate is used to catalyse the reaction, producing an average yield of 50.5% [58]. However without being able to replicate the exact testing conditions used by Aresta *et al.* it is impossible to definitively say whether γ -ZrP is a better catalyst than the doped or un-doped AlPOs.

One hypothesis as to why lower yields of glycerol carbonate were obtained (compared to when using a γ -ZrP catalyst) is that the catalysts synthesised during this project exhibit lower surface areas. A lower surface area means there will be fewer potential acid sites available for the catalytic reaction to take place and therefore more catalyst is required to produce the same yield. The lower surface area is in part caused by the chosen method of synthesis, which produces a larger crystal structure compared to other methods. It is also important to note the differences between the gamma and alpha forms of zirconium phosphate and their related catalytic effectiveness. Comparing the results obtained by Aresta *et al.* using γ -ZrP compared to the testing carried out on α -ZrP it appears that γ -ZrP is a better catalyst than α -ZrP. This could possibly be explained by difference in the chemical structure of the two forms: whereas α -ZrP $[\text{Zr}(\text{HPO}_4)_2 \cdot \text{H}_2\text{O}]$ is much more tightly bonded and co-ordinated when compared with γ -ZrP $[\text{Zr}(\text{PO}_4)(\text{H}_2\text{PO}_4) \cdot 2\text{H}_2\text{O}]$, which has an inherently more “flexible” structure because of its higher water content.

Another factor to consider is that of selectivity of the catalyst and the effect of the template present in the AlPOs synthesised. It was decided that after synthesising the AlPOs that they would not be calcined to remove the ethylenediamine template as this could lead to a possible collapse of the layered structure. Instead it was postulated that since the reaction is carried out at a temperature slightly greater than that of the boiling point of ethylenediamine, it would be removed from the AlPO structure during the reaction and instead the glycerol/urea reaction media would enter the catalyst allowing the catalytic reaction to take place more efficiently. Since the reaction was carried out at just above the boiling point of ethylenediamine the template should have evaporated, especially since the reaction was carried out under a reduced pressure thus reducing the boiling point further. However, traces of ethylenediamine should still be present in the reaction mixture at the end of the reaction. After studying the ^{13}C NMRs taken of the reaction solutions, there is no peak at approximately 44ppm, which would be indicative of ethylenediamine being present (see NMR below).

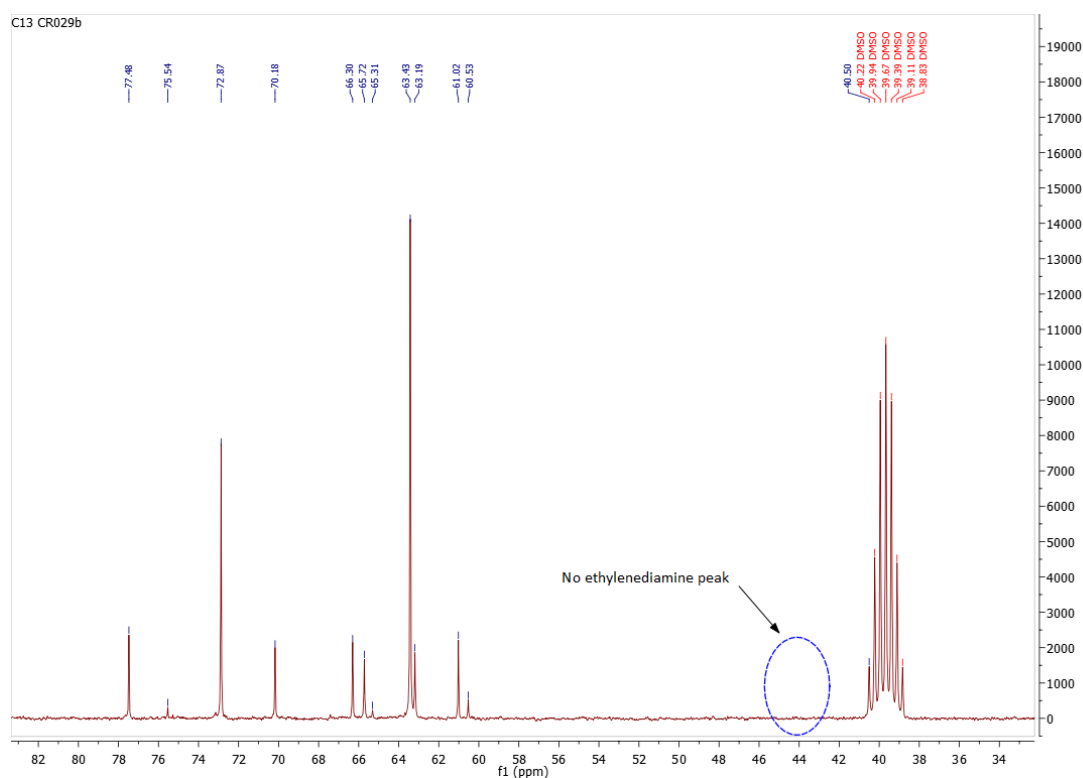


Figure 4.1: ^{13}C NMR of catalytic reaction showing no ethylenediamine peak

The absence of the ethylenediamine peak suggests that the template did not leave the catalysts as planned and therefore this could potentially explain why the AlPO catalysts did not perform as well as the α -ZrP catalyst. With the template still present in the

structure the majority of the internal surface would be blocked, denying any internal acid sites to the reaction. This greatly reduces the efficiency of the AlPO catalysts as all catalytic reactions would have to take place on the external surface only. Similarly, the proposed structure of the AlPOs (see Figure 4.2), suggests that if the template does not come out of the structure during the reaction then the hydrogen bonding interactions between the internal bridging hydroxyls (Brønsted acid sites) and the basic NH_2 groups in the ethylenediamine template will effectively reduce the acidity of the AlPO catalysts.

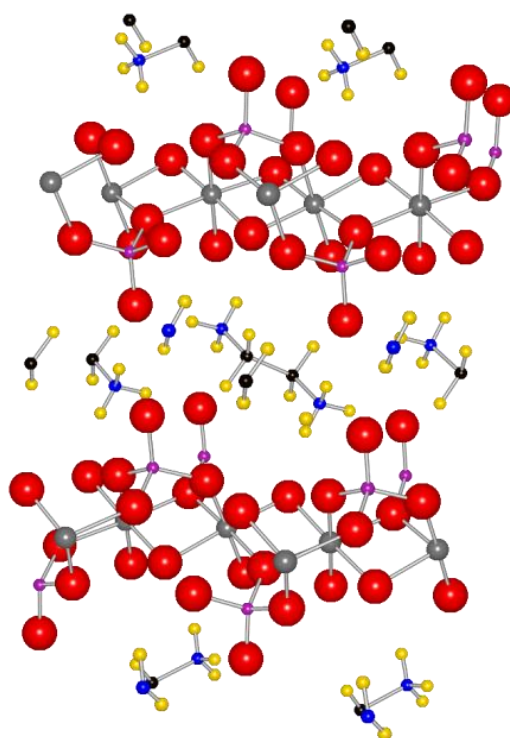


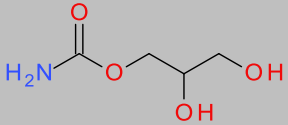
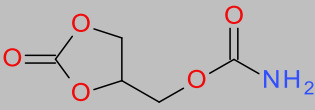
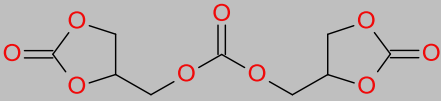
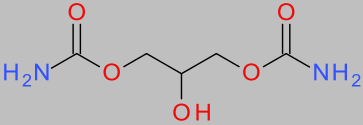
Figure 4.2: Proposed structure of undoped AlPO with template. Adapted from [59]
Key: Grey - aluminium, Red - oxygen, Purple – phosphorus, Black - carbon, Blue – nitrogen, Yellow - hydrogen

Similarly when comparing the ^{13}C NMR spectra of the reaction mixtures (Appendix 5.5) it is apparent that there are more peaks present than those which were anticipated (the peaks for glycerol, urea and glycerol carbonate). This suggests that side-products are forming in the reaction as well as glycerol carbonate. However analysing and quantifying these side-products is difficult for reasons listed previously. Since several of the compounds are chiral the ^1H NMRs display multiple sets of overlapping peaks making it almost impossible to differentiate between the “real” and other peaks caused by the chirality of the compounds. This makes the determination

of the products by NMR extremely difficult. Since it is also believed that the side-products will contain similar functional groups to those of both the starting materials and glycerol carbonate, they cannot be identified by FT-IR and as the compounds are not fluorescent this rules out analysis by UV-VIS spectroscopy.

This only leaves analysis by mass spectroscopy. However, this again presents a problem as the side-products are likely to have similar structures, therefore different compounds could produce similar mass fragments, especially since the compounds are quite bulky and therefore likely to be broken up when ionised. There are 4 unknown peaks in the 60 ppm to 80 ppm and 3 unknown peaks between 150 ppm and 158 ppm. Shown in the table below are the most likely unknown compounds that could match with the unknown ^{13}C peaks and results from GC-MS analysis.

Table 4.1: Potential unknown compounds found in reaction mixtures

Potential side-products identified	
	
Mass: 135.12 Type: reaction intermediate	Mass: 161.11 Type: side-product
	
Mass: 262.17 Type: side-product	Mass: 178.43 Type: side-product

It is interesting to find the reaction intermediate glycerol carbamate present in the GC-MS results, as it was thought that the carbamate would readily cyclise and form glycerol carbonate and not remain as glycerol carbamate. This points to a potential reason as to why the yield of glycerol carbonate was relatively low when compared to the work of Aresta *et al.* It suggests that there was not enough energy provided to the reaction to force the cyclisation (suggesting that the reaction had not completed after 3 hours) or that the catalyst present in the reaction did not reduce the activation energy of the second step sufficiently for it to proceed at a much quicker rate. This

could be caused by either the catalyst becoming poisoned/losing its efficiency too quickly or that the catalyst is instead more suited to catalysing the first stage and not the second stage of the reaction.

Although it has been confirmed that it is possible to dope different metals of different oxidation states into the AlPO structure, there appears to be no direct correlation between the amount doped in and any chemical properties of the metal chosen. This is unusual as it would be expected that metal atoms with a larger ionic radius than that of aluminium would find it harder to be doped into the structure. However, based on EDX analysis the following amounts of metals were substituted in place of aluminium; 35% for titanium, 42% for zinc, 22% for gallium and 5% for cobalt (all values based on atom% in the samples analysed). This suggests that other factors such as the solubility of the metal salt in the reaction mixture and the dispersion of the metal salt in the reaction mixture need to be examined.

4.2: Future work

There are several areas of potential future work within this project, including; acidity determination, structural differences between doped and un-doped catalysts, continuing to test the remaining synthesised catalysts, different catalyst to reactant ratios and forming catalysts with different templates.

Since the catalysts synthesised are being developed for their acidic properties, it is important to determine how acidic they are and how they compare to other known solid acid catalysts. The easiest and one of the most common methods of carrying out acidity testing is by temperature-programmed desorption of ammonia (NH₃-TPD). This method, as outlined by Takahara *et al.* [60], uses mass spectrometry to monitor the evolved ammonia during the test. However, the AlPO catalysts which were synthesised in this project still contain the ethylenediamine template, which when heated to decomposition will produce several products including ammonia. This would therefore, provide erroneous results and another method should be sought.

Another common way of determining the acidity of solid catalysts is to use FT-IR and treat the acid catalyst with a probe molecule. The most common probe molecule used is pyridine as it can be used to detect both Brønsted and Lewis acid sites. As reported by Reddy *et al.* [61] Brønsted acid sites show up 1540 cm⁻¹ and Lewis acid sites at 1450 cm⁻¹. The IR spectra were recorded between 1350 cm⁻¹ and 1650 cm⁻¹ using a DRIFTS cell attachment. The samples are heated for 1 hour at 100°C to remove any water that may be present in the sample. The sample (approx. 50 mg) is placed in the sample holder and exposed to a small quantity of pyridine. It is then placed into an oven at 120°C for 1 hour to remove any physisorbed pyridine. After allowing the sample to cool, it is placed in the DRIFTS cell and run for 250 scans with KBr used for the background. Alternatively, Zecchina *et al.* [62] have studied the use of ammonia and Armaroli *et al.* [63] have used the weakly basic acetonitrile as potential probe molecules for acid site determination using both FT-IR and DRIFTS techniques.

Schrader and Cheng [64] have used Raman spectroscopy to characterise the acid sites present in Co-Mo/ γ -Al₂O₃ catalysts using adsorbed pyridine as the probe molecule. For the samples to be tested the catalysts were prepared by pressing them into 13 cm disks. To analyse one of the disks, it was placed in a rotating cell (atmosphere controlled) and evacuated to 1.333×10^{-8} bar for 2 hours. After 2 hours the cell was exposed to pyridine vapours for 1 hour and then the Raman spectra were collected at room temperature. The rotating cell is required to prevent signal loss caused by the laser beam continually hitting the same point, resulting in damage to the sample.

Compared to NH₃-TPD and IR/Raman spectroscopy, solid state NMR is a relatively new technique for determining the acidity of solid catalysts. Zheng *et al.* [65] have reviewed 4 different molecules for their potential as probe molecules in conjunction with NMR analysis. The four different molecules chosen were; perdeuterated pyridine (pyridine-*d*₅), trimethylphosphine (³¹P-TMP), trimethylphosphine oxide (³¹P-TMPO) and ¹³C-acetone (2-¹³C-acetone). An idea as to the strength of the acid sites can be given by observing the chemical shift of the peak(s) in the NMR spectra whereas the peak intensity will give an indication of the number of acid sites present in the sample. By running multiple calibration standards the acidity of the solid catalysts can be determined with reasonable accuracy, however there are still several issues with using solid state NMR which need to be resolved. Both pyridine-*d*₅ and 2-¹³C-acetone can only be used to determine the Brønsted acidity of the catalysts, unlike ³¹P-TMP and ³¹P-TMPO which can be used to detect both Lewis and Brønsted acid sites. However, ³¹P-TMP is extremely pyrophoric and both ³¹P-TMP and ³¹P-TMPO are highly toxic meaning that sample preparation is much more complex. The other point for consideration is that the probe molecules reviewed are currently relatively expensive, however other potential and much cheaper probe molecules such as acetonitrile (acetonitrile-*d*₃) have been proposed for future study.

Similarly another area of potential work is that of altering the ratio of catalyst to reactant. As shown by the results from the doped AlPOs, the catalysts do help speed up the initial stage of the reaction however their effect tends to lessen mid-way

through the reaction cycle and ends up producing a similar amount of product as the un-catalysed reaction. As they do show an initial increase over that of the un-catalysed reaction, it is reasonable to assume that the doped metal AlPOs lose their catalytic properties much more quickly than that of DJP015. This means that if there was an increase in the amount of catalyst (in relation to the starting materials) present in the reaction, the yield of glycerol carbonate could be improved.

Another potential avenue of future work is to change the template used to synthesise the layered phosphate catalysts. Ethylenediamine is a short chained flat molecule and therefore the interlayer spacing in the structure of the AlPOs will be small, as the templating agent will lie in the plane that provides the least resistance (x,z not x,y). By varying the template, the interlayer spacing can be increased or decreased accordingly. If a template such as urea, or another branched chain molecule, was to be used in synthesising layered phosphate catalysts the interlayer spacing could be increased (due to its more “3-Dimensional shape”) increasing the surface area and potentially increasing the catalytic activity of the catalysts.

During this project several other doped metal phosphate catalysts were synthesised. Both the vanadium (V) and chromium (Cr) doped AlPOs contained approximately 25% doped metal, whereas both the gold (Au) and praseodymium (Pr) containing AlPOs were doped to approximately 10%. Both gold (0.85Å)[66] and praseodymium (0.99Å)[66] have much larger ionic radii when compared to the ionic radius of aluminium (0.535Å)[66], almost a 100% increase. Therefore although both metals were introduced in their +3 states, making it easier to form the doped AlPO, it was decided that in an attempt to keep the crystal structure similar to that of un-doped aluminium phosphate, a smaller quantity of the chosen metals would be doped in. However, the catalytic properties of these metals or the effect of the different crystal structures have on the glycerolysis reaction have yet to be tested and therefore, this remains one area that should be explored further.

4.3: Summary

During this project a series of doped and undoped metal phosphate catalysts have been successfully synthesised and characterised by various analytical means. Both the undoped AlPO and α -ZrP were highly crystalline single phase materials, with the doped AlPOs varying from a relatively pure single phase to amorphous materials. The catalysts ability in aiding the glycerolysis of urea was also tested and compared to work previously conducted by Aresta *et al.* [45]. Although glycerol carbonate was successfully synthesised the yields obtained were unfortunately comparable to that of the uncatalysed control reaction, an average yield of 23%. However, the results do provide an indication as to which catalysts display the highest selectivity, namely α -ZrP and DJP019; conversely the undoped AlPO was the least selective of the catalysts tested. Therefore, it is possible to say that the catalytic activity is as follows; DJP019>DJP016>DJP018>DJP011>DJP017>DJP015. This indicates that the dopent metal also has an effect on potential catalytic properties of the catalysts as well as their structure.

Several reasons as to why the catalysts did not perform in a similar manner to γ -ZrP have been discussed. This has led to possible future avenues of work which could potentially increase the catalytic effectiveness of the doped AlPOs; including doping different metals into the structure, changing the templating agent and calcining the catalysts before the reaction.

Appendices

Appendix 5.1: Ammonia capture data

Appendix 5.2: XRF spectra

Appendix 5.3: ^{27}Al NMR spectra

Appendix 5.4: 1D-MQMAS NMR spectra

Appendix 5.5: Annotated catalytic reaction NMRs

Appendix 5.6: Refined lattice and unit cell parameters

Appendix 5.1: Ammonia capture data

Table 5.1: Ammonia capture data for DJP011

Sample Number	Time (minutes)	Aliquot	Quantity of 1M HCl used (ml)	Quantity of Ammonia captured (g)	Standard Deviation of sample	Average quantity of Ammonia captured (g)	Cumulative average amount captured (g)
0	0	a	0.00	0.000	0.00000	0.000	0.000
		b	0.00	0.000			
		c	0.00	0.000			
1	30	a	3.80	1.332	0.00826	0.444	0.444
		b	3.85	1.349			
		c	3.85	1.349			
2	60	a	5.40	1.892	0.00826	0.631	1.075
		b	5.40	1.892			
		c	5.45	1.910			
3	90	a	4.55	1.594	0.00826	0.531	1.606
		b	4.50	1.577			
		c	4.50	1.577			
4	120	a	4.90	1.717	0.00826	0.572	2.178
		b	4.90	1.717			
		c	4.85	1.699			
5	150	a	3.60	1.261	0.00826	0.420	2.599
		b	3.65	1.279			
		c	3.65	1.279			
6	180	a	3.75	1.314	0.00826	0.438	3.037
		b	3.80	1.332			
		c	3.75	1.314			

Table 5.2: Ammonia capture data for DJP015

Sample Number	Time (minutes)	Aliquot	Quantity of 1M HCl used (ml)	Quantity of Ammonia captured (g)	Standard Deviation of sample	Average quantity of Ammonia captured (g)	Cumulative average amount captured (g)
0	0	a	0.00	0.000	0.00000	0.000	0.000
		b	0.00	0.000			
		c	0.00	0.000			
1	30	a	3.75	1.314	0.01652	0.438	0.438
		b	3.65	1.279			
		c	3.75	1.314			
2	60	a	5.70	1.997	0.01652	0.666	1.104
		b	5.70	1.997			
		c	5.60	1.962			
3	90	a	5.20	1.822	0.00826	0.607	1.711
		b	5.20	1.822			
		c	5.25	1.840			
4	120	a	4.40	1.542	0.01431	0.514	2.225
		b	4.45	1.559			
		c	4.35	1.524			
5	150	a	4.40	1.542	0.00826	0.514	2.739
		b	4.45	1.559			
		c	4.40	1.542			
6	180	a	4.20	1.472	0.00826	0.491	3.230
		b	4.20	1.472			
		c	4.15	1.454			

Table 5.3: Ammonia capture data for DJP016

Sample Number	Time (minutes)	Aliquot	Quantity of 1M HCl used (ml)	Quantity of Ammonia captured (g)	Standard Deviation of sample	Average quantity of Ammonia captured (g)	Cumulative average amount captured (g)
0	0	a	0.00	0.000	0.00000	0.000	0.000
		b	0.00	0.000			
		c	0.00	0.000			
1	30	a	4.60	1.612	0.01012	0.537	0.537
		b	4.60	1.612			
		c	4.65	1.629			
2	60	a	5.90	2.067	0.01012	0.689	1.226
		b	5.95	2.085			
		c	5.90	2.067			
3	90	a	6.30	2.208	0.01012	0.736	1.962
		b	6.30	2.208			
		c	6.25	2.190			
4	120	a	5.80	2.032	0.01012	0.677	2.640
		b	5.85	2.050			
		c	5.85	2.050			
5	150	a	3.60	1.261	0.00000	0.420	3.060
		b	3.60	1.261			
		c	3.60	1.261			
6	180	a	4.40	1.542	0.01012	0.514	3.574
		b	4.45	1.559			
		c	4.40	1.542			

Table 5.4: Ammonia capture data for DJP017

Sample Number	Time (minutes)	Aliquot	Quantity of 1M HCl used (ml)	Quantity of Ammonia captured (g)	Standard Deviation of sample	Average quantity of Ammonia captured (g)	Cumulative average amount captured (g)
0	0	a	0.00	0.000	0.00000	0.000	0.000
		b	0.00	0.000			
		c	0.00	0.000			
1	30	a	4.65	1.629	0.01012	0.543	0.543
		b	4.70	1.647			
		c	4.70	1.647			
2	60	a	5.20	1.822	0.01012	0.607	1.150
		b	5.15	1.805			
		c	5.20	1.822			
3	90	a	5.30	1.857	0.01012	0.619	1.770
		b	5.35	1.875			
		c	5.35	1.875			
4	120	a	4.45	1.559	0.00000	0.520	2.289
		b	4.45	1.559			
		c	4.45	1.559			
5	150	a	3.70	1.296	0.01012	0.432	2.721
		b	3.65	1.279			
		c	3.70	1.296			
6	180	a	4.40	1.542	0.01012	0.514	3.235
		b	4.45	1.559			
		c	4.40	1.542			

Table 5.5: Ammonia capture data for DJP018

Sample Number	Time (minutes)	Aliquot	Quantity of 1M HCl used (ml)	Quantity of Ammonia captured (g)	Standard Deviation of sample	Average quantity of Ammonia captured (g)	Cumulative average amount captured (g)
0	0	a	0.00	0.000	0.00000	0.000	0.000
		b	0.00	0.000			
		c	0.00	0.000			
1	30	a	3.95	1.384	0.01012	0.461	0.461
		b	3.90	1.367			
		c	3.90	1.367			
2	60	a	5.20	1.822	0.01012	0.607	1.069
		b	5.25	1.840			
		c	5.25	1.840			
3	90	a	4.50	1.577	0.00000	0.526	1.594
		b	4.50	1.577			
		c	4.50	1.577			
4	120	a	4.55	1.594	0.01012	0.531	2.126
		b	4.60	1.612			
		c	4.60	1.612			
5	150	a	4.80	1.682	0.00000	0.561	2.686
		b	4.80	1.682			
		c	4.80	1.682			
6	180	a	4.05	1.419	0.01012	0.473	3.159
		b	4.05	1.419			
		c	4.00	1.402			

Table 5.6: Ammonia capture data for DJP019

Sample Number	Time (minutes)	Aliquot	Quantity of 1M HCl used (ml)	Quantity of Ammonia captured (g)	Standard Deviation of sample	Average quantity of Ammonia captured (g)	Cumulative average amount captured (g)
0	0	a	0.00	0.000	0.00000	0.000	0.000
		b	0.00	0.000			
		c	0.00	0.000			
1	30	a	2.70	0.946	0.04046	0.315	0.315
		b	2.50	0.876			
		c	2.50	0.876			
2	60	a	3.10	1.086	0.02023	0.362	0.677
		b	3.10	1.086			
		c	3.00	1.051			
3	90	a	5.35	1.875	0.01012	0.625	1.302
		b	5.35	1.875			
		c	5.30	1.857			
4	120	a	6.50	2.278	0.01012	0.759	2.062
		b	6.50	2.278			
		c	6.55	2.295			
5	150	a	5.10	1.787	0.01012	0.596	2.657
		b	5.15	1.805			
		c	5.15	1.805			
6	180	a	4.70	1.647	0.01012	0.549	3.206
		b	4.75	1.664			
		c	4.70	1.647			

Table 5.7: Ammonia capture data for un-catalysed reaction

Sample Number	Time (minutes)	Aliquot	Quantity of 1M HCl used (ml)	Quantity of Ammonia captured (g)	Standard Diviation of sample	Average quantity of Ammonia captured (g)	Cumulative average amount captured (g)
0	0	a	0.00	0.000	0.00000	0.000	0.000
		b	0.00	0.000			
		c	0.00	0.000			
1	30	a	2.40	0.841	0.00000	0.280	0.280
		b	2.40	0.841			
		c	2.40	0.841			
2	60	a	4.45	1.559	0.01012	0.520	0.800
		b	4.40	1.542			
		c	4.40	1.542			
3	90	a	6.60	2.313	0.02023	0.771	1.571
		b	6.50	2.278			
		c	6.60	2.313			
4	120	a	4.70	1.647	0.00000	0.549	2.120
		b	4.70	1.647			
		c	4.70	1.647			
5	150	a	4.50	1.577	0.00000	0.526	2.646
		b	4.50	1.577			
		c	4.50	1.577			
6	180	a	4.60	1.612	0.01012	0.537	3.183
		b	4.65	1.629			
		c	4.65	1.629			

Appendix 5.2: XRF spectra

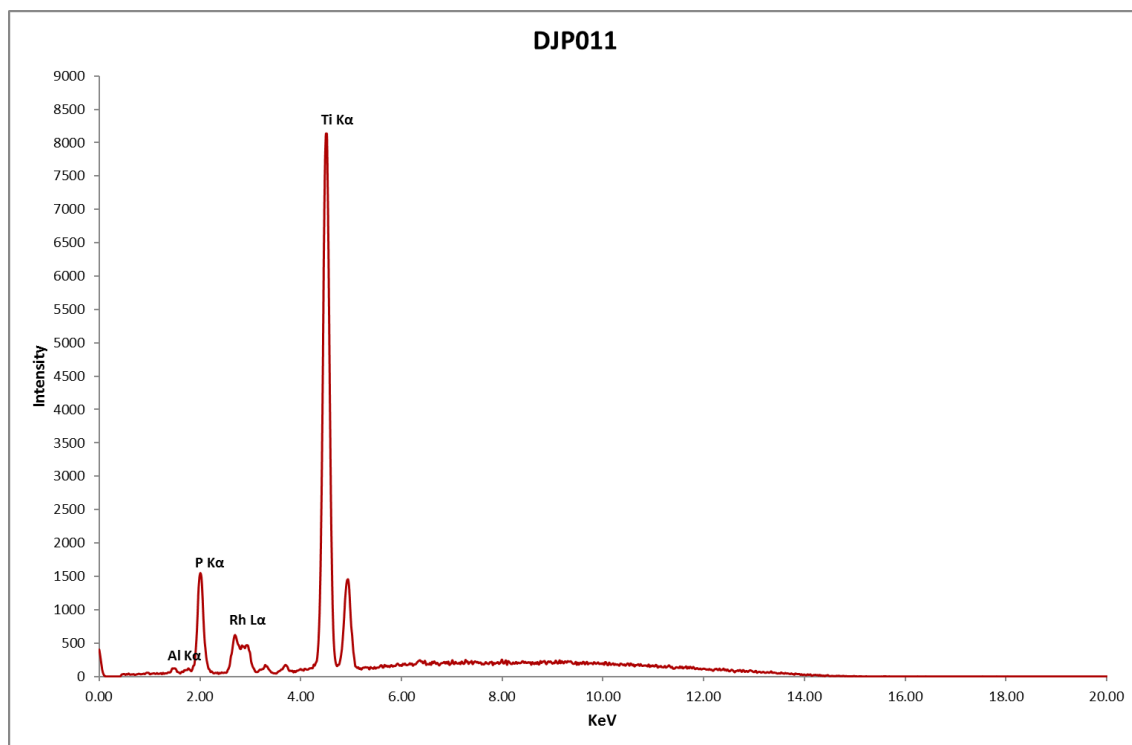


Figure 5.1: XRF spectrum for DJP011

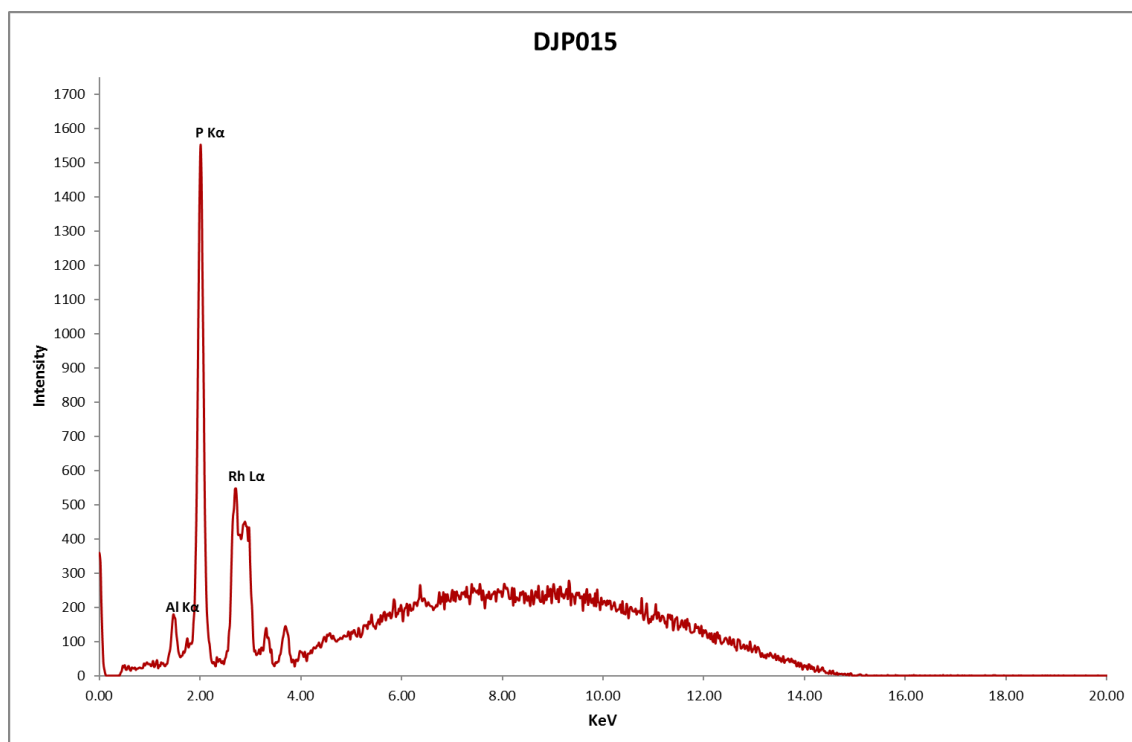


Figure 5.2: XRF spectrum for DJP015

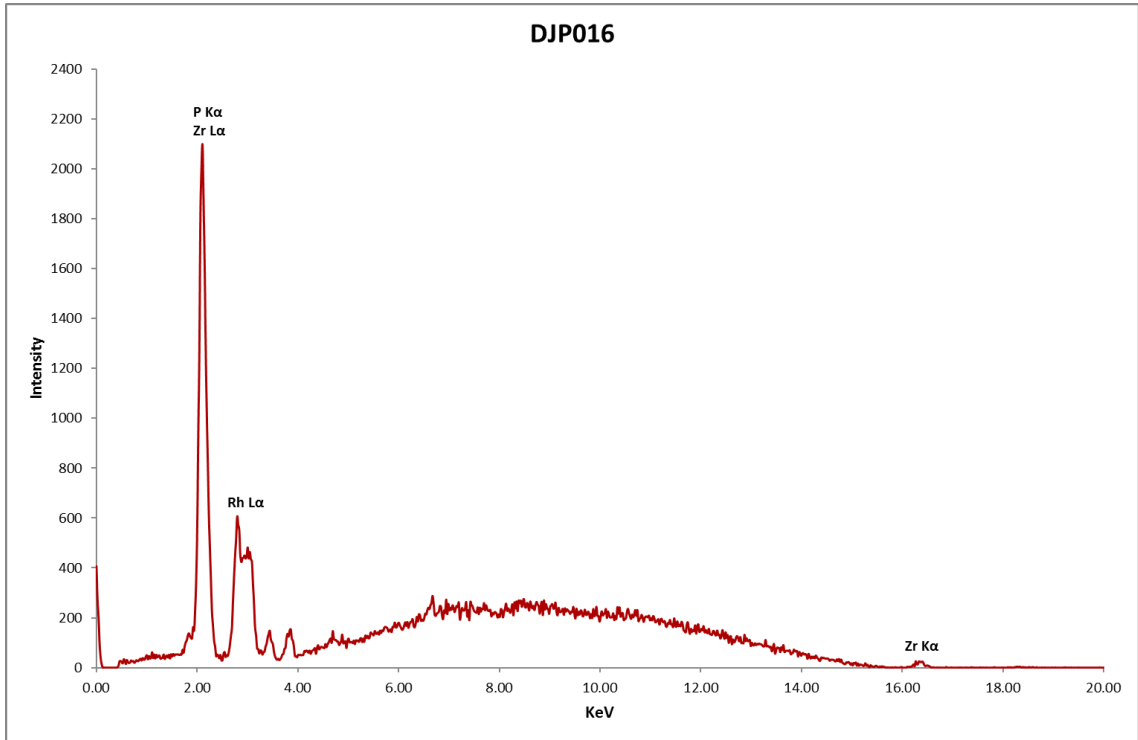


Figure 5.3: XRF spectrum for DJP016

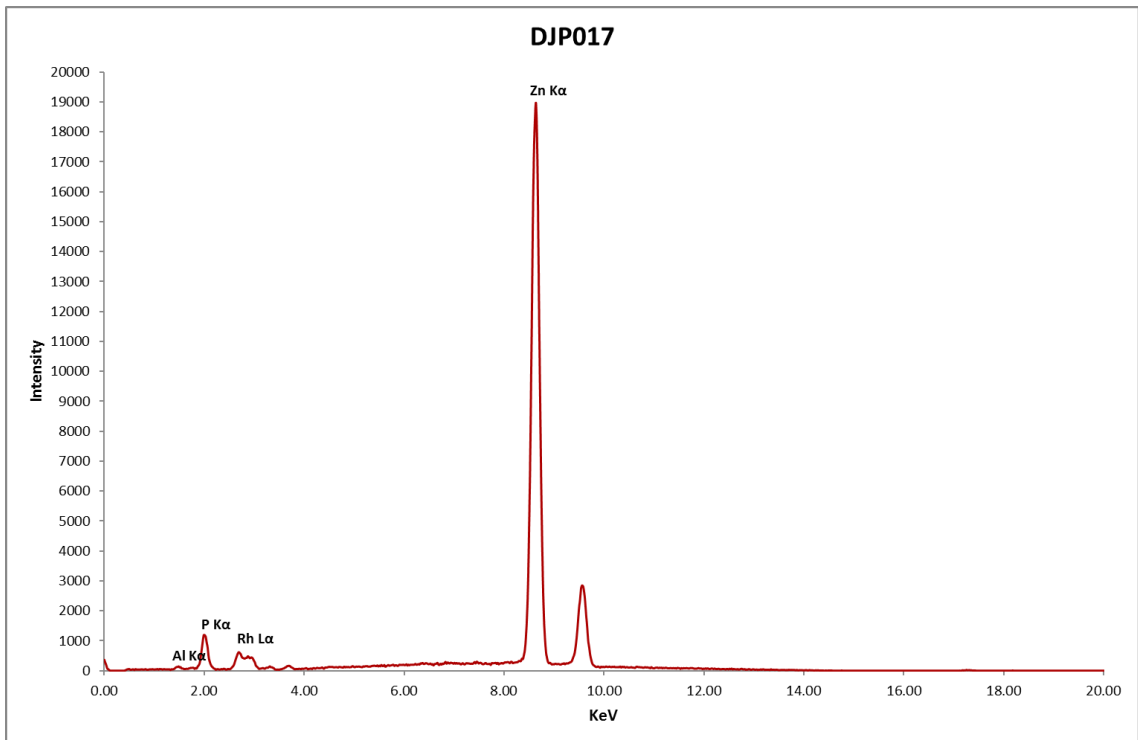


Figure 5.4: XRF spectrum for DJP017

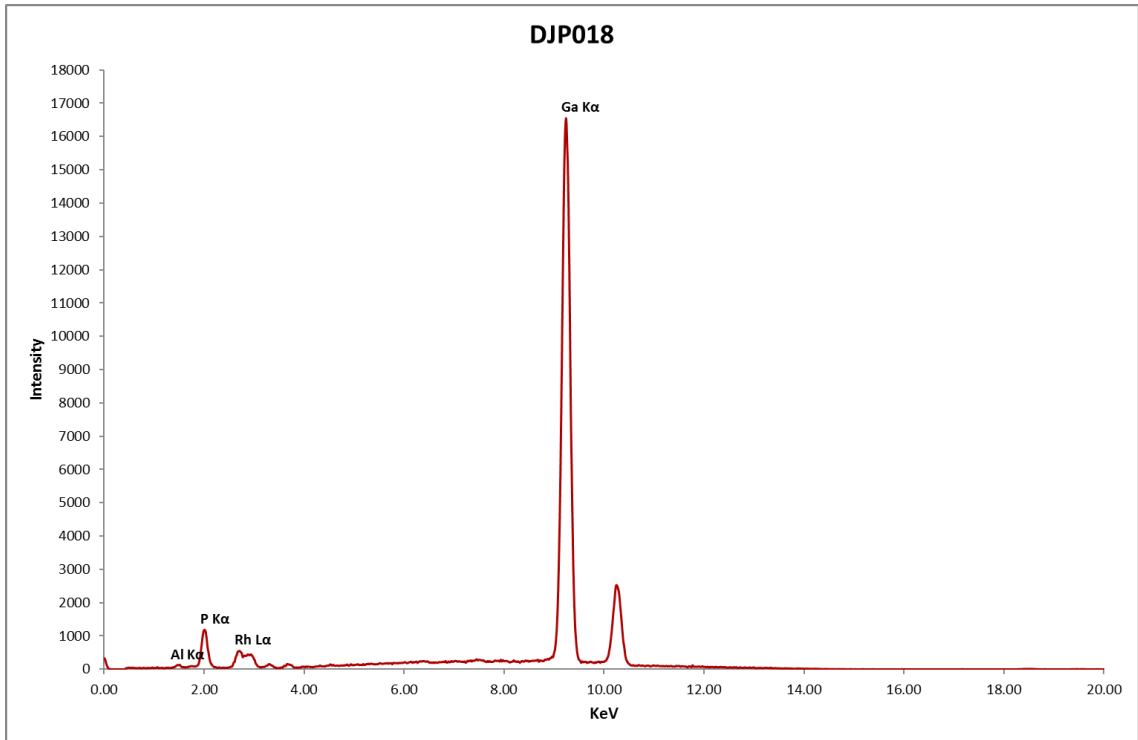


Figure 5.5 XRF spectrum for DJP018

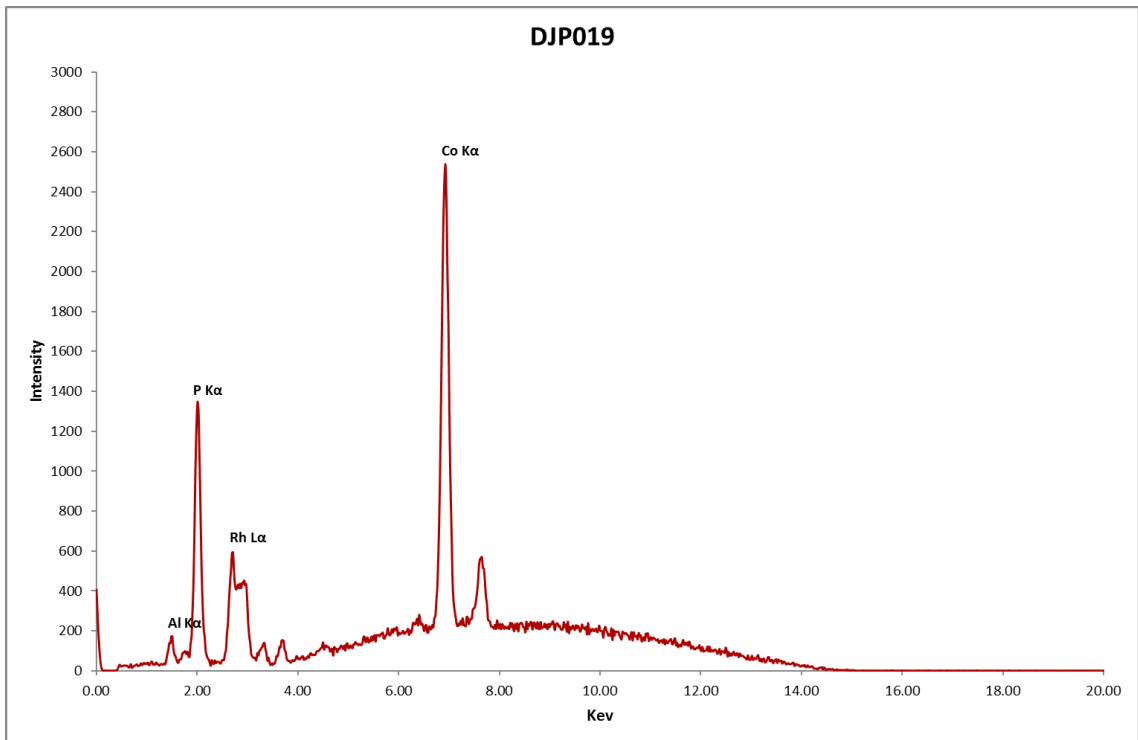


Figure 5.6 XRF spectrum for DJP019

Appendix 5.3: ^{27}Al NMR spectra

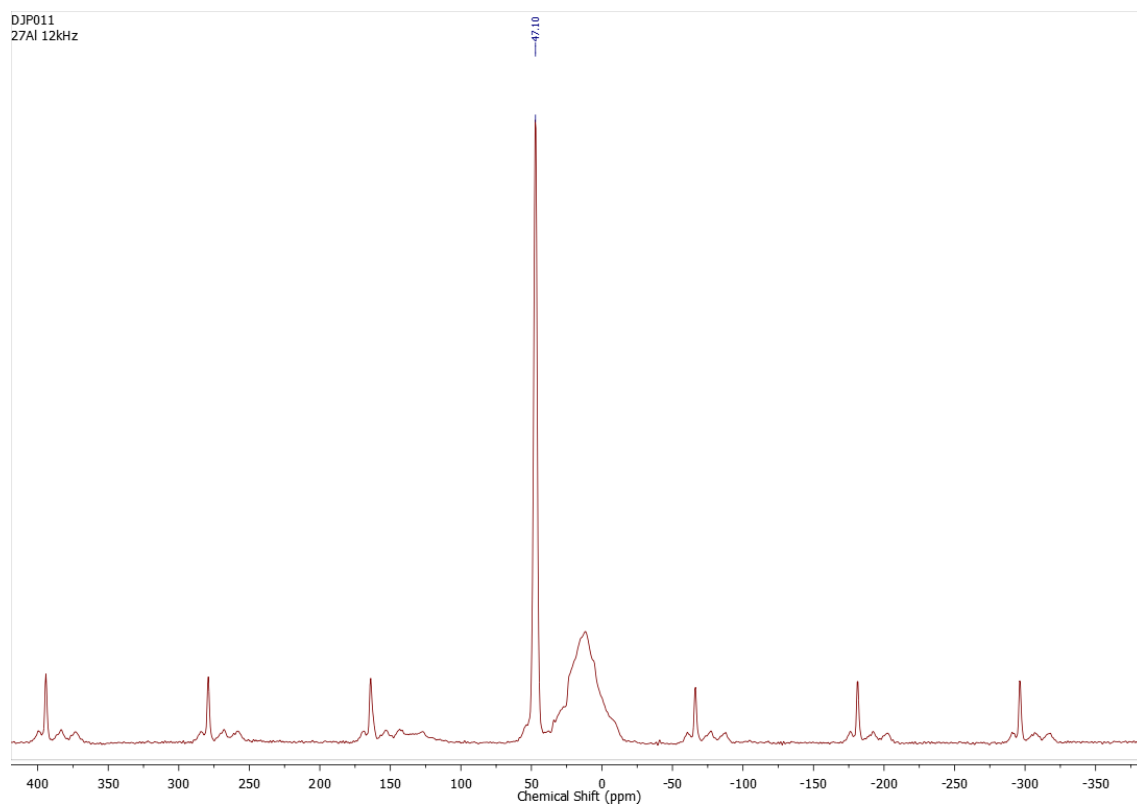


Figure 5.7: ^{27}Al NMR spectrum of DJP011

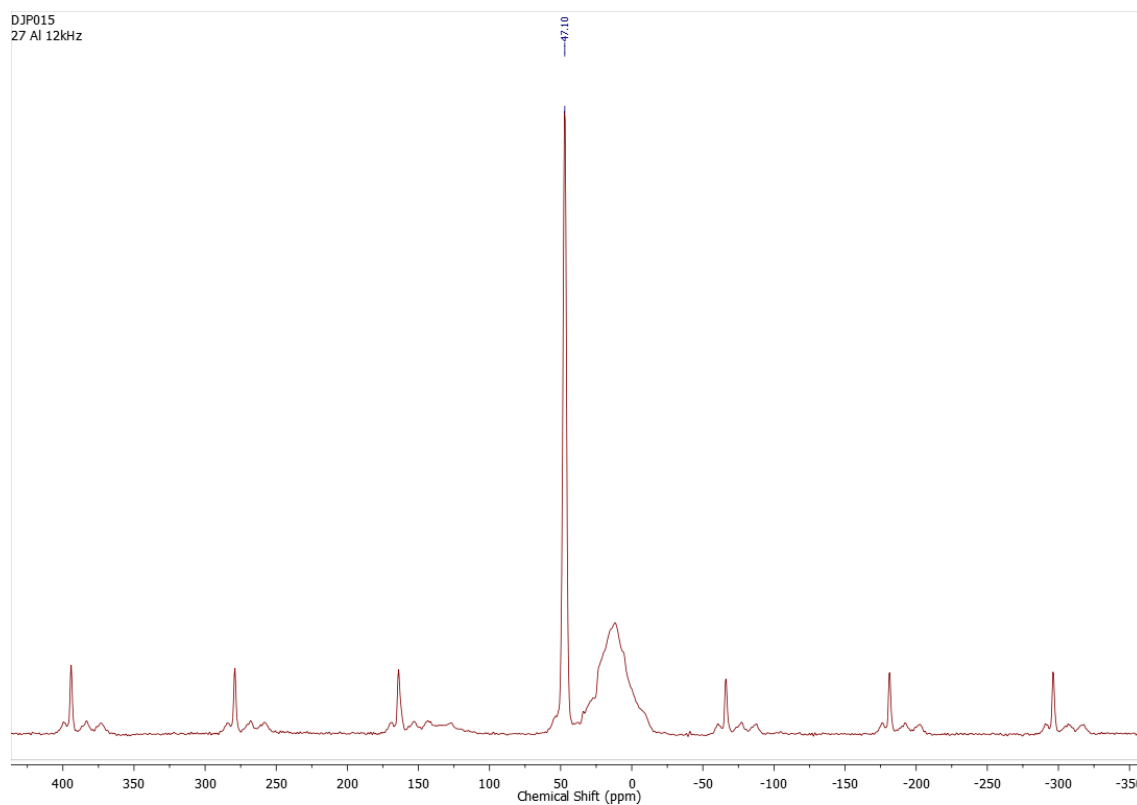


Figure 5.8: ^{27}Al NMR spectrum of DJP015

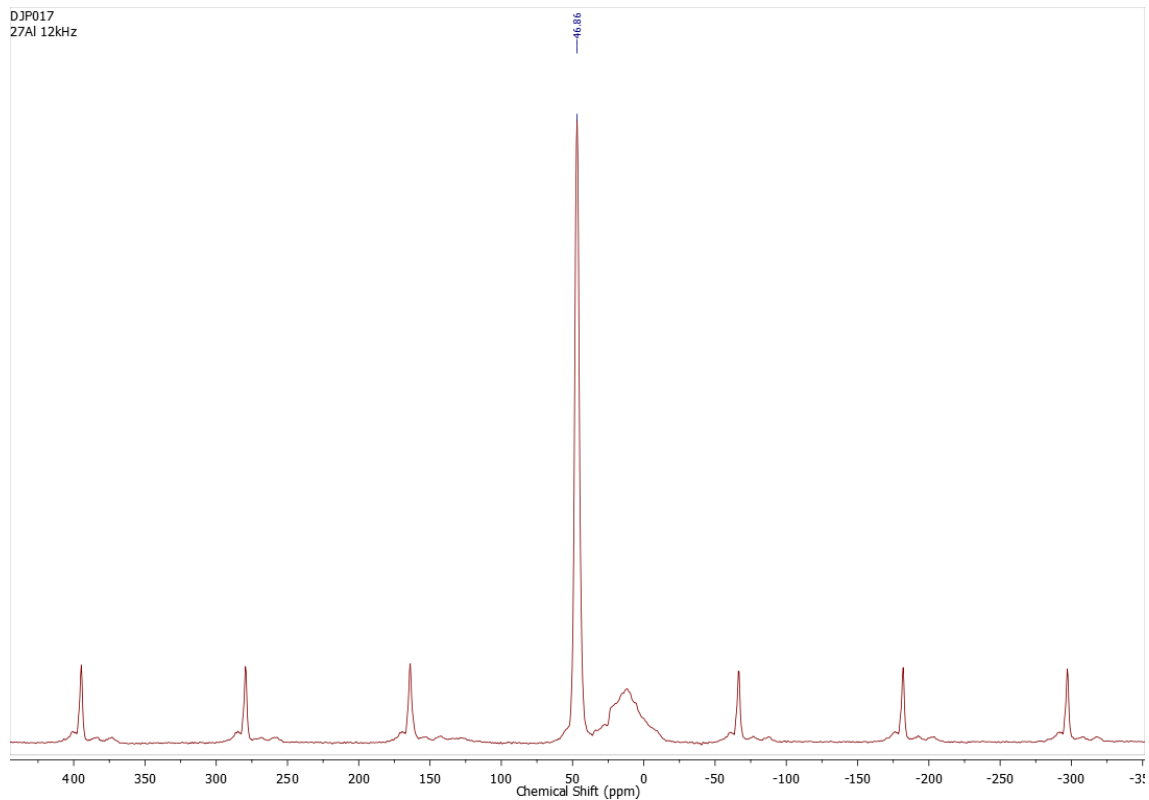


Figure 5.9: ^{27}Al NMR spectrum of DJP017

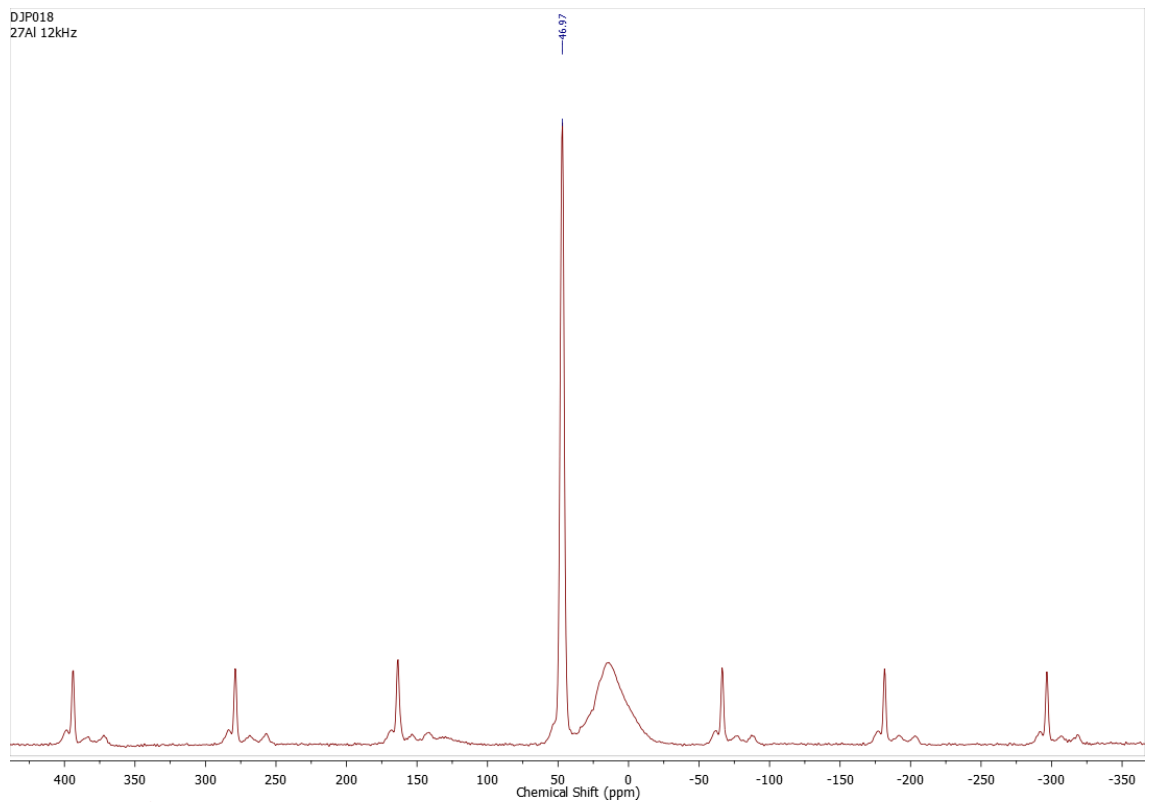


Figure 5.10: ^{27}Al NMR spectrum of DJP018

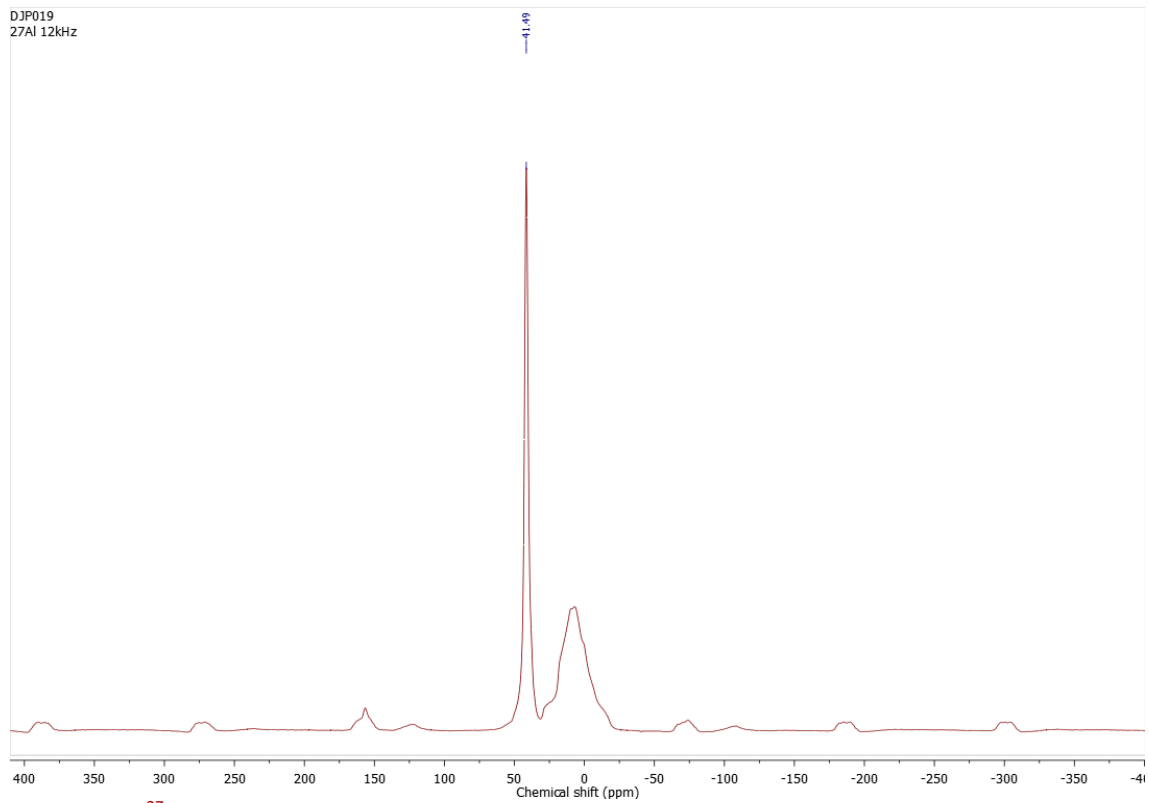


Figure 5.11: ^{27}Al NMR spectrum of DJP019

Appendix 5.4: 1D-MQMAS NMR spectra

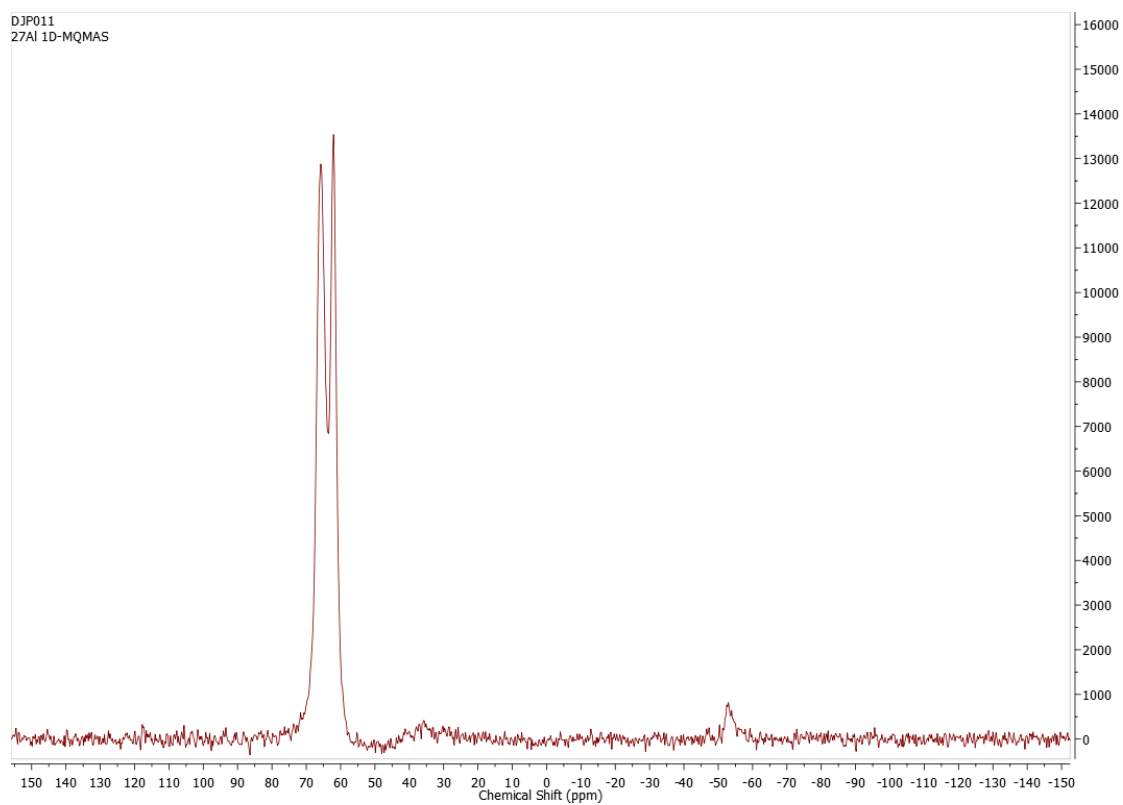


Figure 5.12: 1D-MQMAS spectrum of DJP011

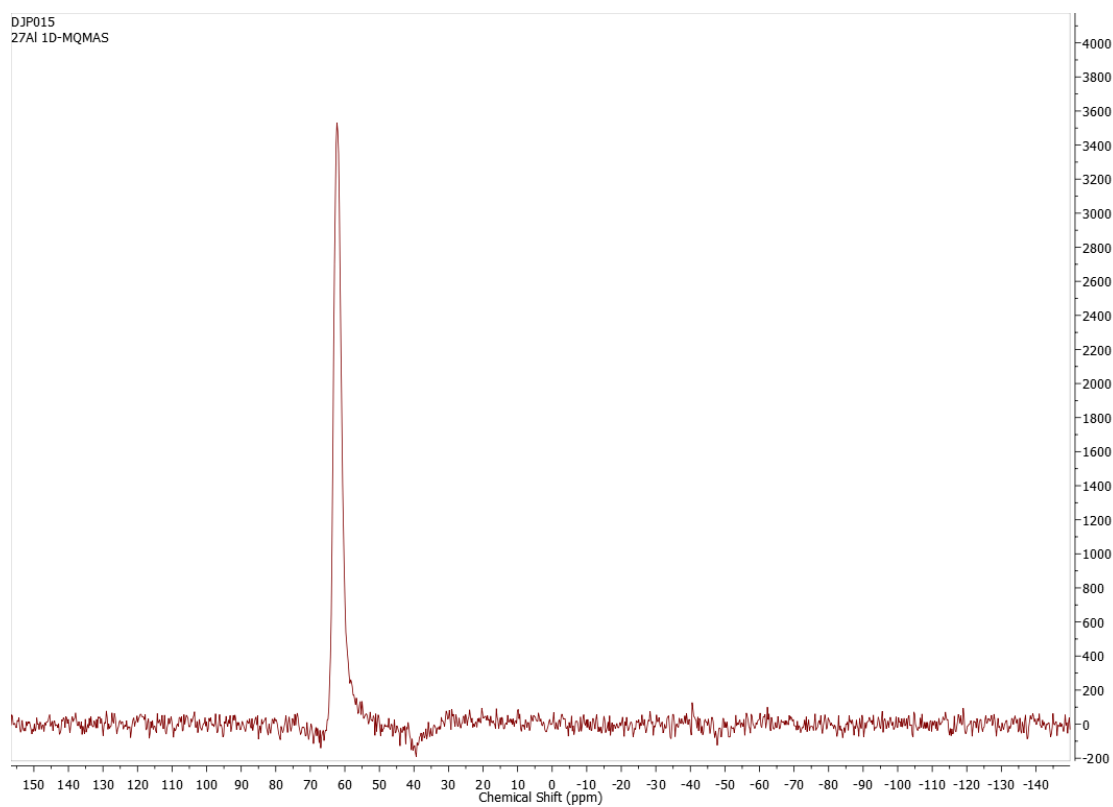


Figure 5.13: 1D-MQMAS spectrum of DJP015

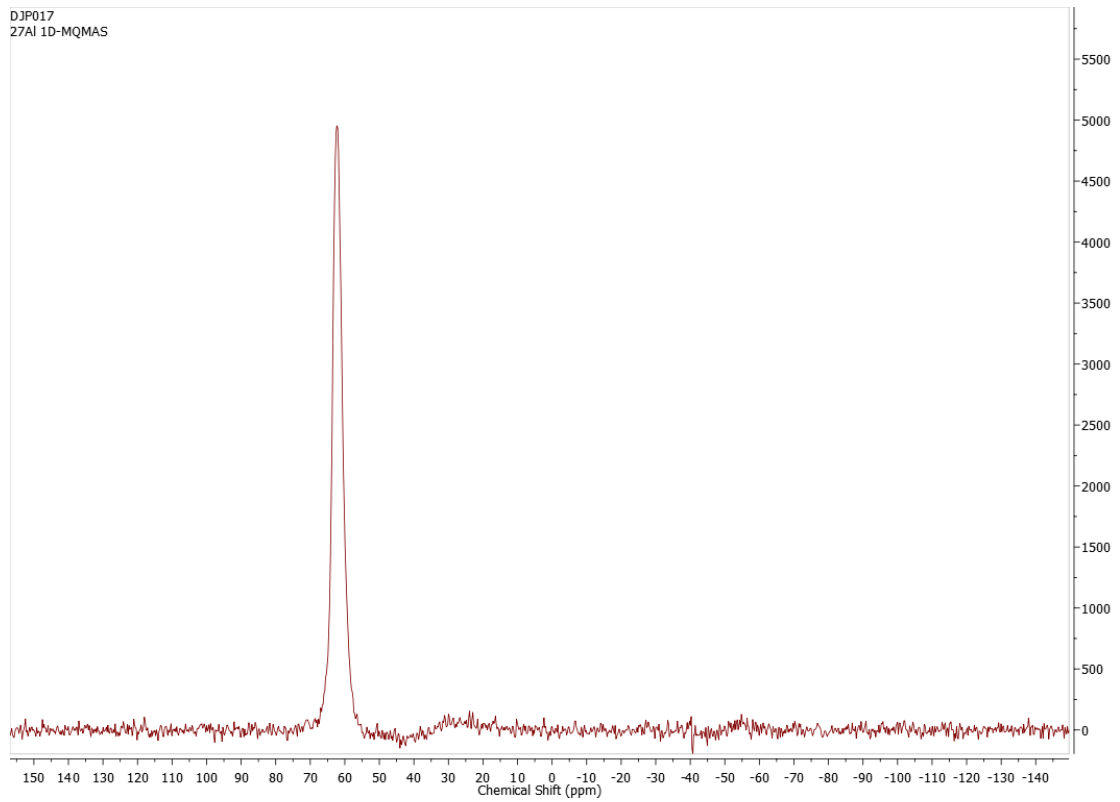


Figure 5.14: 1D-MQMAS spectrum of DJP017

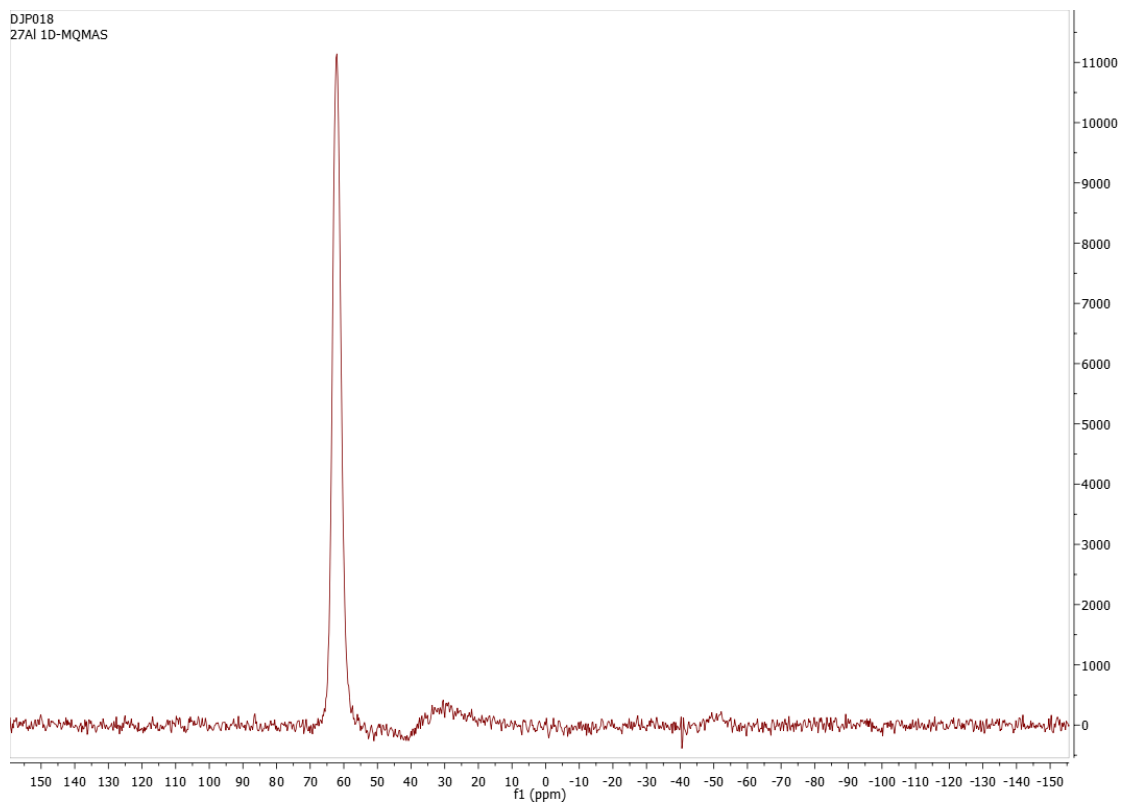


Figure 5.15: 1D-MQMAS spectrum of DJP018

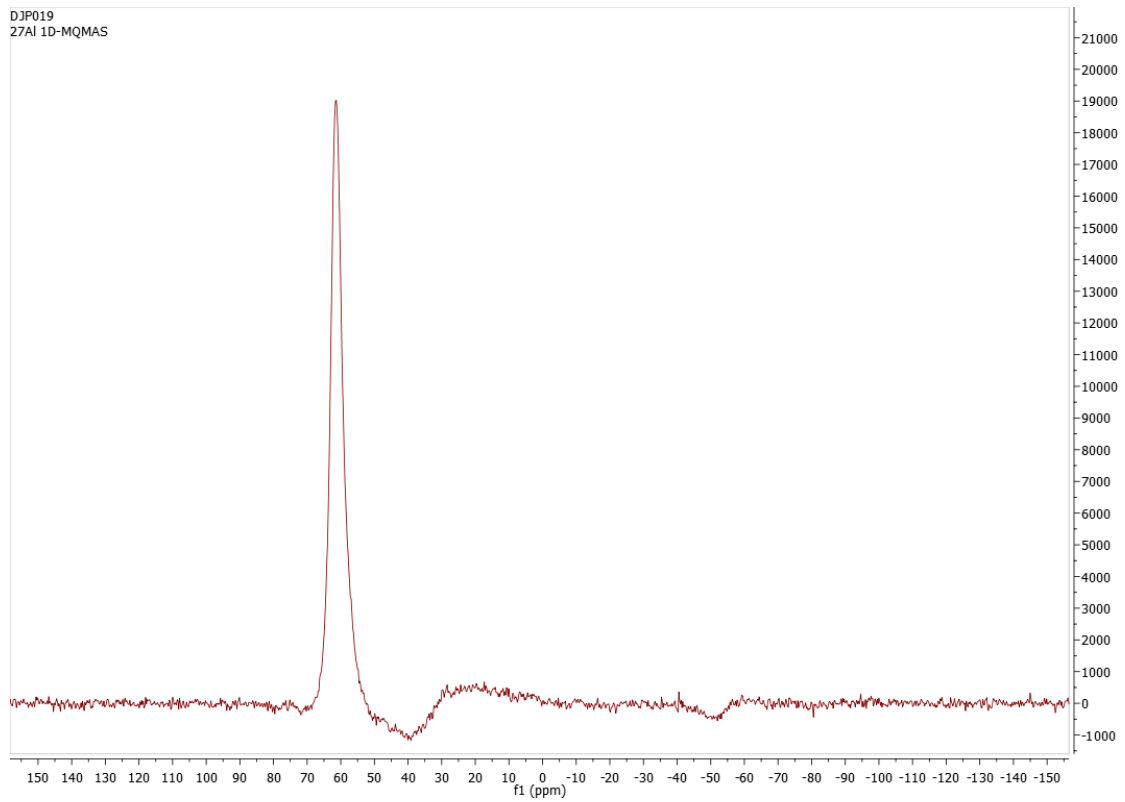


Figure 5.16: 1D-MQMAS spectrum of DJP019

Appendix 5.5: Annotated catalytic reaction NMRs

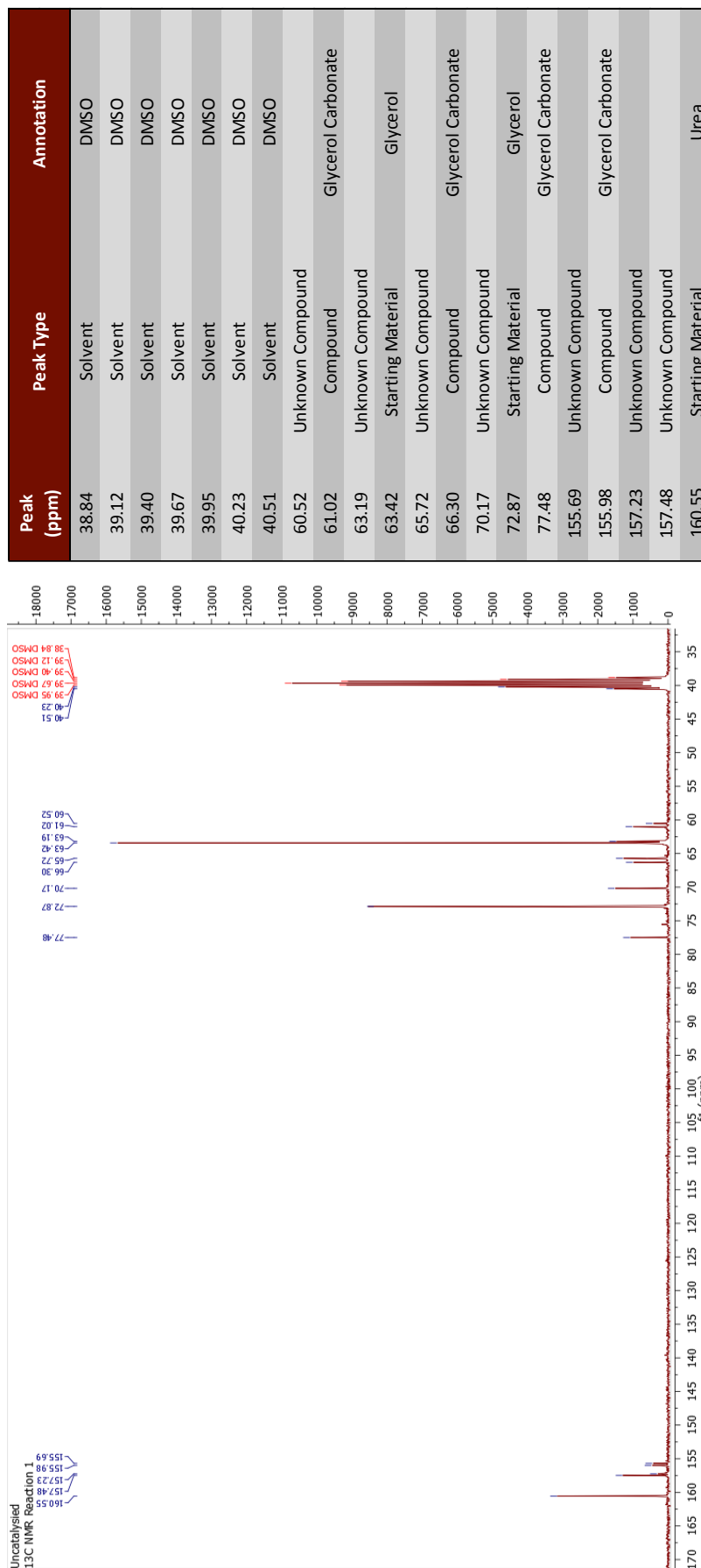


Figure 5.17: Annotated ^{13}C NMR for DJP000 (reaction 1)

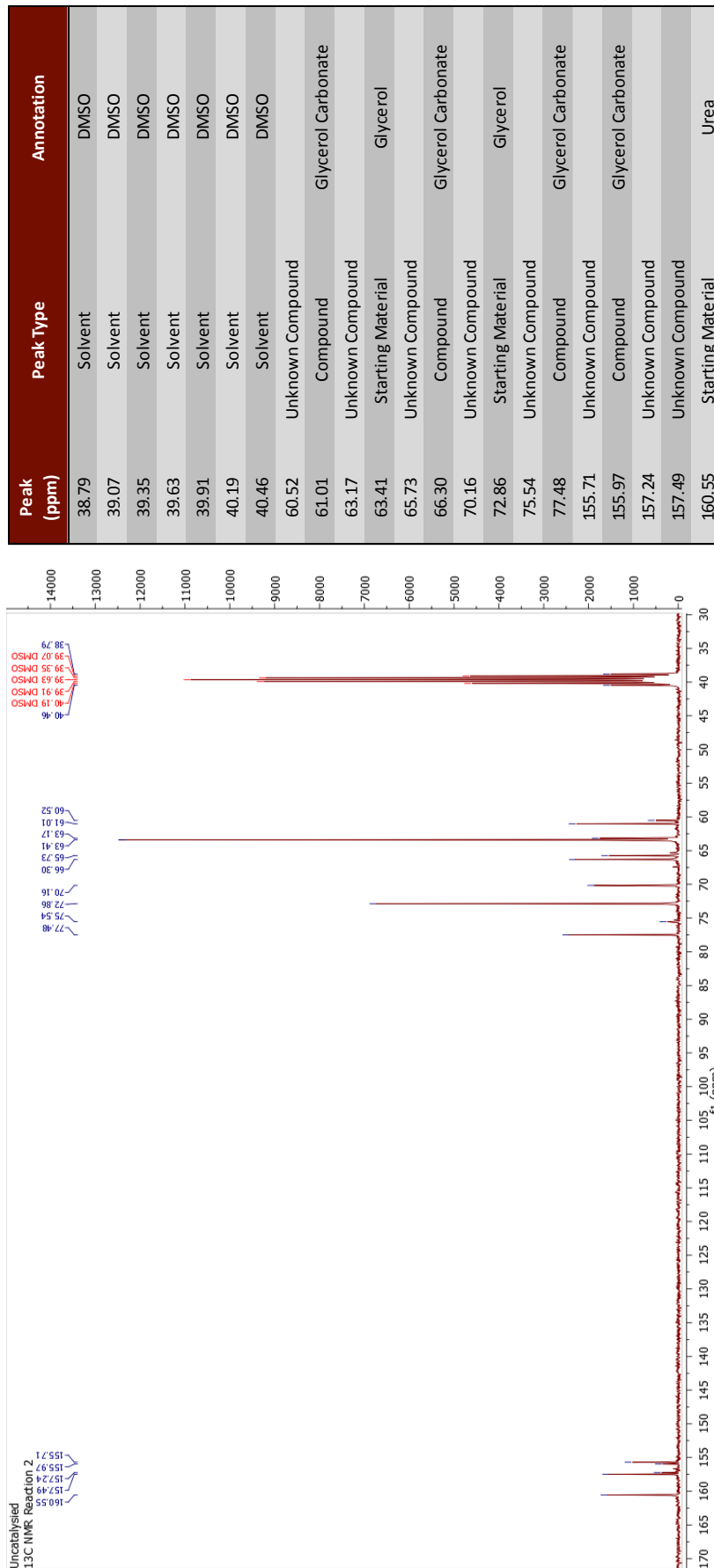


Figure 5.18: Annotated ¹³C NMR for DJP000 (reaction 2)

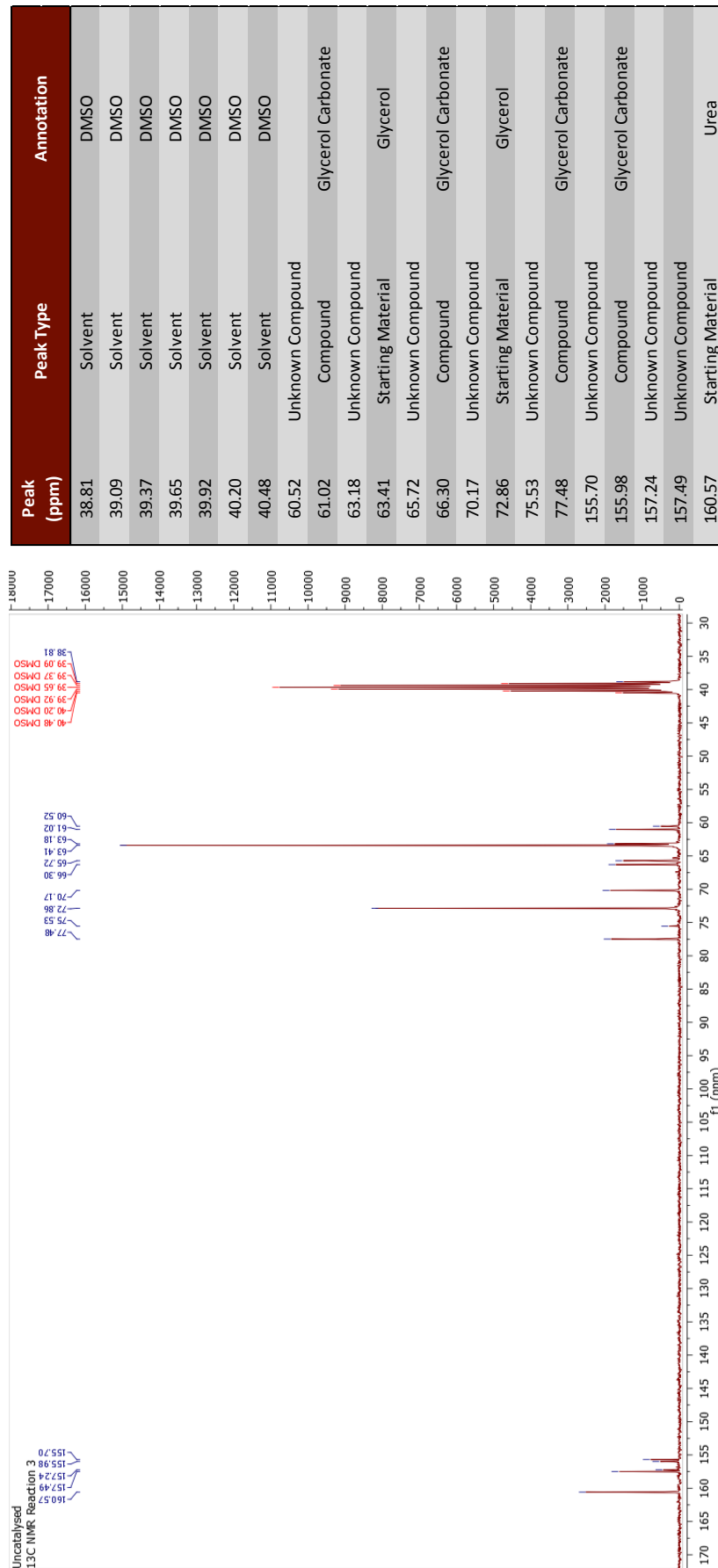


Figure 5.19: Annotated ^{13}C NMR for DJP000 (reaction 3)

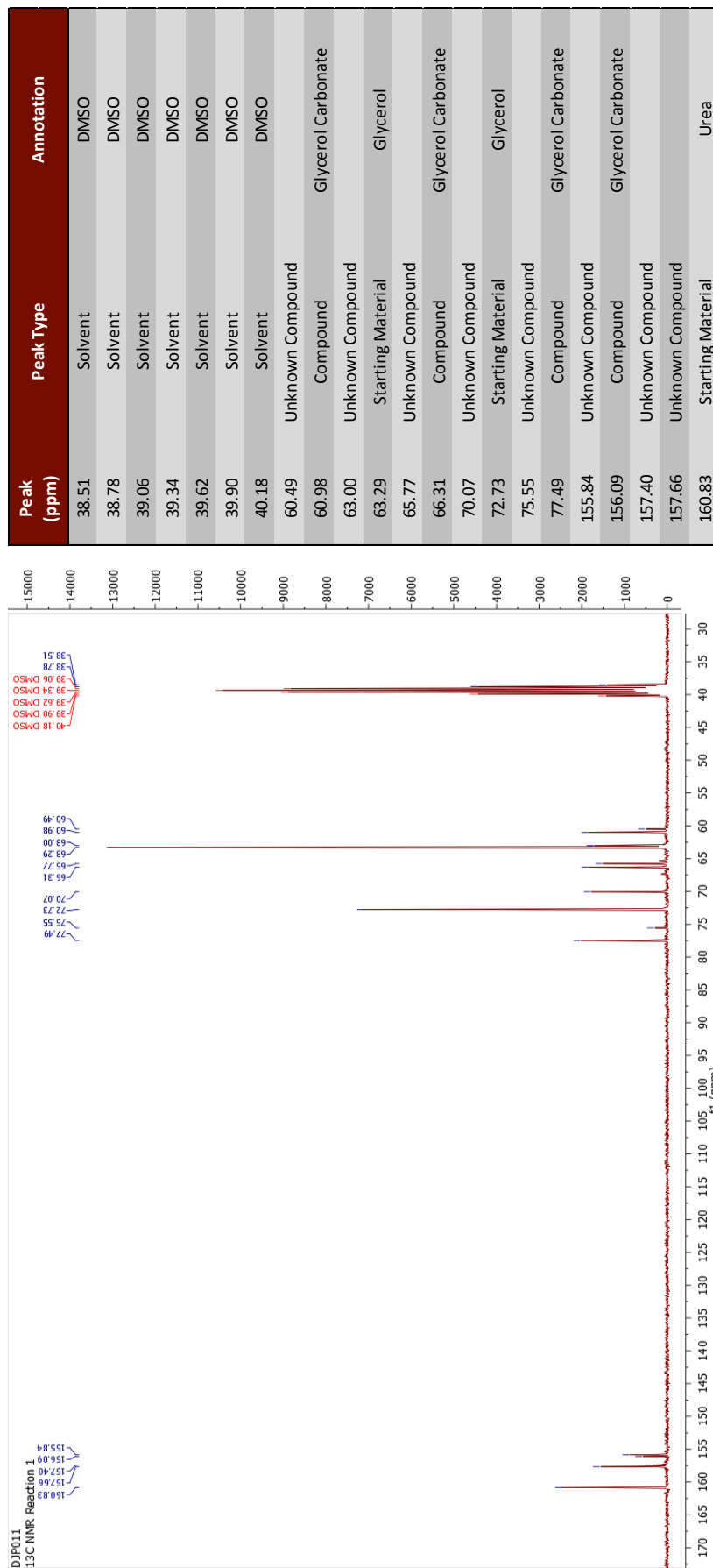


Figure 5.20: Annotated ¹³C NMR for DJP011 (reaction 1)

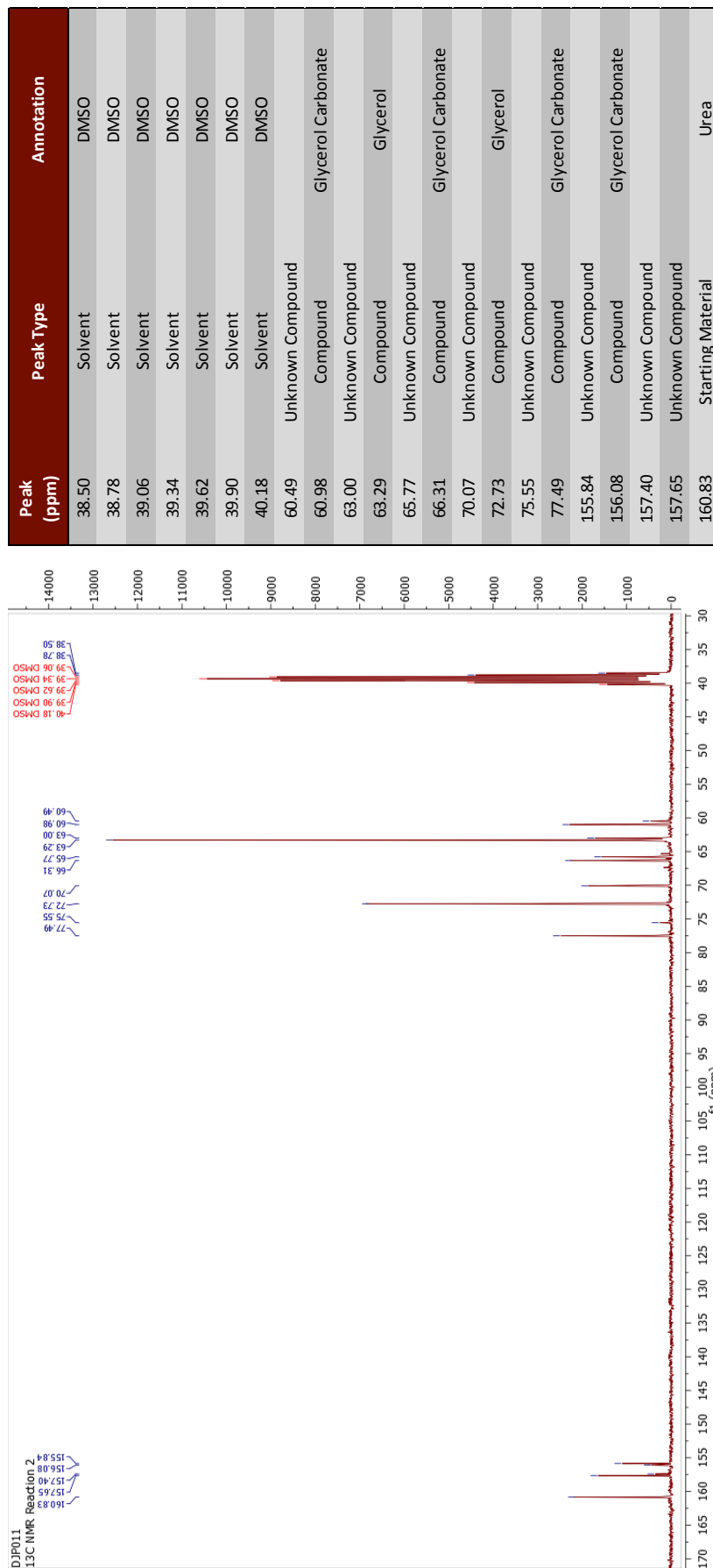


Figure 5.21: Annotated ¹³C NMR for DJP011 (reaction 2)

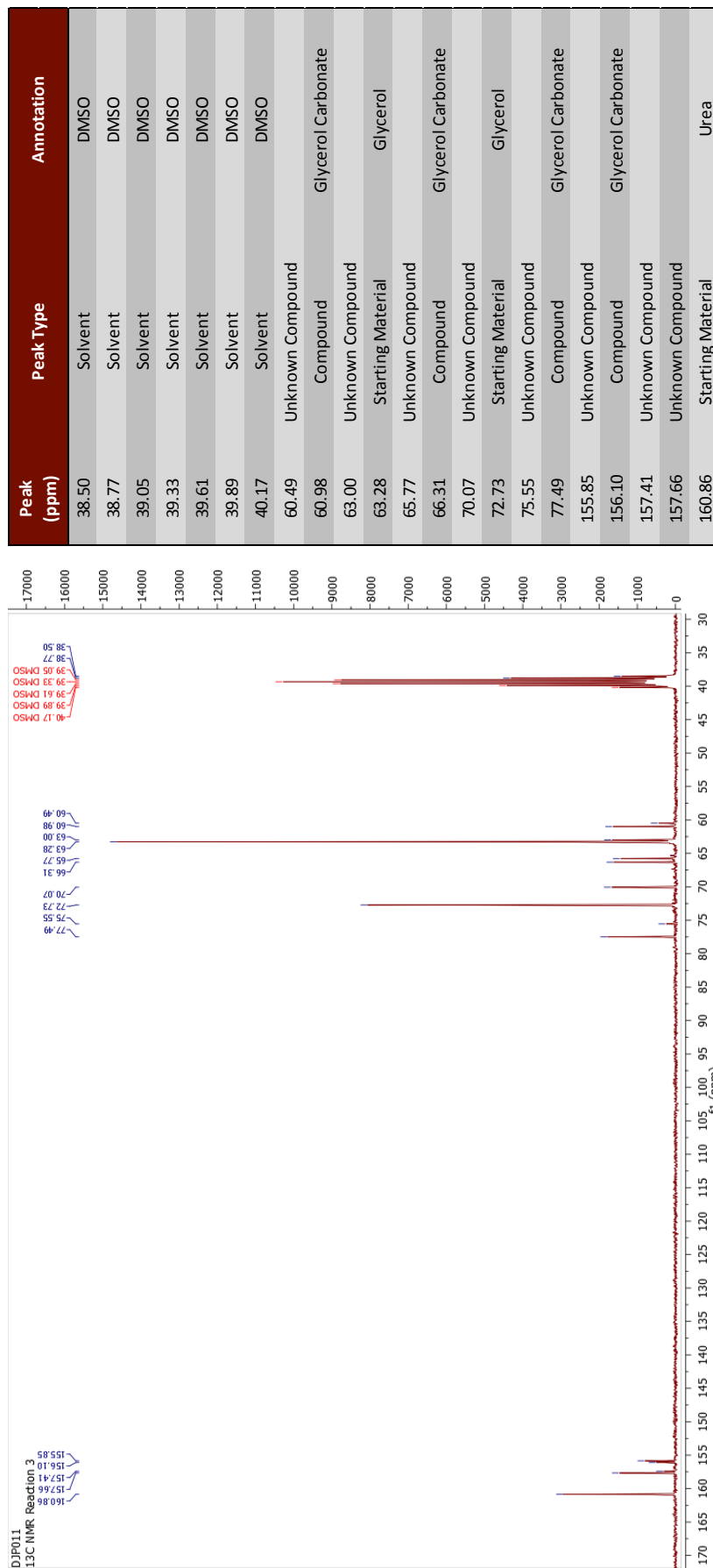


Figure 5.22: Annotated ¹³C NMR for DJP011 (reaction 3)

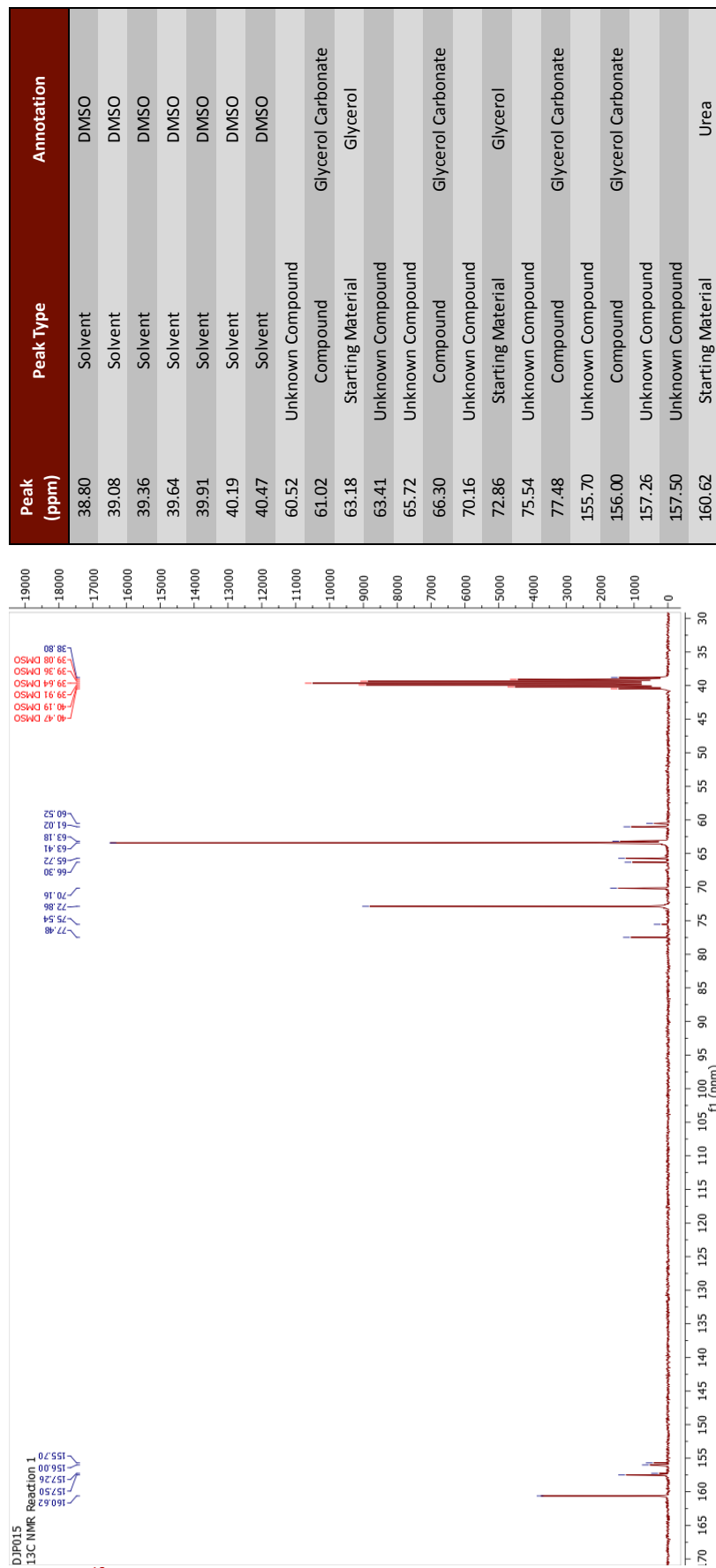


Figure 5.23: Annotated ¹³C NMR for DJP015 (reaction 1)

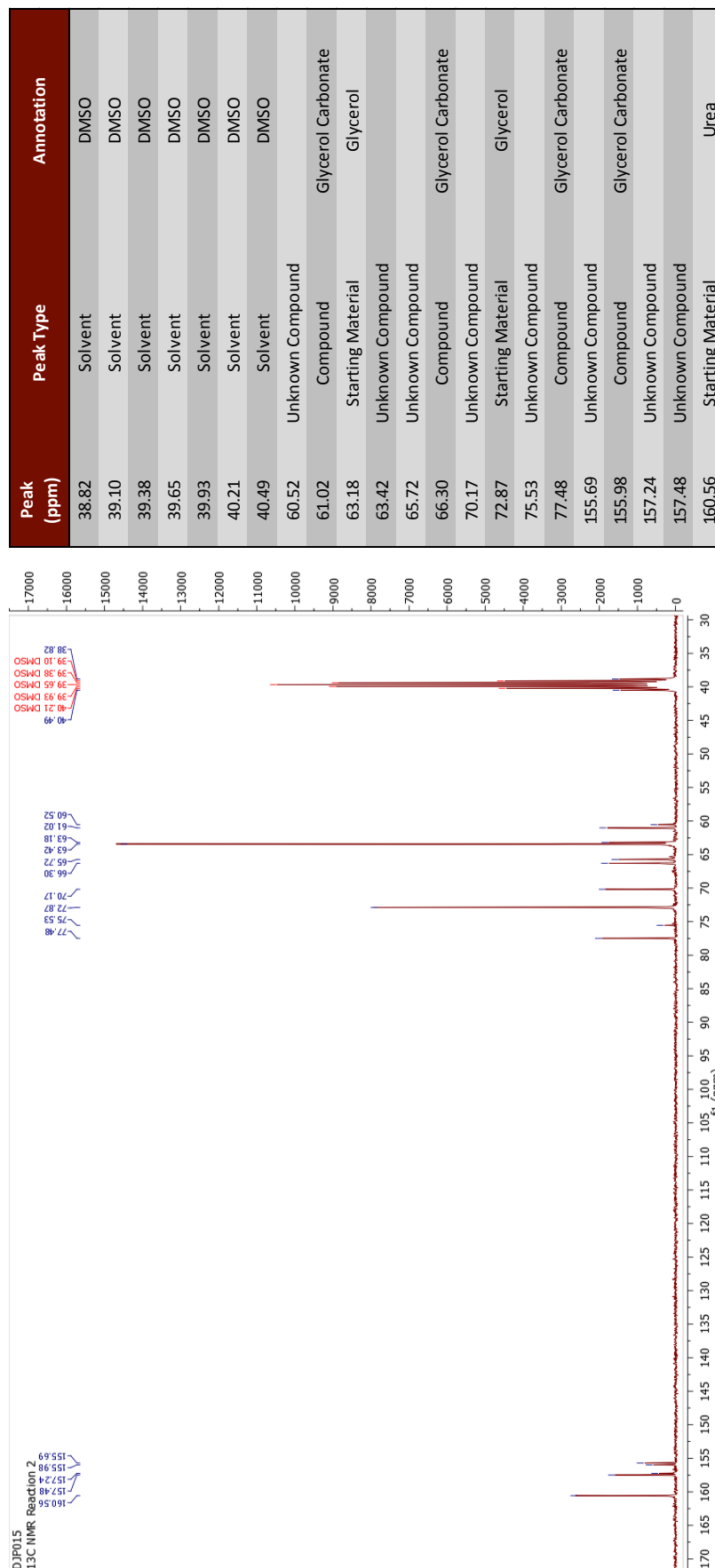


Figure 5.24: Annotated ¹³C NMR for DJP015 (reaction 2)

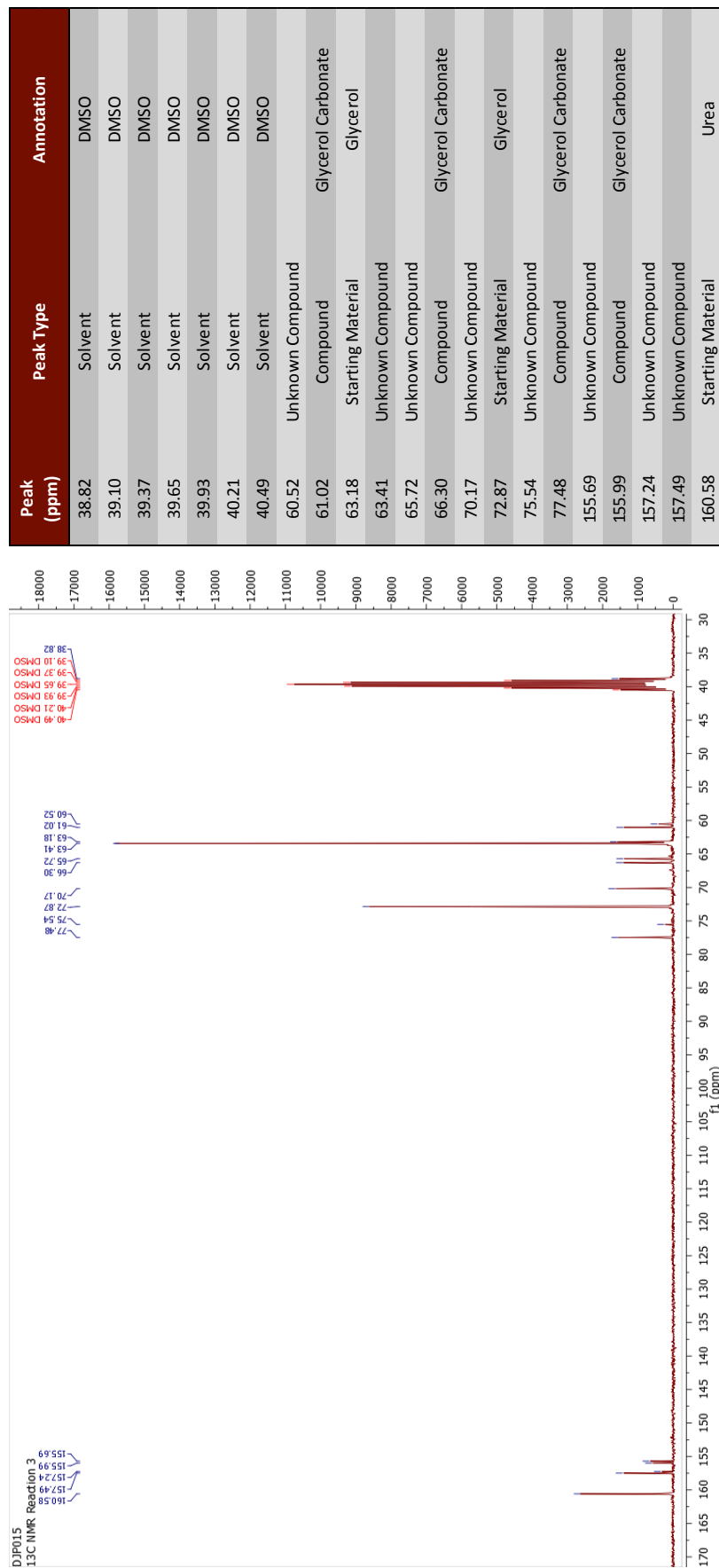


Figure 5.25: Annotated ¹³C NMR for DJP015 (reaction 3)

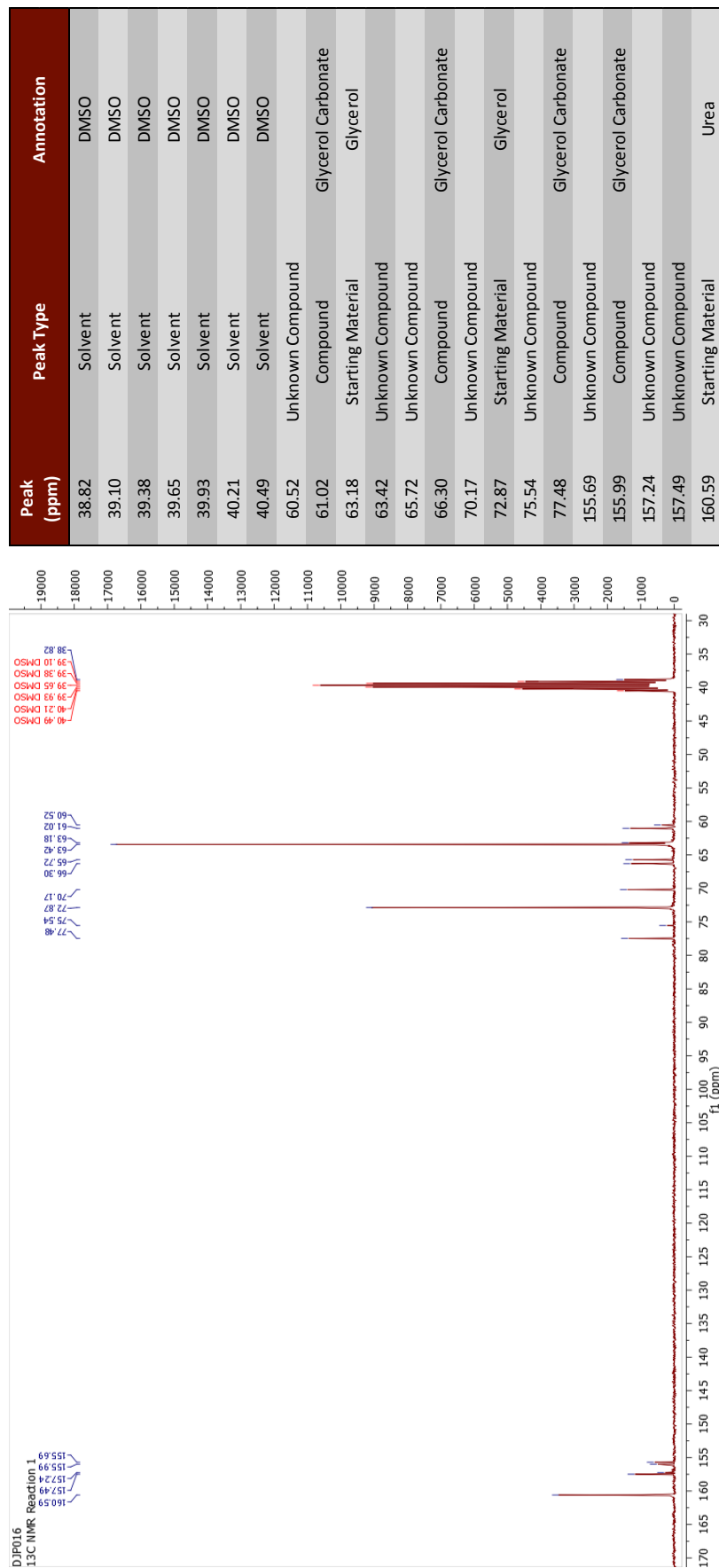


Figure 5.26: Annotated ¹³C NMR for DJP016 (reaction 1)

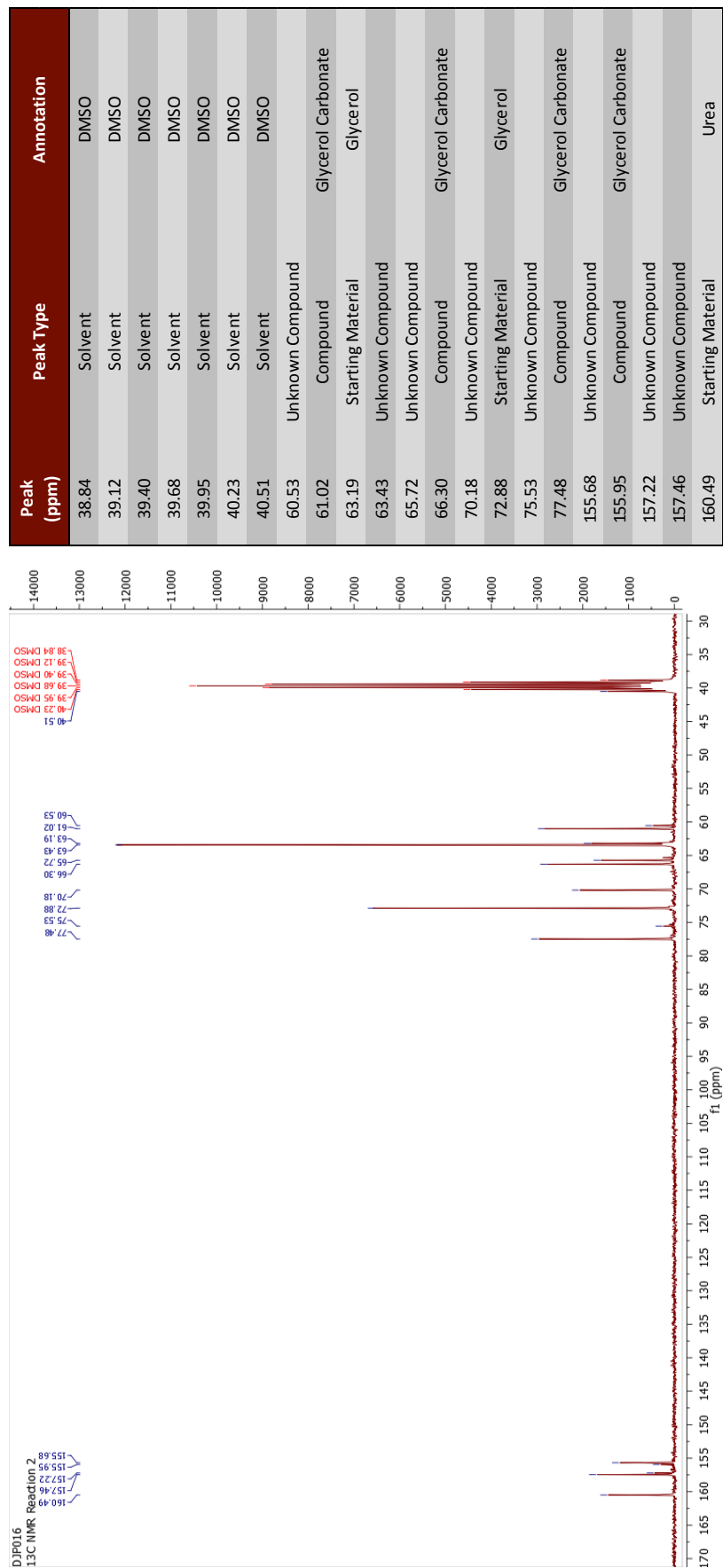


Figure 5.27: Annotated ¹³C NMR for DJP016 (reaction 2)

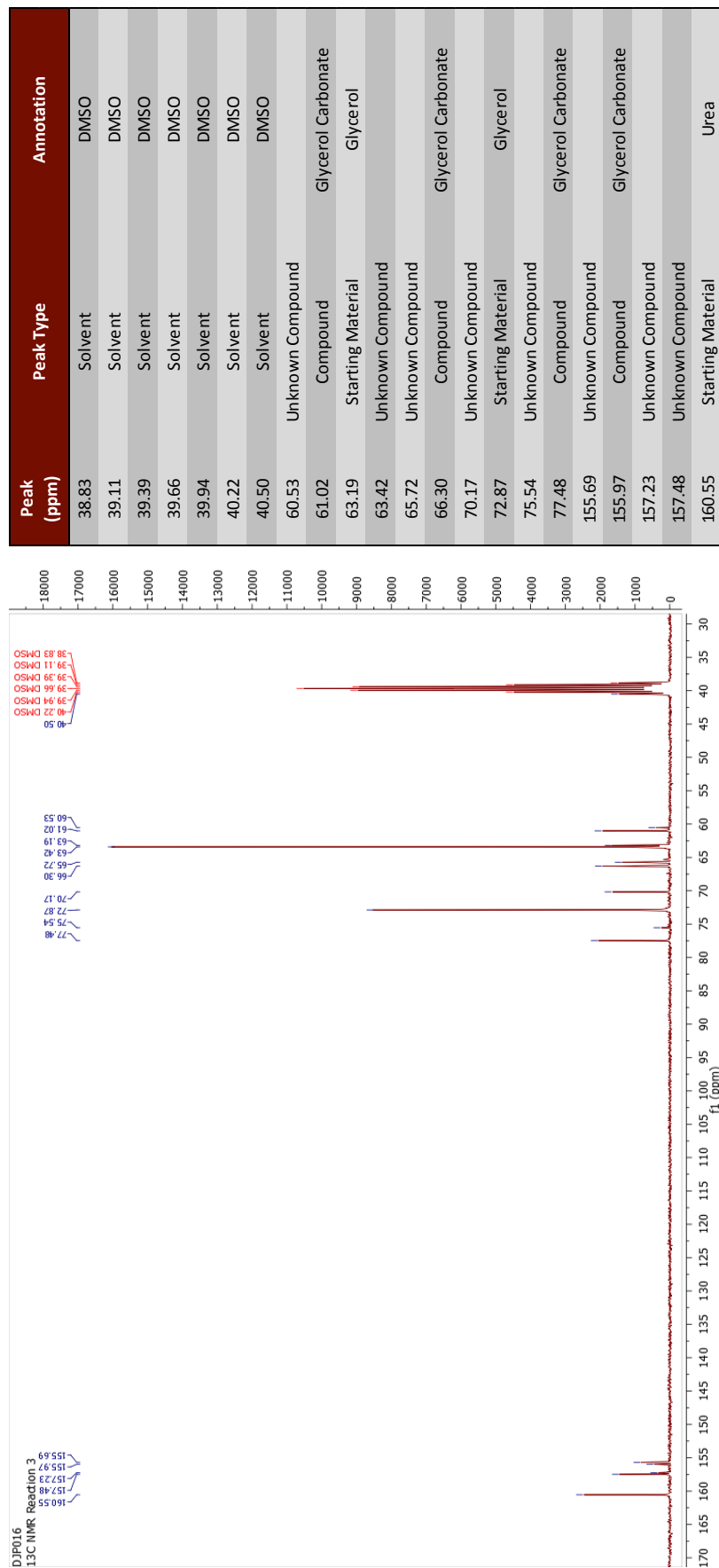


Figure 5.28: Annotated ¹³C NMR for DJP016 (reaction 3)

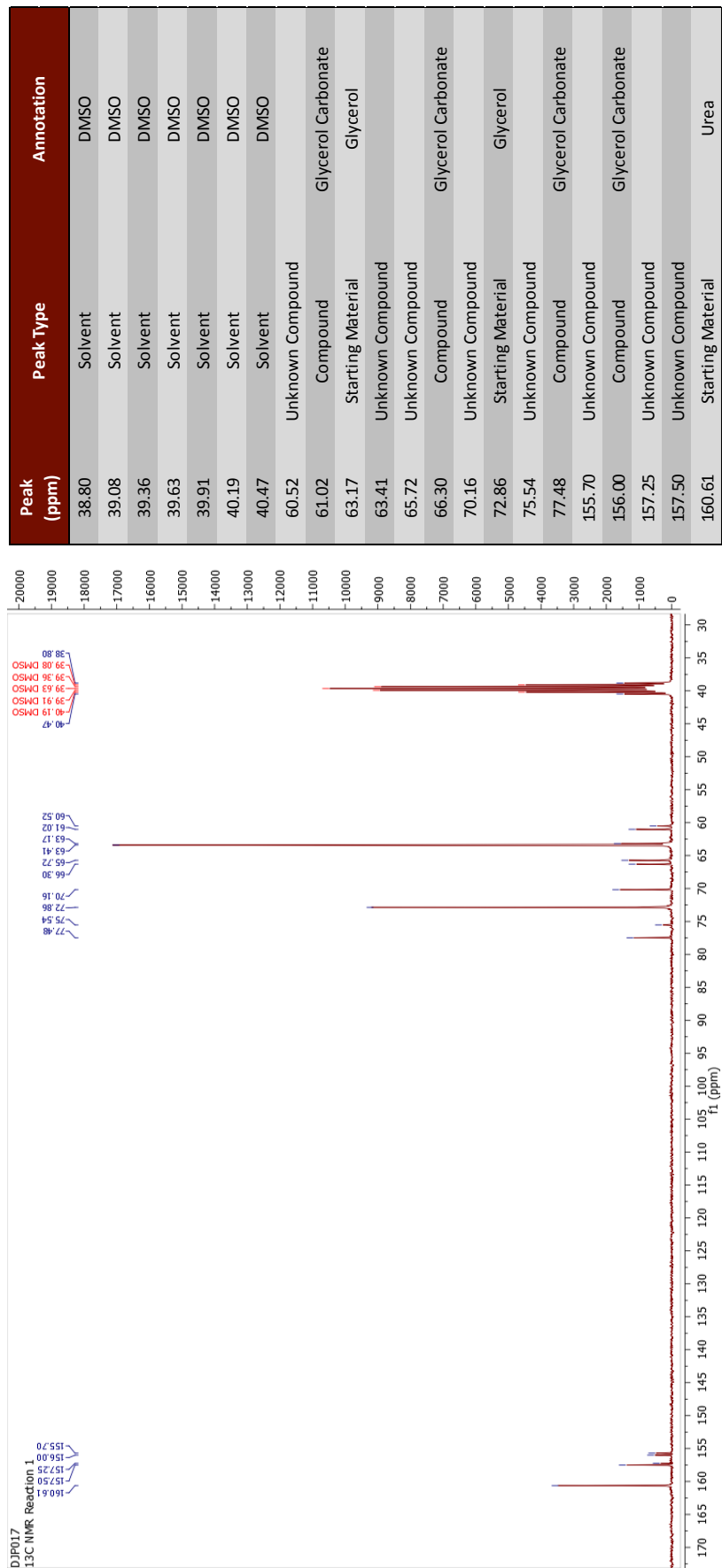


Figure 5.29: Annotated ¹³C NMR for DJP017 (reaction 1)

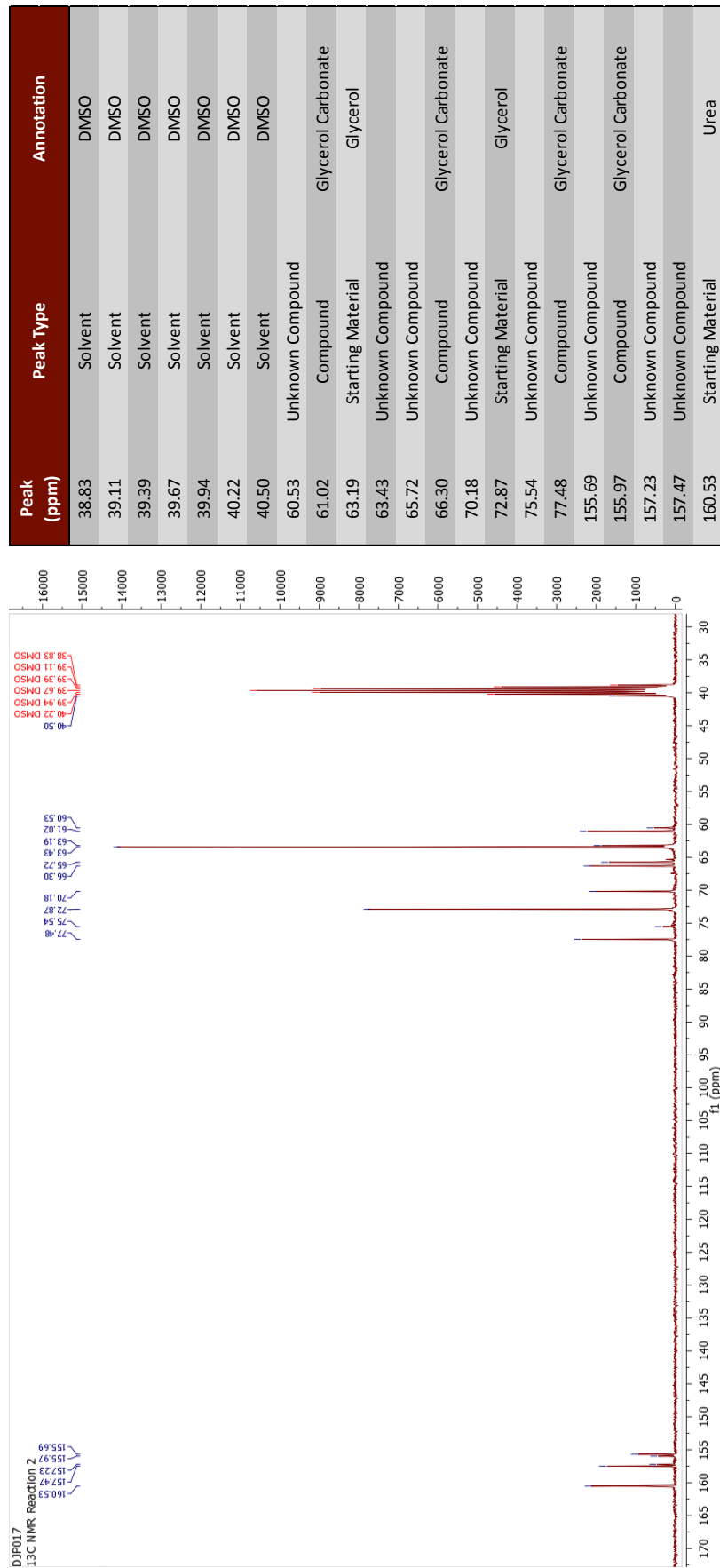


Figure 5.30: Annotated ¹³C NMR for DJP017 (reaction 2)

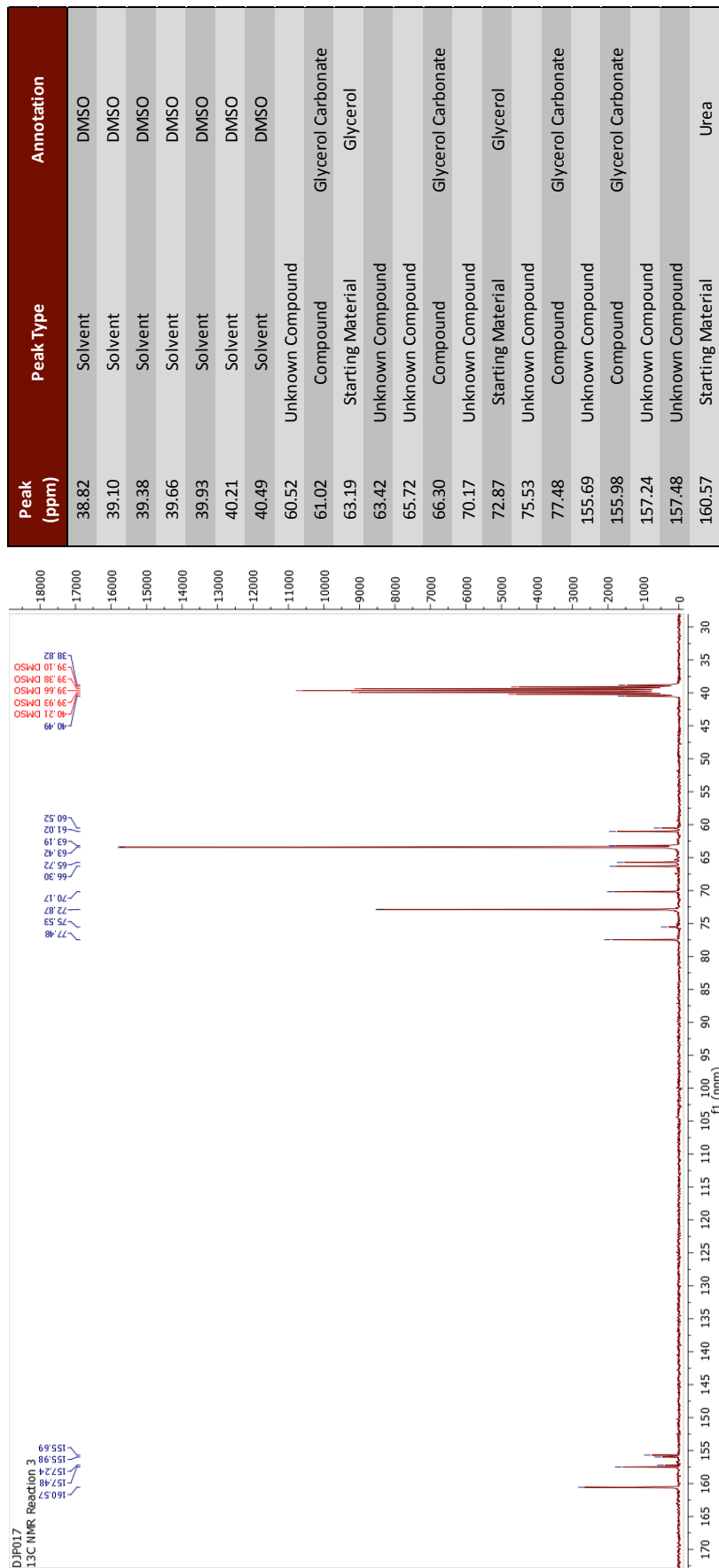


Figure 5.31: Annotated ¹³C NMR for DJP017 (reaction 3)

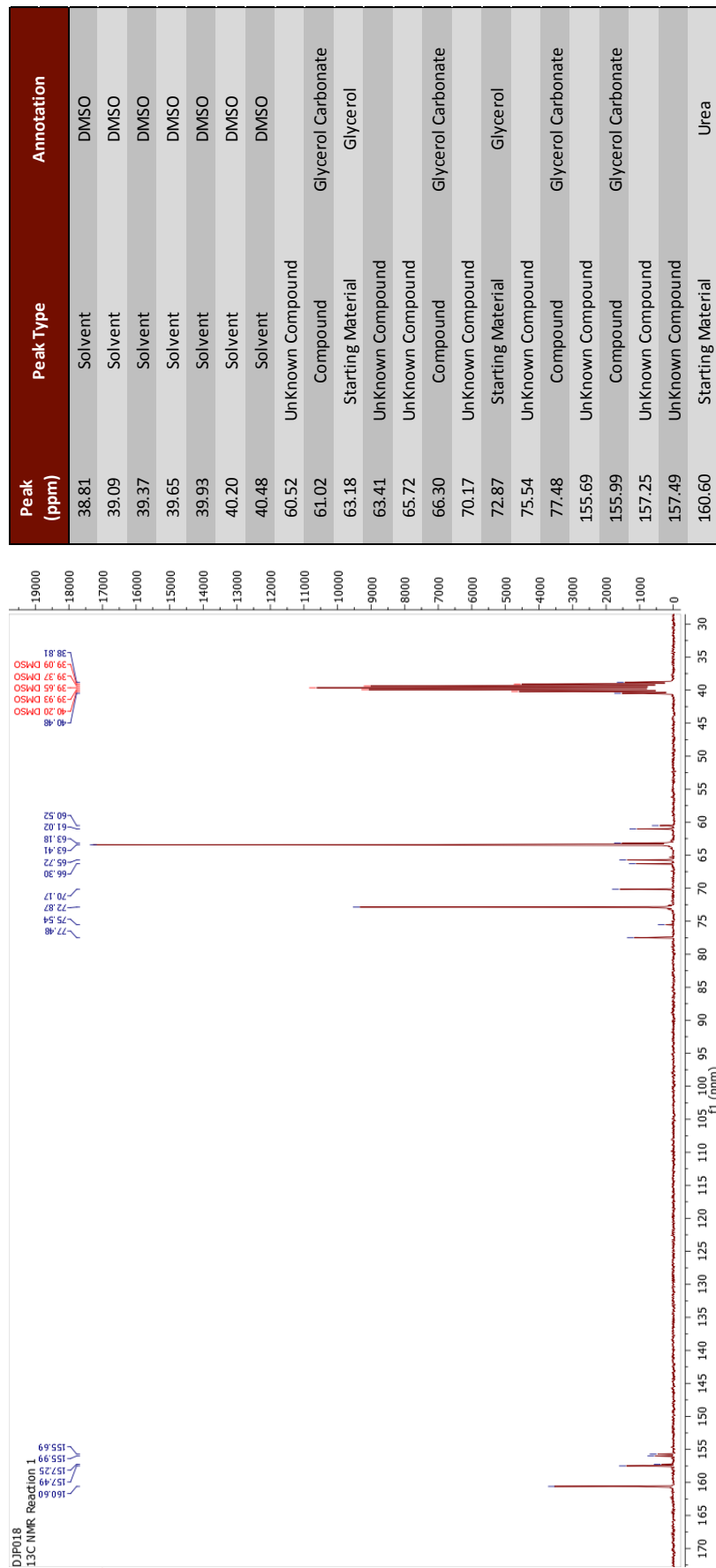


Figure 5.32: Annotated ¹³C NMR for DJP018 (reaction 1)

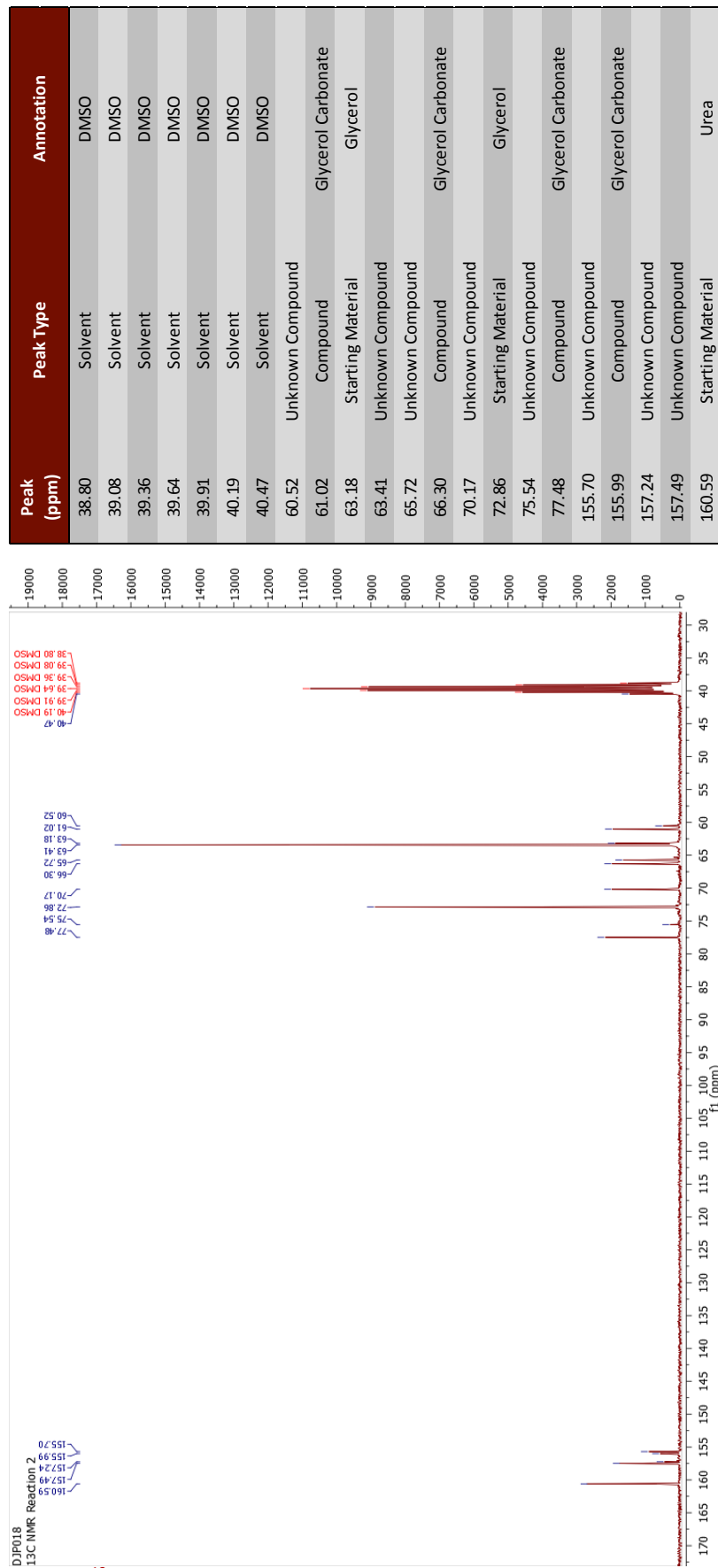


Figure 5.33: Annotated ¹³C NMR for DJP018 (reaction 2)

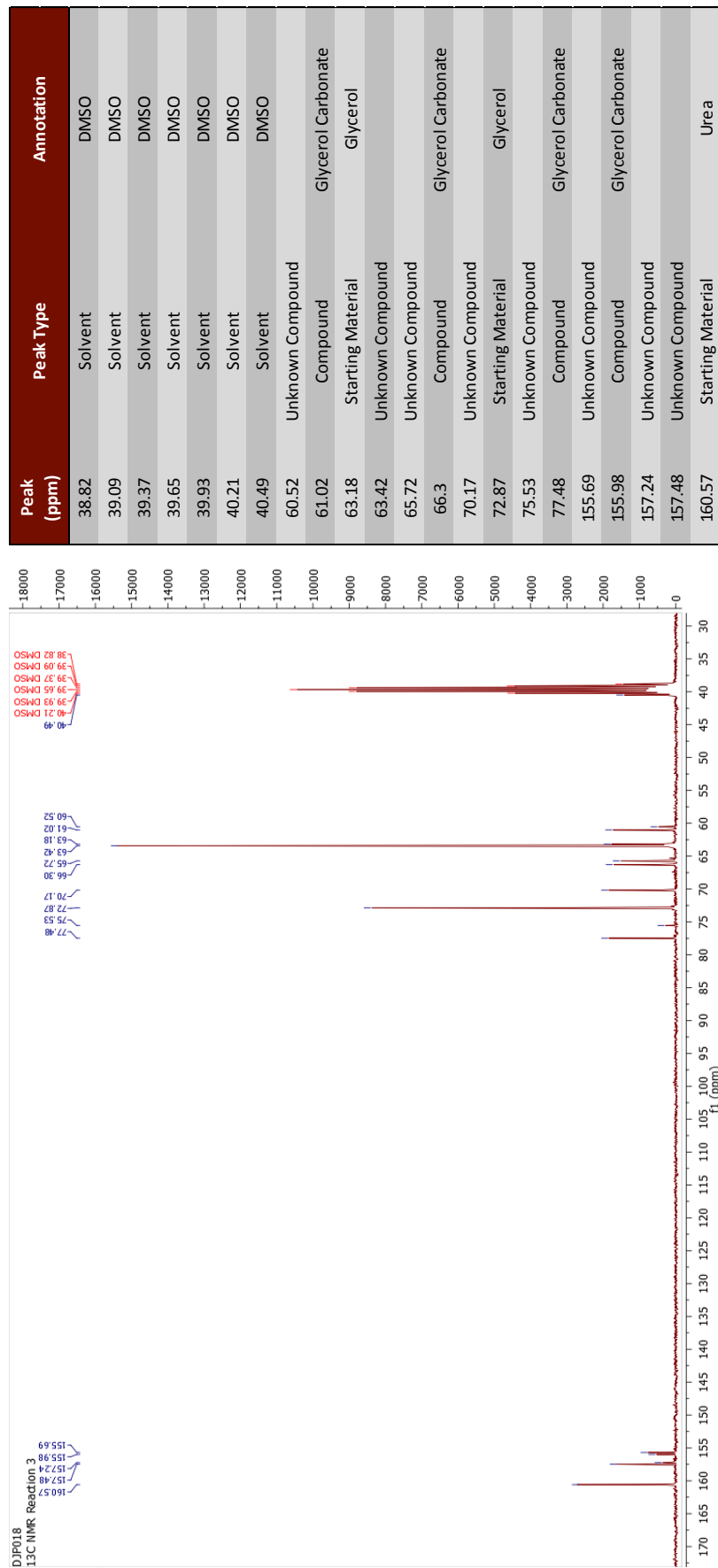


Figure 5.34: Annotated ¹³C NMR for DJP018 (reaction 3)

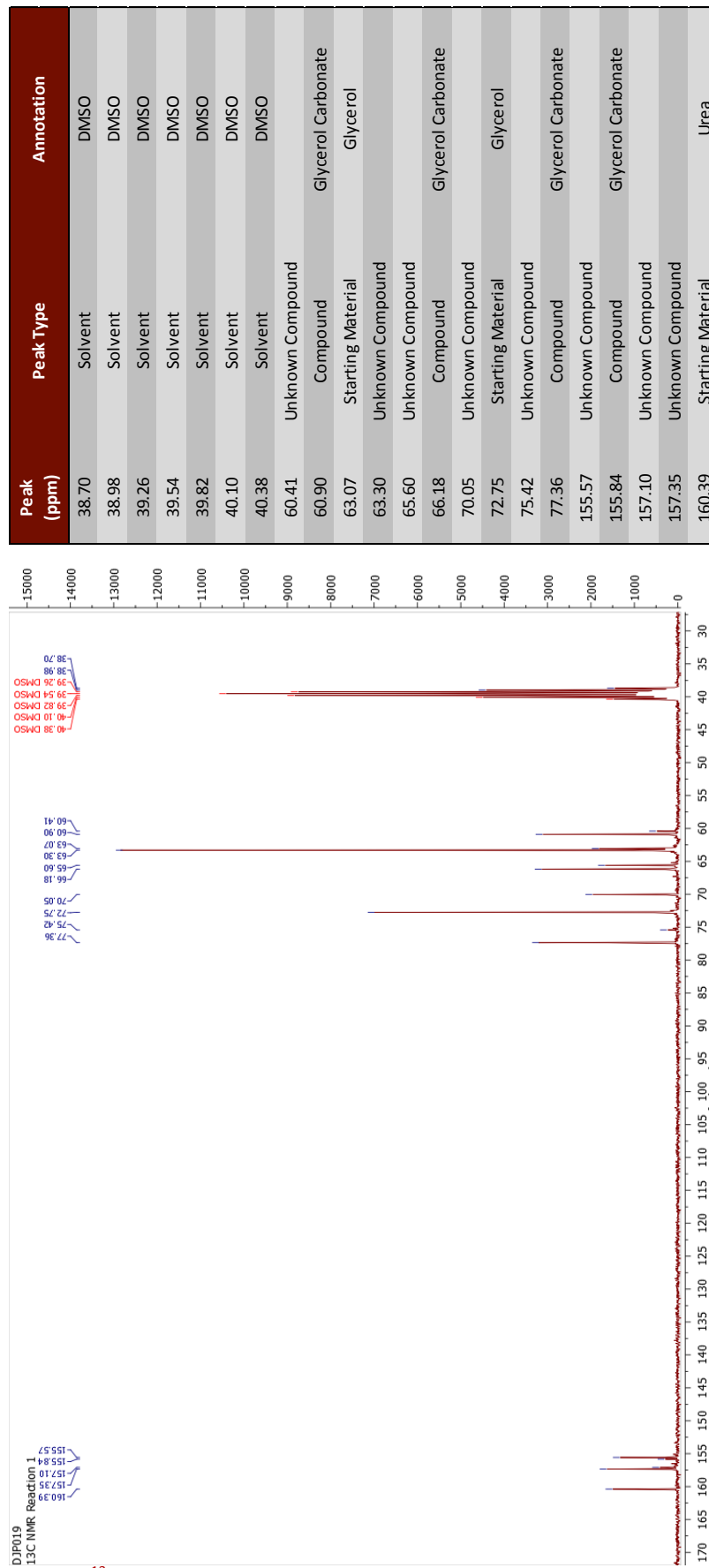


Figure 5.35: Annotated ¹³C NMR for DJP019 (reaction 1)

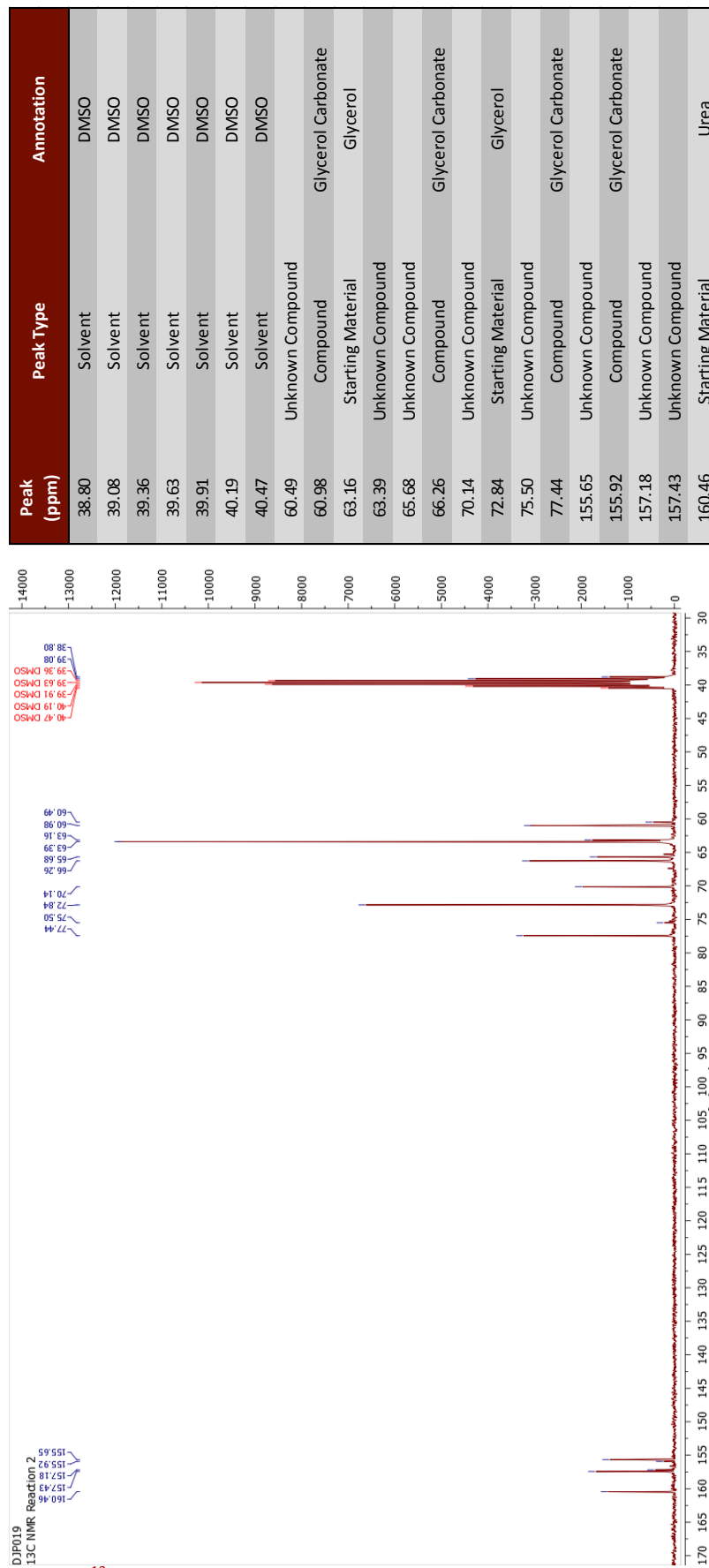


Figure 5.36: Annotated ¹³C NMR for DJP019 (reaction 2)

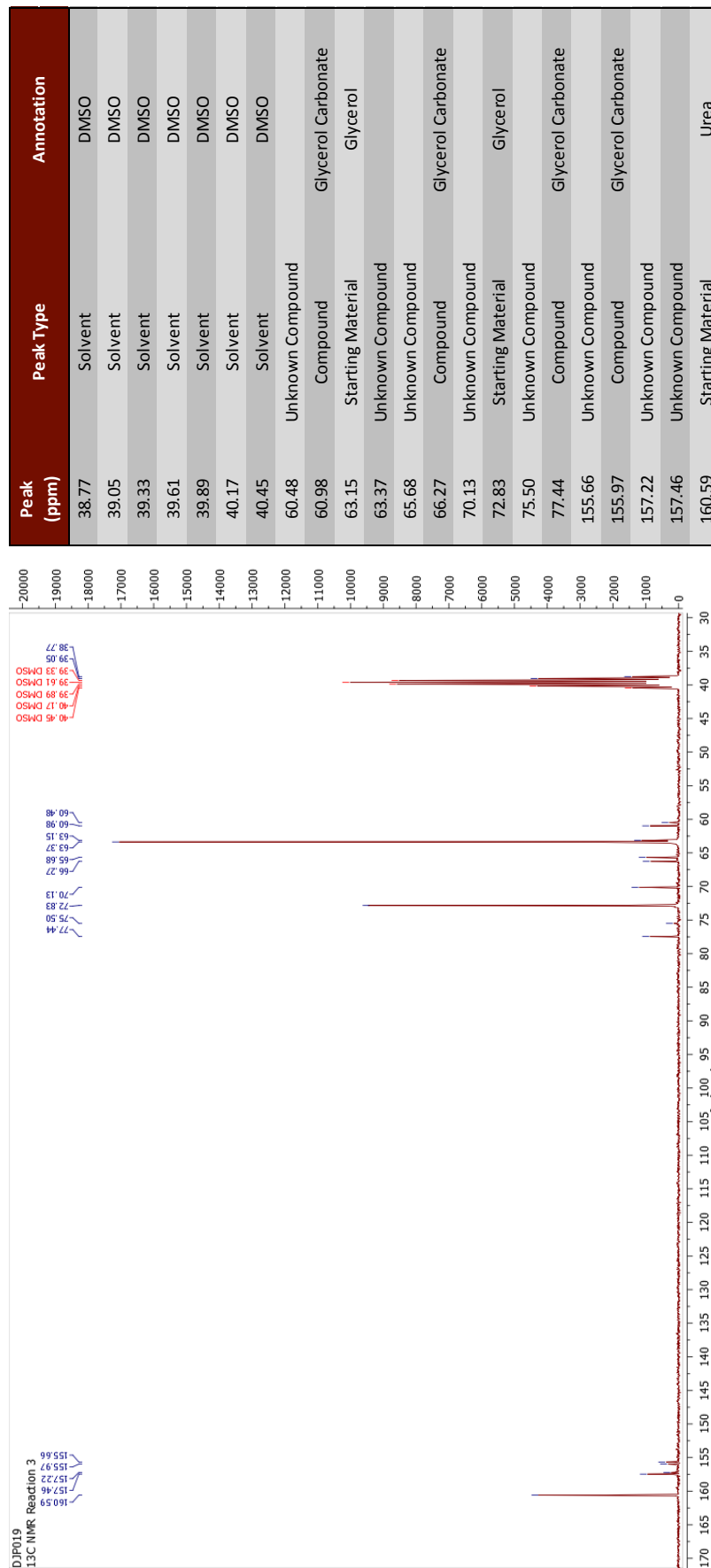


Figure 5.37: Annotated ¹³C spectrum for DJP019 (reaction 3)

Appendix 5.6: Refined lattice parameters

Table 5.8: Refined lattice parameters for DJP011

Refined Lattice Parameters for DJP011					
H	K	L	2 θ (obs)	2 θ (cal)	Difference
-1	0	1	6.1832	6.1791	0.0041
0	1	1	9.7371	9.7436	-0.0065
-1	1	1	10.4202	10.3278	0.0924
1	1	1	11.2119	11.2610	-0.0491
0	1	2	13.2326	13.2256	0.0070
-1	0	3	15.1862	15.2083	-0.0221
3	0	1	15.9065	15.9141	-0.0076
1	0	3	17.1152	17.0932	0.0220
-2	1	3	18.3152	18.3309	-0.0157
-1	2	2	19.6054	19.6016	0.0038
-2	0	4	20.8710	20.8575	0.0135
3	2	0	21.7514	21.7649	-0.0135
0	1	4	22.3316	22.3190	0.0126
3	0	3	23.0663	23.0357	0.0306
1	2	3	23.8475	23.8993	-0.0518
-3	2	3	25.0117	25.0221	-0.0104
-1	3	1	25.7965	25.7550	0.0415
0	2	4	26.6198	26.6316	-0.0118
0	1	5	27.2581	27.2785	-0.0204
-1	3	3	29.3800	29.3726	0.0074
2	1	5	30.6732	30.6463	0.0269
4	2	3	31.6591	31.6791	-0.0200
-7	1	1	33.4439	33.4411	0.0028
0	4	1	33.9231	33.9329	-0.0098

Refined Unit Cell

A= 19.4021(41), B= 10.6952(6), C= 17.5564(34), α = 90.00, β = 102.06(357), γ = 90.00

Table 5.9: Refined lattice parameters for DJP015

Refined Lattice Parameters for DJP015					
H	K	L	2 θ (obs)	2 θ (cal)	Difference
1	0	0	6.1970	6.1456	0.0514
1	1	0	11.2523	11.2336	0.0187
2	0	0	12.3194	12.3090	0.0104
0	1	1	13.2517	13.2356	0.0161
-1	1	1	14.0398	14.0237	0.0161
-2	1	1	17.1820	17.1647	0.0173
3	0	0	18.5055	18.5084	-0.0029
0	2	0	18.8643	18.8528	0.0115
1	2	0	19.8543	19.8466	0.0077
1	0	2	20.4969	20.5059	-0.0090
-2	0	2	20.8789	20.8638	0.0151
-3	1	1	21.6464	21.6847	-0.0383
1	2	1	22.3370	22.3395	-0.0025
1	1	2	22.6195	22.5979	0.0216
-2	1	2	22.9452	22.9247	0.0205
2	0	2	23.8970	23.8817	0.0153
2	2	1	25.1456	25.1496	-0.0040
-3	1	2	26.1852	26.1953	-0.0101
3	2	0	26.5214	26.5391	-0.0177
-1	2	2	26.7746	26.7459	0.0287
1	2	2	27.9800	27.9951	-0.0151
3	0	2	28.2823	28.2807	0.0016
3	2	1	29.0557	29.0778	-0.0221
-1	1	3	29.5300	29.5418	-0.0118
0	3	1	29.9862	29.9868	-0.0006
-1	3	1	30.3886	30.3563	0.0323
1	3	1	30.9125	30.9197	-0.0072
1	1	3	31.2364	31.2445	-0.0081
5	1	0	32.5937	32.5509	0.0428
2	3	1	33.0252	33.0556	-0.0304
4	0	2	33.3304	33.3428	-0.0124
0	2	3	34.0801	34.1072	-0.0271
-2	2	3	34.9110	34.9115	-0.0005
-2	1	4	39.3685	39.3557	0.0128
-6	1	2	40.7655	40.7854	-0.0199

Refined Unit Cell

A= 14.5338(5), B= 9.4145(3), C= 9.6076(3), α = 90.00, β = 98.290, γ = 90.00

Table 5.10: Refined lattice parameters for DJP016

Refined Lattice Parameters for DJP016					
H	K	L	2 θ (obs)	2 θ (cal)	Difference
-1	0	1	10.5458	10.5140	0.0318
2	0	0	11.7937	11.7202	0.0735
1	0	1	12.6136	12.5883	0.0253
-3	0	1	18.4583	18.4207	0.0376
-1	1	1	19.8656	19.8269	0.0387
0	0	2	20.1048	20.0838	0.0210
3	0	1	22.0367	22.0258	0.0109
-3	1	1	25.0360	25.0046	0.0314
2	0	2	25.3348	25.3318	0.0030
-2	1	2	27.0848	27.0824	0.0024
3	1	1	27.8169	27.8067	0.0102
4	1	0	29.0984	29.0594	0.0390
0	2	0	33.9079	33.8965	0.0114
4	0	2	34.2286	34.2285	0.0001
1	2	1	36.2907	36.2923	-0.0016
5	1	1	37.4128	37.4501	-0.0373
3	0	3	38.3781	38.4039	-0.0258
-6	1	2	41.1812	41.1874	-0.0062
-4	2	1	41.7432	41.7594	-0.0162
2	2	2	42.7915	42.7864	0.0051
-4	2	2	44.3577	44.3699	-0.0122
6	0	2	44.8872	44.9227	-0.0355
7	1	1	48.5766	48.5824	-0.0058
-6	2	2	51.2975	51.3109	-0.0134
-5	2	3	51.9165	51.8814	0.0351
1	2	4	55.4423	55.4516	-0.0093
0	3	2	56.1509	56.1654	-0.0145
3	3	2	60.7759	60.7816	-0.0057

Refined Unit Cell

A= 15.425(6), B= 5.2894(2), C= 9.032(5), α = 90.00, β = 101.75, γ = 90.00

Table 5.11: Refined lattice parameters for DJP017

Refined Lattice Parameters for DJP017					
H	K	L	2 θ (obs)	2 θ (cal)	Difference
0	-1	0	6.1994	6.2109	-0.0115
-1	-1	0	8.5022	8.5700	-0.0678
-1	1	0	9.5683	9.5464	0.0219
-1	0	1	11.2475	11.3059	-0.0584
0	-1	1	11.5891	11.5787	0.0104
0	1	1	13.2546	13.2607	-0.0061
-2	-1	0	13.9764	14.0075	-0.0311
0	-2	1	15.1811	15.1603	0.0208
-2	-2	0	17.1836	17.1884	-0.0048
1	-2	1	17.9462	18.0089	-0.0627
-1	2	1	18.5029	18.5367	-0.0338
2	0	1	18.8617	18.9017	-0.0400
2	-2	0	19.1739	19.1599	0.0140
-3	0	0	19.8710	19.9041	-0.0331
1	-3	0	20.4914	20.5262	-0.0348
-1	-1	2	20.8817	20.8787	0.0030
0	0	2	21.6462	21.6505	-0.0043
-3	-2	0	22.3214	22.3566	-0.0352
2	-2	1	22.5662	22.5501	0.0161
2	2	1	22.9425	22.8315	0.1110
0	1	2	23.4072	23.4700	-0.0628
-1	3	1	23.8912	23.8972	-0.0060
-3	-3	1	25.1410	25.0484	0.0926
3	-1	1	25.6967	25.6728	0.0239
-2	-3	2	26.2144	26.2930	-0.0786
-2	-4	1	26.5192	26.4920	0.0272
0	2	2	26.7712	26.7032	0.0680
-3	1	2	27.9983	28.0275	-0.0292
-2	2	2	28.2889	28.2480	0.0409
2	1	2	29.0806	29.0819	-0.0013
1	4	1	29.5264	29.5782	-0.0518
-3	3	1	30.3796	30.3602	0.0194
3	3	1	30.9062	30.9299	-0.0237
-4	2	1	31.2310	31.2272	0.0038
-2	3	2	32.5970	32.5882	0.0088
-1	-3	3	34.0567	34.0199	0.0368
4	-3	0	34.4368	34.4238	0.0130
1	0	3	34.9130	34.9131	-0.0001
0	-3	3	35.2324	35.2294	0.0030
-5	-2	3	40.7813	40.7782	0.0031

Refined Unit Cell

A= 13.8877(18), B= 14.5656(19), C= 8.5739(10), α = 100.67(84), β = 104.24(80), γ = 81.49(82)

Table 5.12: Refined lattice parameters for DJP018

Refined Lattice Parameters for DJP018					
H	K	L	2 θ (obs)	2 θ (cal)	Difference
1	0	0	6.1938	6.1337	0.0601
1	1	0	11.2236	11.1995	0.0241
2	0	0	12.3072	12.2851	0.0221
0	1	1	13.2248	13.2078	0.0170
-1	1	1	14.0109	13.9952	0.0157
1	1	1	15.1740	15.1312	0.0428
-2	1	1	17.1461	17.1309	0.0152
3	0	0	18.4819	18.4723	0.0096
0	2	0	18.8048	18.7863	0.0185
1	2	0	19.7871	19.7796	0.0075
1	0	2	20.4753	20.4864	-0.0111
-2	0	2	20.8569	20.8465	0.0104
-3	1	1	21.6208	21.6425	-0.0217
1	2	1	22.2748	22.2750	-0.0002
1	1	2	22.5807	22.5662	0.0145
-2	1	2	22.9037	22.8951	0.0086
2	0	2	23.8621	23.8516	0.0105
2	2	1	25.0812	25.0811	0.0001
-3	1	2	26.1476	26.1582	-0.0106
3	2	0	26.4806	26.4654	0.0152
-1	2	2	26.7038	26.6897	0.0141
1	2	2	27.9168	27.9347	-0.0179
-2	2	2	28.2208	28.2049	0.0159
3	2	1	28.9956	29.0033	-0.0077
-1	1	3	29.4842	29.5144	-0.0302
0	3	1	29.8770	29.8881	-0.0111
1	3	1	30.8048	30.8198	-0.0150
1	1	3	31.1766	31.2097	-0.0331
-5	1	1	32.5350	32.5532	-0.0182
-3	1	3	32.9346	32.9243	0.0103
4	0	2	33.2787	33.2874	-0.0087
0	2	3	34.0249	34.0526	-0.0277
-2	2	3	34.8374	34.8571	-0.0197
3	3	1	36.0934	36.0990	-0.0056
-3	2	3	36.9037	36.9239	-0.0202
2	2	3	37.7876	37.7520	0.0356
1	0	4	39.2687	39.2705	-0.0018
-3	0	4	39.8501	39.8030	0.0471
-6	1	2	40.6971	40.7147	-0.0176

Refined Unit Cell

A= 14.5611(8), B= 9.4475(4), C= 9.6135(4), α = 90.00, β = 92.26(66), γ = 90.00

Table 5.13: Refined lattice parameters for DJP019

Refined Lattice Parameters for DJP018					
H	K	L	2 θ (obs)	2 θ (cal)	Difference
1	0	0	6.1729	6.1466	0.0263
1	1	0	11.2708	11.2351	0.0357
2	0	0	12.3270	12.3109	0.0161
0	1	1	13.2604	13.2394	0.021
-1	1	1	14.0531	14.0316	0.0215
1	1	1	15.2000	15.1634	0.0366
-2	1	1	17.1880	17.1754	0.0126
3	0	0	18.5172	18.5112	0.006
0	2	0	18.8692	18.8551	0.0141
1	0	2	20.4930	20.5085	-0.0155
-2	0	2	20.8913	20.8830	0.0083
-3	1	1	21.6566	21.6971	-0.0405
1	2	1	22.3395	22.3410	-0.0015
1	1	2	22.6243	22.6008	0.0235
-2	1	2	22.9376	22.9427	-0.0051
2	0	2	23.8942	23.8800	0.0142
2	2	1	25.1453	25.1494	-0.0041
3	2	0	26.5226	26.5428	-0.0202
-1	2	2	26.7697	26.7579	0.0118
3	0	2	28.2685	28.2763	-0.0078
3	2	1	29.0543	29.0768	-0.0225
0	3	1	29.9908	29.9915	-0.0007
1	3	1	30.9142	30.9226	-0.0084
1	1	3	31.2392	31.2513	-0.0121
-5	0	2	34.0679	34.0527	0.0152
-2	2	3	34.9109	34.9340	-0.0231

Refined Unit Cell

A= 14.5294(12), B= 9.4133(4), C= 9.6018(7), α = 90.00, β = 98.23(121), γ = 90.00

References

1. Johnson, D. T.; Taconi, K. A., The glycerin glut: Options for the value-added conversion of crude glycerol resulting from biodiesel production. *Environmental Progress* **2007**, *26* (4), 338-348.
2. US Energy Information Administration. *Monthly Biodiesel Production Report (October 2013)*; US Department of Energy: Washington, DC, 2013.
3. Pagliaro, M.; Ciriminna, R.; Kimura, H.; Rossi, M.; Della Pina, C., From Glycerol to Value-Added Products. *Angewandte Chemie International Edition* **2007**, *46* (24), 4434-4440.
4. Behr, A.; Eilting, J.; Irawadi, K.; Leschinski, J.; Lindner, F., Improved utilisation of renewable resources: New important derivatives of glycerol. *Green Chem* **2008**, *10* (1), 13-30.
5. Habe, H.; Shimada, Y.; Yakushi, T.; Hattori, H.; Ano, Y.; Fukuoka, T.; Kitamoto, D.; Itagaki, M.; Watanabe, K.; Yanagishita, H.; Matsushita, K.; Sakaki, K., Microbial Production of Glyceric Acid, an Organic Acid That Can Be Mass Produced from Glycerol. *Appl. Environ. Microbiol.* **2009**, *75* (24), 7760-7766.
6. Carretin, S.; McMorn, P.; Johnston, P.; Griffin, K.; Hutchings, G. J., Selective oxidation of glycerol to glyceric acid using a gold catalyst in aqueous sodium hydroxide. *Chemical Communications* **2002**, (7), 696-697.
7. Zeng, A.-P.; Biebl, H., Bulk Chemicals from Biotechnology: The Case of 1,3-Propanediol Production and the New Trends. In *Tools and Applications of Biochemical Engineering Science*, Springer Berlin Heidelberg: 2002; Vol. 74, pp 239-259.
8. Kurosaka, T.; Maruyama, H.; Naribayashi, I.; Sasaki, Y., Production of 1,3-propanediol by hydrogenolysis of glycerol catalyzed by Pt/WO₃/ZrO₂. *Catalysis Communications* **2008**, *9* (6), 1360-1363.
9. Di Serio, M.; Casale, L.; Tesser, R.; Santacesaria, E., New Process for the Production of Glycerol tert-Butyl Ether†. *Energy & Fuels* **2010**, *24* (9), 4668-4672.

10. Xiao, L.; Mao, J.; Zhou, J.; Guo, X.; Zhang, S., Enhanced performance of HY zeolites by acid wash for glycerol etherification with isobutene. *Applied Catalysis A: General* **2011**, *393* (1–2), 88-95.
11. Soares, R. R.; Simonetti, D. A.; Dumesic, J. A., Glycerol as a Source for Fuels and Chemicals by Low-Temperature Catalytic Processing. *Angewandte Chemie International Edition* **2006**, *45* (24), 3982-3985.
12. Simonetti, D. A.; Kunkes, E. L.; Dumesic, J. A., Gas-phase conversion of glycerol to synthesis gas over carbon-supported platinum and platinum–rhenium catalysts. *Journal of Catalysis* **2007**, *247* (2), 298-306.
13. Sonnati, M. O.; Amigoni, S.; de Givenchy, E. P. T.; Darmanin, T.; Choulet, O.; Guittard, F., Glycerol carbonate as a versatile building block for tomorrow: synthesis, reactivity, properties and applications. *Green Chem* **2013**, *15* (2), 283-306.
14. Aresta, M.; Dibenedetto, A.; Nocito, F.; Pastore, C., A study on the carboxylation of glycerol to glycerol carbonate with carbon dioxide: The role of the catalyst, solvent and reaction conditions. *Journal of Molecular Catalysis A: Chemical* **2006**, *257* (1–2), 149-153.
15. Vieville, C.; Yoo, J. W.; Pelet, S.; Mouloungui, Z., Synthesis of glycerol carbonate by direct carbonatation of glycerol in supercritical CO₂ in the presence of zeolites and ion exchange resins. *Catalysis Letters* **1998**, *56* (4), 245-247.
16. Hammond, C.; Lopez-Sanchez, J. A.; Hasbi Ab Rahim, M.; Dimitratos, N.; Jenkins, R. L.; Carley, A. F.; He, Q.; Kiely, C. J.; Knight, D. W.; Hutchings, G. J., Synthesis of glycerol carbonate from glycerol and urea with gold-based catalysts. *Dalton Transactions* **2011**, *40* (15), 3927-3937.
17. Climent, M. J.; Corma, A.; De Frutos, P.; Iborra, S.; Noy, M.; Velty, A.; Concepción, P., Chemicals from biomass: Synthesis of glycerol carbonate by transesterification and carbonylation with urea with hydrotalcite catalysts. The role of acid–base pairs. *Journal of Catalysis* **2010**, *269* (1), 140-149.

18. Ochoa-Gómez, J. R.; Gómez-Jiménez-Aberasturi, O.; Maestro-Madurga, B.; Pesquera-Rodríguez, A.; Ramírez-López, C.; Lorenzo-Ibarreta, L.; Torrecilla-Soria, J.; Villarán-Velasco, M. C., Synthesis of glycerol carbonate from glycerol and dimethyl carbonate by transesterification: Catalyst screening and reaction optimization. *Applied Catalysis A: General* **2009**, *366* (2), 315-324.
19. Wilson, S. T.; Lok, B. M.; Messina, C. A.; Cannan, T. R.; Flanigen, E. M., Aluminophosphate Molecular-Sieves - a New Class of Microporous Crystalline Inorganic Solids. *J Am Chem Soc* **1982**, *104* (4), 1146-1147.
20. Oliver, S.; Kuperman, A.; Ozin, G. A., A New Model for Aluminophosphate Formation: Transformation of a Linear Chain Aluminophosphate to Chain, Layer, and Framework Structures. *Angewandte Chemie International Edition* **1998**, *37* (1-2), 46-62.
21. Brill, R.; Debretteville, A. P., On the chemical bond type in AlPO₄. *Acta Crystallographica* **1955**, *8* (9), 567-570.
22. Middelkoop, V.; Jacques, S. M.; O'Brien, M.; Beale, A.; Barnes, P., Hydrothermal/autoclave synthesis of AlPO-5: a prototype space/time study of crystallisation gradients. *J Mater Sci* **2008**, *43* (7), 2222-2228.
23. Wilson, S. T.; Lok, B. M.; Messina, C. A.; Cannan, T. R.; Flanigen, E. M., Aluminophosphate molecular sieves: a new class of microporous crystalline inorganic solids. *J Am Chem Soc* **1982**, *104* (4), 1146-1147.
24. Jones, R. H.; Thomas, J. M.; Chen, J.; Xu, R.; Huo, Q.; Li, S.; Ma, Z.; Chippindale, A. M., Structure of an Unusual Aluminium Phosphate ($[Al_5P_6O_{24}H]^{2-} \cdot 2[N(C_2H_5)_3H]^+ \cdot 2H_2O$) JDF-20 with Large Elliptical Apertures. *J Solid State Chem* **1993**, *102* (1), 204-208.
25. Chippindale, A. M.; Turner, C., The Synthesis and Characterization of a One-Dimensional Aluminophosphate: $[C_{10}N_2H_9] [Al(PO_4)(PO_2(OH)_2)]$. *J Solid State Chem* **1997**, *128* (2), 318-322.
26. Chippindale, A. M.; Cowley, A. R., Heteroatom-substituted microporous gallium phosphates. *Microporous and Mesoporous Materials* **1998**, *21* (4-6), 271-279.

27. Wragg, D. S.; Slawin, A. M. Z.; Morris, R. E., The role of added water in the ionothermal synthesis of microporous aluminium phosphates. *Solid State Sciences* **2009**, *11* (2), 411-416.
28. Parnham, E. R.; Morris, R. E., The Ionothermal Synthesis of Cobalt Aluminophosphate Zeolite Frameworks. *J Am Chem Soc* **2006**, *128* (7), 2204-2205.
29. Kannan, C.; Sivakami, K.; Ilavarasi Jeyamalar, J., A simple method for the synthesis of thermally stable large pore mesoporous aluminophosphate molecular sieves. *Materials Letters* **2013**, *113* (0), 93-95.
30. Sreenivasulu, P.; Nandan, D.; Kumar, M.; Viswanadham, N., Synthesis and catalytic applications of hierarchical mesoporous $\text{AlPO}_4/\text{ZnAlPO}_4$ for direct hydroxylation of benzene to phenol using hydrogen peroxide. *Journal of Materials Chemistry A* **2013**, *1* (10), 3268-3271.
31. Shiju, N. R.; Fiddy, S.; Sonntag, O.; Stockenhuber, M.; Sankar, G., Selective oxidation of benzene to phenol over FeAlPO catalysts using nitrous oxide as oxidant. *Chemical Communications* **2006**, (47), 4955-4957.
32. Zhou, L.; Xu, J.; Chen, C.; Wang, F.; Li, X., Synthesis of Fe, Co, and Mn substituted AlPO-5 molecular sieves and their catalytic activities in the selective oxidation of cyclohexane. *J Porous Mater* **2008**, *15* (1), 7-12.
33. ChandraKishore, S.; Pandurangan, A., Synthesis and characterization of Y-shaped carbon nanotubes using Fe/AlPO₄ catalyst by CVD. *Chemical Engineering Journal* **2013**, *222* (0), 472-477.
34. Clearfield, A.; Stynes, J. A., The preparation of crystalline zirconium phosphate and some observations on its ion exchange behaviour. *Journal of Inorganic and Nuclear Chemistry* **1964**, *26* (1), 117-129.
35. Poojary, D. M.; Shpeizer, B.; Clearfield, A., X-Ray powder structure and Rietveld refinement of [gamma]-zirconium phosphate, $\text{Zr}(\text{PO}_4)(\text{H}_2\text{PO}_4)\cdot 2\text{H}_2\text{O}$. *Journal of the Chemical Society, Dalton Transactions* **1995**, (1), 111-113.

36. Troup, J. M.; Clearfield, A., Mechanism of ion exchange in zirconium phosphates. 20. Refinement of the crystal structure of α -zirconium phosphate. *Inorganic Chemistry* **1977**, *16* (12), 3311-3314.
37. Trobajo, C.; Khainakov, S. A.; Espina, A.; García, J. R., On the Synthesis of α -Zirconium Phosphate. *Chemistry of Materials* **2000**, *12* (6), 1787-1790.
38. Sun, L.; Boo, W. J.; Sue, H.-J.; Clearfield, A., Preparation of [small α]-zirconium phosphate nanoplatelets with wide variations in aspect ratios. *New Journal of Chemistry* **2007**, *31* (1), 39-43.
39. Naik, A. H.; Thakkar, N. V.; Dharwadkar, S. R.; Singh Mudher, K. D.; Venugopal, V., Microwave assisted low temperature synthesis of sodium zirconium phosphate ($\text{NaZr}_2\text{P}_3\text{O}_{12}$). *J Therm Anal Calorim* **2004**, *78* (3), 707-713.
40. Burnell, V. A.; Readman, J. E.; Tang, C. C.; Parker, J. E.; Thompson, S. P.; Hriljac, J. A., Synthesis and structural characterisation using Rietveld and pair distribution function analysis of layered mixed titanium-zirconium phosphates. *J Solid State Chem* **2010**, *183* (9), 2196-2204.
41. Clearfield, A.; Frianeza, T. N., On the mechanism of ion exchange in zirconium phosphates—XXII mixed zirconium titanium phosphates. *Journal of Inorganic and Nuclear Chemistry* **1978**, *40* (11), 1925-1932.
42. Kapoor, M. P.; Inagaki, S.; Yoshida, H., Novel Zirconium–Titanium Phosphates Mesoporous Materials for Hydrogen Production by Photoinduced Water Splitting. *The Journal of Physical Chemistry B* **2005**, *109* (19), 9231-9238.
43. Scheetz, B. E.; Agrawal, D. K.; Breval, E.; Roy, R., Sodium zirconium phosphate (NZP) as a host structure for nuclear waste immobilization: A review. *Waste Management* **1994**, *14* (6), 489-505.
44. Rao, K. N.; Sridhar, A.; Lee, A. F.; Tavener, S. J.; Young, N. A.; Wilson, K., Zirconium phosphate supported tungsten oxide solid acid catalysts for the esterification of palmitic acid. *Green Chem* **2006**, *8* (9), 790-797.

45. Aresta, M.; Dibenedetto, A.; Nocito, F.; Ferragina, C., Valorization of bio-glycerol: New catalytic materials for the synthesis of glycerol carbonate via glycerolysis of urea. *Journal of Catalysis* **2009**, *268* (1), 106-114.
46. Readman, J. E. The synthesis and Characterisation of some Aluminium Phosphates and Related Phases. Oxford Univeristy, Pembroke College, Oxford, 1996.
47. Chippindale, A. M.; Walton, R. I., [C₉H₂₀N][Al₂(HPO₄)₂(PO₄)]: An Aluminium Phosphate with a New Layer Topology. *J Solid State Chem* **1999**, *145* (2), 731-738.
48. Bond, A. D.; Chippindale, A. M.; Cowley, A. R.; Readman, J. E.; Powell, A. V., Synthesis and characterisation of transition-metal-substituted gallium phosphates with the laumontite structure. *Zeolites* **1997**, *19* (5-6), 326-333.
49. AXS, B. *DIFFRAC.EVA*, 3.0; Bruker: 2012.
50. Nakamoto, K., *Infrared Spectra of Inorganic and Coordination Compounds*. John Wiley & Sons, Inc.: USA, 1963.
51. Socrates, G., *Infrared and Raman Characterisitic Group Frequencies*. 3rd ed.; John Wiley & Sons Ltd.: Chichester, England, 2001.
52. Visser, J., A fully automatic program for finding the unit cell from powder data. *Journal of Applied Crystallography* **1969**, *2* (3), 89-95.
53. Altomare, A.; Giacovazzo, C.; Guagliardi, A.; Moliterni, A. G. G.; Rizzi, R.; Werner, P.-E., New techniques for indexing: N-TREOR in EXPO. *Journal of Applied Crystallography* **2000**, *33* (4), 1180-1186.
54. Boultif, A.; Louer, D., Indexing of powder diffraction patterns for low-symmetry lattices by the successive dichotomy method. *Journal of Applied Crystallography* **1991**, *24* (6), 987-993.
55. David, W. I. F.; Shankland, K.; McCusker, L. B.; Baerlocher, C., *Structure Determination from Powder Diffraction Data*. Oxford University Press Inc.: United States, 2011.

56. Blake, A. J.; Clegg, W.; Cole, J. M.; Evans, J. S. O.; Main, P.; Parsons, S.; Watkin, D. J., *Crystal Structure Analysis Principles and Practice*. 2nd ed.; Oxford University Press: Great Britain, 2009.
57. Horsley, S. E.; Nowell, D. V.; Stewart, D. T., The infrared and Raman spectra of α -zirconium phosphate. *Spectrochimica Acta Part A: Molecular Spectroscopy* **1974**, *30* (2), 535-541.
58. Dubois, J.-L.; Aresta, M. Synthesis process of polyol carbonate from polyols, conducted in using a solvent selective for polyols carbonates. EP2174937, 08/10/2008, 2013.
59. Jones, R. H.; Thomas, J. M.; Huo, Q.; Xu, R.; Hursthouse, M. B.; Chen, J., The synthesis and crystal structure of a novel clay-like gallophosphate with sub-unit-cell intergrowths of ethylenediamine: $[\text{GaPO}_4(\text{OH})]^- \cdot 0.5(\text{H}_3\text{NCH}_2\text{CH}_2\text{NH}_3)^{2+}$. *Journal of the Chemical Society, Chemical Communications* **1991**, (21), 1520-1522.
60. Takahara, I.; Saito, M.; Inaba, M.; Murata, K., Dehydration of Ethanol into Ethylene over Solid Acid Catalysts. *Catalysis Letters* **2005**, *105* (3-4), 249-252.
61. Ravindra Reddy, C.; Nagendrappa, G.; Jai Prakash, B. S., Surface acidity study of Mn⁺-montmorillonite clay catalysts by FT-IR spectroscopy: Correlation with esterification activity. *Catalysis Communications* **2007**, *8* (3), 241-246.
62. Zecchina, A.; Marchese, L.; Bordiga, S.; Pazè, C.; Gianotti, E., Vibrational Spectroscopy of NH₄⁺ Ions in Zeolitic Materials: An IR Study. *The Journal of Physical Chemistry B* **1997**, *101* (48), 10128-10135.
63. Armaroli, T.; Busca, G.; Carlini, C.; Giuttari, M.; Raspolli Galletti, A. M.; Sbrana, G., Acid sites characterization of niobium phosphate catalysts and their activity in fructose dehydration to 5-hydroxymethyl-2-furaldehyde. *Journal of Molecular Catalysis A: Chemical* **2000**, *151* (1-2), 233-243.
64. Schrader, G. L.; Cheng, C. P., Laser Raman spectroscopy of cobalt-molybdenum/ γ -aluminum oxide catalysts. Characterization using pyridine adsorption. *The Journal of Physical Chemistry* **1983**, *87* (19), 3675-3681.

65. Zheng, A.; Liu, S.-B.; Deng, F., Acidity characterization of heterogeneous catalysts by solid-state NMR spectroscopy using probe molecules. *Solid State Nuclear Magnetic Resonance* **2013**, 55–56 (0), 12-27.
66. Shannon, R., Revised effective ionic radii and systematic studies of interatomic distances in halides and chalcogenides. *Acta Crystallographica Section A* **1976**, 32 (5), 751-767.